# Stony Brook University

**Influence of deformable substrates on macroscopic and microscopic phenomenon of tissue**

A Dissertation Presented

by

**Divya Bhatnagar**

to

The Graduate School

in Partial Fulfillment of the

Requirements

for the Degree of

**Doctor of Philosophy**

in

**Materials Science and Engineering**

Stony Brook University

**August 2012**

**Stony Brook University**

The Graduate School

**Divya Bhatnagar**

We, the dissertation committee for the above candidate for the

**Doctor of Philosophy** degree,

hereby recommend acceptance of this dissertation.

**Dr. Miriam H. Rafailovich – Dissertation Advisor**
**Distinguished Professor, Materials Science and Engineering**

**Dr. Jonathan C. Sokolov - Chairperson of Defense**
**Professor, Materials Science and Engineering**

**Dr. Vladimir Jurukovski**
**Associate Professor, Materials Science and Engineering**

**Dr. Marcia Simon**
**Professor, Department of Oral Biology and Pathology, Stony Brook University**

This dissertation is accepted by the Graduate School

Charles Taber
Interim Dean of the Graduate School

Abstract of the Dissertation

**Influence of deformable substrates on macroscopic and microscopic phenomenon of tissue**

by

**Divya Bhatnagar**

**Doctor of Philosophy**

in

**Materials Science and Engineering**

Stony Brook University

**2012**

One of the most important aspects by which cells adapt to their environment is their interaction with their extracellular matrix. The goal of this thesis is to design deformable substrates with controllable mechanical and biochemical properties and to understand cell-substrate interaction at both microscopic and macroscopic scales. First part of the thesis aims to develop biodegradable hydrogels as delivery vehicles for cellular and small molecular therapeutics and also for potential tissue engineering constructs. The second part deals with development of an assessment tool for analyzing changes in tissue mechanics.

In the first part of this thesis, we studied the interaction of the dental pulp stem cells with enzymatically crosslinked gelatin hydrogels of tunable stiffness (8KPa-0.1KPa). Dental pulp

stem cells (DPSCs) are known to undergo odontogenesis when grown with Dexamethasone (Dex). The purpose of this study was to investigate the odontogenic impact of substrates on DPSCs in the absence of Dex. Through our experiments we identified hydrogels that support DPSC biomineralization and odontogenesis. These scaffolds were self-mineralizing and may prove useful as a biodegradable scaffold for dentin regeneration.

In the second part, we prepared physically crosslinked polymer composite hydrogels of variable stiffness. We studied the rheological properties of these hydrogel scaffolds and related it to the type of bonding, degree of crosslinking and mechanical structure of the hydrogels. We showed the successful application of these hydrogels as potential drug delivery vehicles by studying the controlled release of Salicylic Acid. Their potential use as tissue engineered constructs was also shown by dermal fibroblasts adhesion and proliferation.

In the last part of this thesis, we successfully developed a non-invasive Digital Image Speckle Correlation (DISC) technique for the precise quantification of the magnitude and duration of facial muscle paralysis inflicted by the Botulinum toxin (BTX-A). We were able to precisely characterize the mechanics of skin abnormalities and macroscopic response of collective cellular motion. Due to the generality of this method we were able to extend the use of DISC for diagnosis and prognosis of patients with vestibular schwannomas. Our results are based on successful human clinical trials of vestibular schwannomas and facial paralysis patients.

*Dedicated to*

***My Family***

***For their love and support***

# TABLE OF CONTENTS

**List of Figures** ..... x

Chapter 1 ..... x

Chapter 2 ..... xii

Chapter 3 ..... xiii

Chapter 4 ..... xiv

**List of Tables** ..... xv

**List of Abbreviations** ..... xvi

**Acknowledgments** ..... xviii

**List of Patents and Publications** ..... xxi

**Introduction** ..... 1

*Background* ..... 1

*Outline of the chapters* ..... 2

**Chapter 1** ..... 7

**The behavior of human dental pulp stem cells on enzymatically crosslinked gelatin hydrogels** ..... 7

**1. Introduction** ..... 7

**2. Materials and Methods** ..... 9

2.1 *Preparation of enzymatically crosslinked gelatin hydrogels* ..... 9

*2.2 Dynamic Rheological characterization* ..... 9

*2.3 Cell culture and Cell Seeding* ..... 10

*2.4 Shear Modulation Force Microscopy (SMFM)* ..... 10

*2.5 Scanning Electron Microscopy (SEM)* ..... 11

*2.6 Confocal Laser Scanning Microscopy* ..... 11

*2.7 RT-PCR* ..... 11

*2.8 Alizarin Red Staining* ..... 12

*2.9 Education* ..... 13

**3. Results** ..... 13

*3.1 Rheological Characterization of Gelatin-mTG hydrogels* ..... 13

*3.2 Cell stiffness* ..... 13

*3.3 Biomineralization of the ECM* ..... 14

*3.3.1 In presence of DPSCs* ..... 14

*3.3.2 In absence of DPSC's* ..... 15

*3.3.3 Gelatin and mTG alone cannot trigger biomineralization* ..... 15
*3.4 ECM mineralization of DPSCs on crosslinked hydrogels* ..... 16
*3.5 Cell Morphology* ..... 16
*3.6 Expression of differentiation markers (RT-PCR)* ..... 17
*3.5 Long term differentiation* ..... 18
*3.5.1 Mineralization after 21 days of incubation* ..... 18
*3.5.2 Expression of Differentiation markers* ..... 18
**4. Discussion** ..... 19
**5. Conclusion** ..... 22
**6. Figures** ..... 23
**Chapter 2** ..... 37
**Hyaluronic Acid and Gelatin Clay composite hydrogels: Substrates for Cell adhesion and controlled drug delivery** ..... 37
**1. Introduction** ..... 37
**2. Materials and Methods** ..... 40
*2.1 Raw Materials* ..... 40
*2.2 Preparation of the hydrogels* ..... 41
*2.2.1 HA-Clay, Gelatin-Clay and HA-Gelatin-Clay Hydrogels* ..... 41
*2.2.2 HA-Clay hydrogel substrates with glucose* ..... 42
*2.3 Dynamic Rheological Characterization* ..... 42
*2.4 Cell Culture* ..... 43
*2.5 Cell attachment* ..... 44
*2.6 Cell Stiffness* ..... 44
*2.7 Salicylic Acid drug delivery* ..... 45
**3. Results and Discussion** ..... 46
*3.1 Synthesis of HA-Clay Hydrogels* ..... 46
*3.2 Rheological Characterization of HA-Clay/Gelatin-Clay/HA-Gelatin-Clay hydrogels.* ..... 47
*3.2.1 Oscillatory stress Sweep* ..... 47
*3.2.2 Oscillatory frequency Sweep* ..... 48
*3.3 Effect of Glucose on the rheological properties* ..... 50
*3.4 In-vitro salicylic acid release* ..... 51
*3.5 In vitro cell culture testing* ..... 52
*3.5 Measurement of cell stiffness* ..... 52

**4. Conclusion** ..... 53

**5. Figures** ..... 55

**Chapter 3** ..... 61

**Non-Invasive Analysis of the Effect and Duration of Treatment with Botulinum Toxin Type A using Digital Image Speckle Correlation** ..... 61

**1. Introduction** ..... 61

**2. Methods** ..... 64

*2.1 DISC Method* ..... 64

*2.2 Experimental protocol* ..... 66

**3. Results** ..... 67

*3.1 Vector and Vertical Displacement Maps* ..... 67

*3.2 Quantification of Muscle Contraction Using DISC* ..... 68

*3.3 FLO-11 and SGA* ..... 69

*3.4 Determination of the Site of Maximum Muscular Tension* ..... 70

**4. Discussion** ..... 71

**5. Conclusion** ..... 73

**6. Figures and tables** ..... 74

**Chapter 4** ..... 85

**An analysis of facial nerve function in patients with vestibular schwannomas using digital image speckle correlation** ..... 85

**1. Introduction** ..... 85

**2. Methods** ..... 87

*2.1 Experimental Protocol* ..... 87

*2.2 The DISC Method* ..... 88

*2.3 Quantifying the displacement or deformation field* ..... 89

*2.4 Statistical Analysis* ..... 89

**3. Results** ..... 90

*3.1 Establishing the degree of facial asymmetry in the control group* ..... 90

*3.2 Quantitative DISC analysis of untreated (no surgery) population* ..... 90

*3.3 Quantitative DISC analysis of gamma knife radiosurgery treated population* ..... 91

*3.4 Quantitative DISC analysis of resection treated population* ..... 92

*3.5 Tumor Size* ..... 92

**4. Discussion** ..... 92

**5. Conclusion** ..... 94
**6. Figures** ..... 95
**Bibliography** ..... 99

# List of Figures

## Chapter 1

FIGURE 1-1: OSCILLATORY SHEAR STRESS SHOWING THE STIFFNESS OF HARD, MEDIUM AND SOFT HYDROGEL (B) CELL STIFFNESS FROM DAY 1 TO DAY 7 IN INDUCED AND NON-INDUCED HARD AND SOFT HYDROGELS. ....23

FIGURE 1-2: SEM MICROGRAPHS OF INDUCED HARD GEL (H+) WITH DPSCS, SHOWING BIOMINERALIZED DEPOSITS ON (A) DAY1 (B) DAY 7 (C) DAY 14 (D) DAY 21 (E) DAY 35. EDAX SPECTRA SHOWING PEAKS FOR CALCIUM PHOSPHATE ON (F) DAY 1 (G) DAY 7 (H) DAY 14 (I) DAY 21 (J) DAY 35. MAGNIFICATION= 1KX; SCALE= 20μM....24

FIGURE 1- 3: SEM MICROGRAPHS OF NON-INDUCED HARD GEL (H-) WITH DPSCS, SHOWING BIOMINERALIZED DEPOSITS ON (A) DAY1 (B) DAY 7 (C) DAY 14 (D) DAY 21 (E) DAY 35. EDAX SPECTRA SHOWING PEAKS OF CALCIUM PHOSPHATE ON (F) DAY 1 (G) DAY 7 (H) DAY 14 (I) DAY 21 AND (J) DAY 35. MAGNIFICATION= 1KX; SCALE= 20μM ....25

FIGURE 1- 4: SEM MICROGRAPHS OF INDUCED SOFT GEL (S+) WITH DPSCS, SHOWING BIOMINERALIZED DEPOSITS ON (A) DAY1 (B) DAY 7 (C) DAY 14 (D) DAY 21 (E) DAY 35. EDAX SPECTRA SHOWING PEAKS OF CALCIUM PHOSPHATE ON (F) DAY 1 (G) DAY 7 (H) DAY 14 (I) DAY 21 (J) DAY 35. MAGNIFICATION= 1KX; SCALE= 20μM ....26

FIGURE 1- 5: SEM MICROGRAPHS OF NON-INDUCED SOFT GEL (S-) WITH DPSCS, SHOWING BIOMINERALIZED DEPOSITS ON (A) DAY1 (B) DAY 7 (C) DAY 14 (D) DAY 21 (E) DAY 35. EDAX SPECTRA SHOWING PEAKS OF CALCIUM PHOSPHATE ON (F) DAY 1 (G) DAY 7 (H) DAY 14 (I) DAY 21 (J) DAY 35. MAGNIFICATION= 1KX; SCALE= 20μM ....27

FIGURE 1- 6: SEM MICROGRAPHS OF NON-INDUCED HARD GEL (H-) WITHOUT DPSCS, SHOWING BIOMINERALIZED DEPOSITS ON (A) DAY1 (B) DAY 7 (C) DAY 14 (D) DAY 21 (E) DAY 35. EDAX SPECTRA SHOWING PEAKS FOR CALCIUM PHOSPHATE ON (F) DAY 1 (G) DAY 7 (H) DAY 14 (I) DAY 21 (J) DAY 35. MAGNIFICATION= 3KX; SCALE= 20μM. ....28

FIGURE 1- 7: SEM MICROGRAPHS AFTER 21 DAYS OF INCUBATION OF DPSCS ON TCP COATED WITH (A) INDUCED MTG (MTG+) (B) NON-INDUCED MTG (MTG-) (C) INDUCED GELATIN (GELATIN+) (D) NON-INDUCED GELATIN (GELATIN-). EDAX SPECTRA AFTER OF DPSCS ON TCP COATED WITH (E) INDUCED MTG (MTG+) (F) NON-INDUCED MTG (MTG-) (G) INDUCED GELATIN (GELATIN+) (H) NON-INDUCED GELATIN (GELATIN-) AFTER 21 DAYS OF INCUBATION. MAGNIFICATION= 3KX; SCALE= 10µM. .....29

FIGURE 1- 8: MINERALIZATION SHOWN THROUGH ALIZARIN RED STAINING AFTER DAY 35 OF INCUBATION ON: INDUCED (A) HARD GEL (H+) WITH DPSCS (B) SOFT GEL (S+) WITH DPSCS (C) HARD GEL (H+) WITHOUT DPSCS (D) SOFT GEL (S+) WITHOUT DPSCS, NON-INDUCED (E) HARD GEL (H-) WITH DPSC (F) SOFT GEL (S-) WITH DPSC (G) HARD GEL (H-) WITHOUT DPSC (H) SOFT GEL (S-) WITHOUT DPSC. MAGNIFICATION=10X .....30

FIGURE 1- 9: MORPHOLOGY OF THE DPSCS AFTER 21 DAYS OF INCUBATION ON INDUCED (A) HARD GEL (H+) (B) SOFT GEL (S+), NON-INDUCED (C) HARD GEL (H-) (D) SOFT GEL (S-). ACTIN FILAMENTS WERE STAINED BY ALEXA FLOUR 488 (GREEN), NUCLEUS WAS STAINED BY PROPIUM IODIDE (RED). MAGNIFICATION= 63X; SCALE = 47.41µM.....31

FIGURE 1- 10: MRNA EXPRESSION OF (A) OSTEOCALCIN (OCN) (B) BONE SIALOPROTEIN (BSP) (C) ALKALINE PHOSPHATASE (ALP) (D) DENTIN SIALOPHOSPHOPROTEIN (DSPP) FROM DAY 1 TO DAY 35 ON CONTROLS (TCP+, TCP-), H+, H-, S+, S-. .....32

FIGURE 1- 11: SEM MICROGRAPHS SHOWING BIOMINERALIZED DEPOSITS OF INDUCED "EDUCATION SAMPLES" WHERE THE DPSCS WERE RE-PLATED ON TCP FOR 21 DAYS AFTER GETTING EXTRACTED FROM (A) INDUCED HARD GEL (H+(+)) (B) INDUCED SOFT GEL (S+(+)) (C) NON-INDUCED HARD GEL (H-(+)) (D)NON-INDUCED SOFT GEL (S-(+). CORRESPONDING EDAX SPECTRA SHOWING CALCIUM PHOSPHATE PEAKS OF INDUCED "EDUCATION SAMPLES" WHERE THE DPSCS WERE RE-PLATED ON TCP FOR 21 DAYS AFTER GETTING EXTRACTED FROM (E) INDUCED HARD GEL (H+(+)) (F) INDUCED SOFT GEL (S+(+)) (G) NON-INDUCED HARD GEL (H-(+)) (H) NON-INDUCED SOFT GEL (S-(+). MAGNIFICATION= 1KX; SCALE=20µM. .....33

FIGURE 1- 12: SEM MICROGRAPHS SHOWING BIOMINERALIZED DEPOSITS OF NON-INDUCED "EDUCATION SAMPLES" WHERE THE DPSCS WERE RE-PLATED ON TCP FOR 21 DAYS AFTER GETTING EXTRACTED FROM (A) INDUCED HARD GEL (H+(-)) (B) INDUCED SOFT GEL (S+(-)) (C) NON-INDUCED HARD GEL (H-(-)) (D) NON-INDUCED SOFT GEL (S-(-)). CORRESPONDING EDAX SPECTRA SHOWING CALCIUM PHOSPHATE PEAKS OF INDUCED "EDUCATION SAMPLES" WHERE THE DPSCS WERE RE-PLATED ON TCP FOR 21 DAYS AFTER GETTING EXTRACTED FROM (E)

INDUCED HARD GEL (H+(-)) (F) INDUCED SOFT GEL (S+(-)) (G) NON-INDUCED HARD GEL (H-(-)) (H) NON-INDUCED SOFT GEL (S-(-). MAGNIFICATION= 1KX; SCALE=20μM.....34

FIGURE 1- 13: COMPARISON OF 21 DAY MRNA EXPRESSION OF (A) OSTEOCALCIN (OCN) (B) ALKALINE PHOSPHATASE (ALP) (C) DENTIN SIALOPHOSPHOPROTEIN (DSPP) ON H+(+), S+(+), H-(-) AND S-(-) EDUCATION SAMPLES AND TCP(+), TCP(-) CONTROLS.....35

FIGURE 1- 14: HARD GELATIN-MTG GEL ON DAY 0 WITHOUT CELLS AND WITHOUT INDUCED/NON-INDUCED MEDIA (A) SEM MICROGRAPH SHOWING THE SURFACE WITH NO MINERALIZED DEPOSITS (B) CORRESPONDING EDAX SPECTRA SHOWING ABSENCE OF CALCIUM PHOSPHATE PEAKS. MAGNIFICATION=1KX; SCALE =20μM.....35

FIGURE 1- 15 BIO-MINERALIZED DEPOSITS (SEM MICROGRAPHS) AFTER DAY1 OF INCUBATION ON NON-INDUCED GELATIN-MTG GELS WITHOUT DPSCS. THESE GELS ARE MADE WITH VARIABLE AMOUNT OF GELATIN AND FIXED AMOUNT OF MTG (A) 3%(W/V) GELATIN (B) 4%(W/V) GELATIN (C) 5%(W/V) GELATIN (D) 6%(W/V) GELATIN (E) 8%(W/V) GELATIN. CORRESPONDING EDAX SPECTRA SHOWING CALCIUM PHOSPHATE PEAK ON GELATIN-MTG GELS WITH (F) 3%(W/V) GELATIN (G) 4%(W/V) GELATIN (H) 5%(W/V) GELATIN (I) 6%(W/V) GELATIN (J) 8%(W/V) GELATIN. MAGNIFICATION=3KX; SCALE=20μM.....36

# Chapter 2

FIGURE 2- 1: (A) SCHEMATIC SHOWING STRUCTURE OF HA MOLECULE. (B) (A) STRUCTURE OF HECTORITE CLAY (B) EXFOLIATED CLAY IN DI WATER [39].....55

FIGURE 2- 2: SCHEMATIC REPRESENTATION OF THE MECHANISM OF FORMATION OF HYDROGELS (A) HA-CLAY (B) GELATIN-CLAY (C) HA-GELATIN-CLAY.....56

FIGURE 2- 3: OSCILLATORY STRESS SWEEP ON DIFFERENT TYPES OF HYDROGELS (A) HA-CLAY (B) GELATIN-CLAY (C) HA-GELATIN-CLAY (D) PLOT OF THE BREAKING STRESS FOR DIFFERENT TYPES OF HYDROGELS.....57

FIGURE 2- 4: OSCILLATORY FREQUENCY SWEEP OF DIFFERENT HYDROGELS TO DETERMINE G' AND G" (A) HA-CLAY (B) GELATIN-CLAY (C) HA-GELATIN-CLAY. .....58

FIGURE 2- 5: 1:20(V/V) HA:CLAY HYDROGEL (A) PLOT OF G'(PA) VS DIFFERENT GLUCOSE CONCENTRATIONS (MG/ML) (B) PLOT OF BREAKING STRESS VS DIFFERENT GLUCOSE CONCENTRATIONS (C) CONTROLLED TIME RELEASE OF SA.....59

FIGURE 2- 6: PH PICTURE OF CELLS ON HA-GELATIN-CLAY HYDROGEL AFTER 3 DAYS OF INCUBATION(A) 1:10 (B) 1:20 (C) AGAROSE DROPLET WITH CELLS ON 1:20 GEL (D) LINEAR RELATIONSHIP BETWEEN DRIVE AND RESPONSE AMPLITUDE (E) CELL MODULUS ON 1:20 AND 1:10 HA-GELATIN-CLAY AFTER DAY 1 (* INDICATES P<0.05).....60

# Chapter 3

FIGURE 3- 1: [BOTULINUM TOXIN TYPE-A] REFERENCE AND DEFORMED IMAGES: (1A) PATIENT'S FACE AT REST (REFERENCE IMAGE); (1B) PATIENT FROWNING (DEFORMED IMAGE); (1C) A SCHEMATIC DIAGRAM OF THE DIGITAL IMAGE CORRELATION ALGORITHM [13].....74

FIGURE 3- 2: [BOTULINUM TOXIN TYPE-A] VECTOR DIAGRAMS GENERATED BY DISC FOR GLABELLAR AREA OF THE PATIENT WHILE FROWNING. PRE-TREATMENT (2A) DAY0; POST-TREATMENT (2B) WEEK1 (2C) WEEK2 (2D) WEEK 21.....75

FIGURE 3- 3: [BOTULINUM TOXIN TYPE-A] VECTOR DIAGRAMS GENERATED DISC FOR FOREHEAD REGION WHILE RAISING EYEBROWS. PRE-TREATMENT (3A) DAY0; POST-TREATMENT (3B) WEEK1 (3C) WEEK2 (3D) WEEK 16. .....76

FIGURE 3- 4: [BOTULINUM TOXIN TYPE-A] VERTICAL PROJECTION OF DISPLACEMENT MAPS IN THE GLABELLAR REGION OF THE PATIENT PRIOR TO THE TREATMENT AND AT SPECIFIC FOLLOW UP TIME POINTS. UNIT: PIXEL. THE COLOR DESIGNATES THE RELATIVE DISPLACEMENT AMPLITUDE. SCALE OF COLOR INTENSITY BAR: 50 TO -50. ..77

FIGURE 3- 5: [BOTULINUM TOXIN TYPE-A] VERTICAL PROJECTION OF DISPLACEMENT MAPS IN THE FOREHEAD REGION OF THE PATIENT PRIOR TO THE TREATMENT AND AT SPECIFIC FOLLOW UP TIME POINTS. UNIT: PIXEL. THE COLOR DESIGNATES THE RELATIVE DISPLACEMENT AMPLITUDE. SCALE OF COLOR INTENSITY BAR: 50 TO -44. ..78

FIGURE 3- 6: [BOTULINUM TOXIN TYPE-A] AVERAGE OF INTENSITY OF DISPLACEMENT DISTRIBUTIONS ALONG THE LOCUS OF POINTS BY DRAWING A HORIZONTAL LINE. .....79

FIGURE 3- 7: [BOTULINUM TOXIN TYPE-A] (GLABELLAR COMPLEX) FLO-11, SGA AND AVERAGE INTENSITY OF DEFORMATION (DISC) PLOTTED AS PERCENTAGE CHANGE FROM THE BASELINE VERSUS TIME (IN WEEKS) FOR ALL THE SIX PATIENTS. .....80

FIGURE 3- 8: [BOTULINUM TOXIN TYPE-A] (FOREHEAD REGION) FLO-11, SGA AND AVERAGE INTENSITY OF DEFORMATION (DISC) PLOTTED AS PERCENTAGE CHANGE FROM THE BASELINE VERSUS TIME (IN WEEKS) FOR ALL THE SIX PATIENTS. .....81

FIGURE 3- 9: [BOTULINUM TOXIN TYPE-A] (PATIENT4) VECTOR DIAGRAM OVERLAY ON THE FACE WHILE (9A) FROWNING (GLABELLAR) (9B) RAISING EYEBROWS (FOREHEAD). BLACK CROSSES ARE THE SITES WHERE BTX-A WAS INJECTED BY THE PHYSICIAN. RED CIRCLES INDICATE THE REGIONS WHERE THE DISC GENERATED VECTORS OF MAXIMAL TENSION PREDICT THE SITE OF INJECTION. .....82

# Chapter 4

FIGURE 4- 1: SCHEMATIC OF A DISC SET UP. (A) CAMERA (B) TRACK HOLDING THE CAMERA AT A FIXED DISTANCE (C) STAND FOR PLACING THE CHIN .....95

FIGURE 4- 2: (A) PATIENT'S FACE AT REST OR NEUTRAL MOTION (REFERENCE IMAGE) (B) PATIENT'S FACE WITH A SLIGHT SMILE (DEFORMED IMAGE) (C) SCHEMATIC OF WORKING PRINCIPLE OF DISC (D) QUANTIFYING THE MAGNITUDE OF DISPLACEMENT ON RIGHT AND LEFT SIDE OF THE FACE USING A COLOR DISPLACEMENT MAP. ....96

FIGURE 4- 3: DISC GENERATED COLOR DISPLACEMENT MAP OF CONTROL FOR (A) FIRST SET OF IMAGES (B) SECOND SET OF IMAGES (C) THIRD SET OF IMAGES. AVERAGE AREA OF DEFORMATION BETWEEN RIGHT AND LEFT SIDE OF THE FACE FOR (D) FIRST SET OF IMAGES (E) SECOND SET OF IMAGES (F) THIRD SET OF IMAGES (G) LINEAR CORRELATION BETWEEN THE RIGHT AND LEFT SIDE OF THE FACE FOR CONTROL POPULATION INDICATING SYMMETRY. .....97

FIGURE 4- 4: OVERLAY OF DISC GENERATED COLOR MAP ON THE DEFORMED IMAGE OF (A) UNTREATED/NO SURGERY PATIENT (B) GAMMA KNIFE TREATED PATIENT (C) RESECTION TREATED PATIENT. AVERAGE AREA OF DEFORMATION BETWEEN RIGHT AND LEFT SIDE OF THE FACE FOR (D) UNTREATED/ NO SURGERY PATIENT (E) GAMMA KNIFE TREATED PATIENT (F) RESECTION TREATED PATIENT .....97

FIGURE 4- 5: PERCENT AREA CHANGE BETWEEN RIGHT AND LEFT SIDE, |R-L|/R COMPARING CONTROL POPULATION AND (A) NO SURGERY/UNTREATED (B) GAMMA RADIATION TREATED (C) RESECTION TREATED. (D) LARGE AND SMALL MAGNITUDE OF MOTION ON THE FACE .....98

FIGURE 4- 6: NO CORRELATION BETWEEN PERCENT AREA CHANGE BETWEEN RIGHT AND LEFT SIDE, |R-L|/R AND TUMOR SIZE OF (A) NO SURGERY/UNTREATED (B) GAMMA KNIFE TREATED (C) RESECTION TREATED .....98

# List of Tables

TABLE 2- 1: PREPARATION OF HA-CLAY, GELATIN-CLAY, HA-GELATIN-CLAY HYDROGELS WITH THEIR STORAGE MODULI AND BREAKING STRESS.....55

TABLE 3- 1: [BOTULINUM TOXIN TYPE-A] SUBJECT DEMOGRAPHICS. INITIAL WRINKLE SEVERITY SUBJECTIVELY ASSESSED USING THE FACIAL WRINKLE SCALE (0=NONE, 1=MILD, 2=MODERATE, 3=SEVERE).....83

TABLE 3- 2: TABLE I. [BOTULINUM TOXIN TYPE-A] INJECTION NUMBER AND LOCATION BASED ON THE 2008 PLASTIC AND RECONSTRUCTIVE SURGERY SUPPLEMENT CONSENSUS RECOMMENDATIONS [24]. (F=FEMALE, M=MALE, U=UNITS) .....82

TABLE 3- 3: [BOTULINUM TOXIN TYPE-A] MUSCLE MASS (SMALL, MEDIUM, LARGE) AND INJECTION VOLUME (UNITS) PER LOCATION IN EACH PATIENT.....84

# List of Abbreviations

| | |
|---|---|
| αMEM | Alpha Minimum Essential Medium |
| ALP | Alkaline Phosphatase |
| AHDFs | Adult Human Dermal Fibroblasts |
| AZ | Alizarin |
| BSP | Bone Sialoprotein |
| BTX-A | Botulinum Toxin type A |
| CaP | Calcium Phosphate |
| DISC | Digital Image Speckle Correlation |
| DMEM | Dulbecco's modified eagle's medium |
| DPSCs | Dental Pulp Stem Cells |
| DSPP | Dentin Sialophosphoprotein |
| Dex | Dexamethasone |
| ECM | Extra Cellular Matrix |
| FBS | Fetal Bovine Serum |
| FLO | Facial Lines Outcome |
| FN | Fibronectin |

| | |
|---|---|
| FWS | Facial wrinkle scale |
| G’ | Storage Modulus |
| G” | Viscous Modulus |
| H+ | Induced Hard hydrogel |
| H- | Non- Induced hard gel |
| HA | Hyaluronic Acid/ Hyaluronan |
| LVR | Linear Viscoelastic Range |
| mTG | Microbial transglutaminase |
| OCN | Osteocalcin |
| PS | Penn Strep |
| S+ | Induced soft gel |
| S- | Non-Induced soft gel |
| SA | Salicylic Acid |
| SGA | Subject Global Assessment |
| SPA | Subject Patient Assessment |
| TCP | Tissue Culture Plastic |
| VS | Vestibular Schwannomas |

# Acknowledgments

This dissertation would not have been possible without the support of my advisor, Professor Miriam Rafailovich. Her dynamic and invigorating attitude towards research filled the atmosphere with amazing ideas. She constantly shared her knowledge and encouraged me to apply my physics background towards the research problems. I would like to thank her for giving me such incredible opportunities to collaborate and perform research in a variety of areas, enabling me to broaden my horizon.

I would also like to thank Prof. Marcia Simon who gave me an opportunity to work in her lab at the Dental School. The close collaboration and invaluable discussions around my work have been of great value in this study. I am very thankful to Dr. Raphael Davis for not only being an enthusiastic collaborator at the Department of Neurosurgery but for also providing me with financial assistance in the time of need. I will always hold high regards for him. My warm thanks to Dr. Alexander Dagum, for giving me an opportunity to work at the Division of Plastic Surgery and for making my research projects enjoyable. I always feel so lucky to have worked with my collaborators on numerous interesting projects. I thank them for their patience and trust in me and for the enjoyable research experience.

I also want to extend my thanks to my other committee members, Prof. Jonathan Sokolov and Dr. Vladimir Jurukovski for their constructive comments and persistent attention on my research. I'm grateful to Dr. Sokolov who helped with confocal experiments on numerous occasions, to Dr. Jurukovski for helping me with my stem cells project through his valuable comments and for preparing media whenever I asked for it!!

During this work, I have collaborated with many colleagues for whom I have great regard, and I wish to extend my warmest thanks to all those who have helped me with my work. I am

grateful to Prof. Mary Cowman at the NYU Polytech, Dr. Jim Marecek at Chemistry Department and Dr. Yizhi Meng. Without your support, I would not have been able to successfully complete my projects. I'm grateful to Dr. Zhi Pan for training me to work with hydrogels and Dr. Jim Quinn for helping me immensely with my SEM experiments and for sharing his jokes with me all the time. Amongst my professors from whom I have taken courses and done TA, I have a special place for Prof. Tobin who has always given me valuable advices and shared his thoughts about history and culture. He is such a nice human being and so kind to appreciate my work. I would like to thank my laboratory members and colleagues: Kate Dorst, Dr. Chunhua Li, Dr. Chungcheuh Chang, Jason Yang, Dr. Chien-Hsu-Lin, Dr. Ying Liu, Dr. Yantian Wang, Sisi Qin, Cheng Pan, Nicole Conkling, Samantha, Allie for their help with my research. My very special thanks go to my fellow officemates Dr. Seongchen Park, Dr. Tatsiana Minorova, Joanne Toye and Suphanee for their wonderful company and helpful research conversations which made my workplace really enjoyable.

During my stay in Stony Brook, I made very special friends who will always remain very important part of my life. Thanks Chee Sheng Fong, Heli Vora, Giulia Suarato, Lamiya, Manideep and Aneel for always being very supportive. I remember all those times when I was sad and needed a friend and each one of you was there to cheer me up and encourage me. I could talk to you about anything and everything, it just made these 5 years so special. You guys will always be friends for life!!

This thesis would be incomplete without mentioning the most important people in my life, my entire family. No words could ever describe how much love I have for my late grandfather who inspired me for higher studies, my grandmother who is my best friend and my strength. I would have never done it without my Dad who always trusted in me and my decisions, my Mom

who sacrificed so much so that I could get everything I wanted. They are the chief architects of who I am today and I know they are proud of me. I cannot imagine how this journey would have been without my younger sister and brother. They bring my home closer to me with their constant cheerfulness and moral support. I am really fortunate to have been a part of a family with such wonderful selfless people.

Last but not the least; I thank the 'miracle' of my life, Sriram. He has seen me grow from who I was to who I am now, standing by me as my pillar of strength, my confidence, and support system in whatever I did. Every single day for past 10 years, even if it was a competition, an exam, a presentation or an interview, he never stopped believing that "I can do anything"!! He never let me fall and has made all these years from college to PhD, so memorable and special. He believes in me and my dreams like no one else and I simply believe him!!!!

# List of Patents and Publications

This thesis is based on the following patents and publications:

1. "Performance of dental pulp stem cells on enzymatically crosslinked gelatin hydrogels," Bhatnagar Divya, Bherwani Aneel, Jurukovski Vladimir, Simon Marcia, Rafailovich Miriam. (Manuscript to be submitted in Biomaterials).
2. "Cross-linked gelatin hydrogels for Tissue Regeneration," Bhatnagar Divya, Bherwani Aneel, Simon Marcia, Rafailovich Miriam (US Patent Serial # 61/604,846; filed February 29, 2012).
3. "Acellular process of bio-mineralization using enzymatically cross-linked gelatin hydrogels," Bhatnagar Divya, Bherwani Aneel, Simon Marcia, Rafailovich Miriam (US Patent Serial # 61/604,974; filed February 29, 2012).
4. "Hyaluronic Acid and Gelatin Clay composite hydrogels: Substrates for Cell adhesion and controlled drug delivery," Bhatnagar Divya, Cowman Mary, Rafailovich Miriam (Manuscript to be submitted in Biomaterials).
5. "Nanocomposite Hyaluronic Acid Clay based hydrogels," Bhatnagar Divya, Cowman Mary, Rafailovich Miriam (US Patent # 20110275572).
6. "Non-Invasive quantification of the duration and effects of treatment with Botulinum toxin type-A using Digital Image Speckle Correlation", Bhatnagar Divya, Conkling Nicole, Rafailovich Miriam, Phillips Brett, Bui Duc T., Khan S. U., Dagum Alexander B. (Manuscript submitted in Skin Research and Technology).
7. "Digital Image Speckle Correlation (DISC) Analysis for subcutaneous

muscle motion and nerve function," Bhatnagar Divya, Davis Raphael, Rafailovich Miriam (US Patent Serial # 61/482,057; filed May 3, 2011).

8. "An analysis of facial nerve function in patients with vestibular schwannomas using digital image speckle correlation," Davis Raphael, Bhatnagar Divya, Fiore Susan, Rafailovich Miriam. (In preparation to be submitted in Neurosurgery).

*Additional work done by the author during PhD*

9. "Comparison of Native Porcine Skin and a Dermal Substitute using Tensiometry and Digital Image Speckle Correlation", Jason R. Fritz, Brett Phillips, Mitchell Fourman, Nicole Conkling, Mark Melendez, Bhatnagar Divya, Rafailovich Miriam, Dagum Alexander B. (In Press in Annals of Plastic Surgery).
10. "Deformation gradients imprint the direction and speed of en masse fibroblast migration: where to heal," Pan Zhi, Ghosh Kaustabh, Hung Victoria, Macri Lauren, Einhorn Justin, Bhatnagar Divya, Clark Richard A.F., Rafailovich Miriam H. (Under Review in Biomaterials).
11. "Application of Hyaluronic Acid cross-linked thermo reversible pluronic based hydrogels for in-vivo analysis of a prosthetic disc nucleus," Bhatnagar Divya, Rafailovich Miriam, Davis Raphael (US Patent Serial # DM2/2906716.1; filed July 5, 2011).
12. "Digital Image Speckle Correlation for the Clinical Projection of Burn Scarring and Healing Outcome," Clark R., Bhatnagar Divya, Rafailovich M., Fourman M.S. (Filed March, 2012).

13. “Hyaluronic acid-gelatin crosslinked thermoreversible pluronic (F-127) hydrogels”, Bhatnagar Divya, Cowman Mary, Rafailovich Miriam (US Patent Serial # 61/662,724; filed June 21, 2012).

# INTRODUCTION

## *BACKGROUND*

Tissue engineering (TE) has continued to evolve as an exciting and multidisciplinary field, since its emergence in the mid-1980s. It has been aiming to engineer novel biological substitutes that can restore, replace or regenerate defective tissues [1, 2]. The key components of engineered tissue or the TE triad consists of: cells, scaffolds/delivery systems and growth-stimulating signals [3]. Efficient scaffolds should mimic the natural extracellular matrix (ECM) providing the necessary chemical and physical environment to structurally support cell attachment and even control cell functions [4-6]. With regards to the material requirements in TE, hydrogels, specifically polymeric biomaterials based, have long received attention due to their structural integrity, their compositional similarities to the ECM and their ability to support cell proliferation and act as drug delivery vehicles [7]. By definition, hydrogels are simply gels (a class of three-dimensional crosslinked polymeric materials) that swell strongly in aqueous media, and are typically composed of a hydrophilic polymer component that is cross-linked into a network by either covalent or non-covalent interactions [8]. It is the crosslinking that provides for dimensional stability, while the high solvent content gives rise to the fluid-like transport properties. Therefore, hydrogels are considered as deformable viscoelastic materials, where chemical and mechanical properties play a very important role in its applications. Hydrogels can be classified based on the type of crosslinking where eventually the cross-linker controls its tunable mechanical and chemical properties. The classification of hydrogels based on type of cross-linking is as follows:

1) Chemical crosslinking to generate covalent bonds between one or more monomers, 2) physical crosslinking due to chain entanglements, or association bonds including hydrogen bonds or strong van der Waals interactions or ionic interaction between chains [9] and 3) enzymatic crosslinking catalyzing the formation of covalent bonds between protein chains [10]. The applications of hydrogels dates back to 1960, when Wichterle and Lim introduced the use of hydrogels as soft contact lens material [11]. Langer and Vacanti [4] were the first ones to elucidate the techniques of utilizing polymer gels to repair damaged tissues. The fact that hydrogels can absorb from 10-20%, up to thousands of times their dry weight in water, allows the cells to adhere, proliferate, migrate and differentiate [12]. Furthermore, drugs can be incorporated into the hydrogel matrices and be released subsequently depending on hydrogel properties. Thus, hydrogels can function as excellent drug delivery vehicles as well as for tissue regeneration [13].

On a macroscopic scale, we consider the skin on the face to be a deformable substrate. Skin mainly consists of a network of collagen and elastin fibers whose combined effects decide skin's mechanical properties. It is usually considered as an incompressible and anisotropic material that has a visco-elastic behavior and can be deformed [14]. Skin on the face is attached to the underlying muscles and the contraction or stretch of these muscles can determine the skin deformation and abnormalities such as wrinkle formation, vestibular schwannomas, facial paralysis, and various other skin pathologies[15].

In the following chapters of this thesis, I would like to elaborate the study and applications of these deformable substrates on a microscopic and macroscopic scale.

## *OUTLINE OF THE CHAPTERS*

In chapter 1, we focus on the interaction and behavior of Dental Pulp Stem Cells on enzymatically crosslinked hydrogels for dentin regeneration. Using microbial transglutaminase (mTG) as a crosslinker, we catalyze the formation of covalent bonds between individual gelatin strands to form an enzymatically crosslinked gelatin hydrogel. The variable mTG concentration results in a hydrogel with tunable mechanical and biochemical properties. The stiffness was varied from 8KPa (Hard) to 0.15KPa (Soft). We then plated DPSCs on these scaffolds for a period of 35 days and studied the effect of mechanical stiffness and chemical inducer on DPSC differentiation towards odontoblasts. It is well known that bone marrow mesenchymal stem cells when plated on a hard substrate (100 KPa) differentiate towards hard tissue formation. We were able to show that DPSCs could differentiate on scaffolds of very low range of moduli towards odontoblasts to regenerate dentin-like hard tissue. RT-PCR analysis recorded the upregulation of mineralization markers such as Osteocalcin (OCN), Alkaline Phosphatase (ALP) and Dentin Sialophosphoprotein (DSPP), which are required for odontogenic differentiation. Expression of these markers was also seen on non-induced substrates where the chemical inducer, Dex wasn't added. Non-induced hard gel (H-) had the maximum upregulation of the markers, indicating that the odontogenic differentiation can be simulated by the physiochemical environment of the hydrogel. There was abundant CaP biomineralization (SEM and EDAX) which increased from day 1 to day 35, indicating that the mineralized deposits clustered and grew in size. Trace of calcified deposits was also seen on the hydrogel without the cells. Hence, we were able to fabricate a hydrogel scaffold which had the ability to self- mineralize and also induce the DPSCs to differentiate into odontoblasts towards hard tissue formation. Lastly, we were also able to induce permanent differentiation where the cells on hard gel were able to maintain their differentiation when re-plated on a different substrate. They were said to be "educated". Our

results emphasize the importance of biochemical and biophysical stimuli required for differentiation and highlight the potential of our hydrogel as a scaffold for dentin-tissue engineering.

In chapter 2, we focused on the preparation and rheological properties of the physically crosslinked biopolymer composite hydrogels. Hectorite clay was used as a crosslinker to synthesize hyaluronic acid (HA)-clay/ gelatin-clay/ HA-gelatin-clay hydrogels. By varying the polymer:clay content, we produced both non-cell adhesive (HA-Clay) and cell adhesive (Gelatin/HA-gelatin-clay) hydrogels with varied stiffness ranging from 4-11KPa. The oscillatory shear stress sweep tests recorded the G' (storage modulus), Linear Viscoelastic Range (LVR) and the breaking/yield stress whereas, the frequency sweep traced the evolution of g' and G" (viscous modulus) over time. The rheological properties of the hydrogel scaffolds were related to the type of bonding, degree of crosslinking and mechanical structure of the hydrogels. Higher crosslinker content fabricated stiffer gels while using a long chain polymer (HA) resulted in a weaker gel. HA-gelatin-clay hydrogel where both long and short chain polymer chains were adsorbed on the clay surface had the highest range of stiffness. We successfully used the non-cell adhesive HA-clay hydrogels as a drug delivery vehicle for the time release of salicylic acid measured using UV-VIS spectrophotometer. The use of these scaffolds (HA/gelatin/HA-gelatin-clay) was also tested as cell growth substrates by looking at the fibroblasts adhesion, proliferation and migration. We found that our biopolymer-clay composite hydrogel system gave a soft, non-cytotoxic, cell compatible environment for the adult human dermal fibroblasts (AHDFs) where the cells could sense the substrate mechanics, as demonstrated by the SMFM.

In last part of my thesis (chapter 3-chapter 4), we study the response of deformable substrates on a macroscopic scale. We successfully applied a non-invasive imaging technique called DISC

(Digital Image Speckle Correlation) which, on a microscopic scale is used to track the surface deformations induced by cellular traction forces. Macroscopically, DISC can be used to analyze the stretch/contraction of muscular motion, by tracking the pores of the facial skin attached to the underlying muscles. In chapter 3, we applied DISC directly to clinical application by studying the impairment of underlying facial muscles caused by Botulinum toxin-A (BTX-A) injections. We conducted a pilot study of n=6 patients, whose glabellar and forehead complex was paralyzed by BTX-A. Using DISC, we were able to (a) determine the locus of facial muscular tension (b) identify the facial muscles that become impaired in a specific movement; (c) precisely quantify and monitor muscular paralysis and its subsequent return; (d) continuously correlate the appearance of wrinkles and muscular tension to measure treatment efficacy; and (e) corroborate objective data with existing rating scales (Subject Global Assessment and Facial Lines Outcome-11). Maximum paralysis (≥70%) was observed at two weeks, and the rate of recovery varied widely ranging from 2-5 months, with two patients continuing to exhibit reduced contraction at 24 weeks. Vector analysis of pre-treatment contraction correctly predicted injection site and illustrated lines of maximum tension.

In chapter 4, we apply DISC as a clinical tool to identify the muscle impairment caused by pathologies like vestibular schwannomas (VS). A vestibular schwannoma is a benign, usually slow-growing tumor that develops from the balance and hearing nerves supplying the inner ear. The tumor comes from an overproduction of Schwann cells--the cells that normally wrap around nerve fibers to help support and insulate nerves. Vestibular schwannomas influences the facial nerve motor function on a level often undetectable by the human eye during routine clinical examination. These subtle changes to facial nerve motor function may be elucidated through DISC. In a pilot clinical study of n=29 patients, we compare the quantitative facial nerve motor

function of patients with vestibular schwannomas who are untreated (n=13), treated with surgical resection (n=11), or treated with gamma knife radio surgery (n=5), to a control group of individuals (n=14) with no neurologic dysfunction. DISC analysis compared the patients "normal" functioning side of the face with the "affected side (with tumor)" and we revealed that there is almost a fivefold higher asymmetry in the percent area of muscle deformation of the untreated patients compared to the normal population. Over 70% untreated patients showed reduced motion on the opposite side of the tumor, indicating that the presence of vestibular schwannomas can be detected by an asymmetric muscle motion. Following surgery, either resection or gamma knife, 11 out of the 16 patients presented with reduced motion on the side of the tumor and increased motion on the opposing side. No correlation was found between the size of the tumor or the surgical method used to treat it and either the magnitude or the direction of the asymmetry. Hence, the technique of DISC provides a non-invasive method of monitoring the progression of the as well as post-surgical recovery of vestibular schwannomas.

# CHAPTER 1

# THE BEHAVIOR OF HUMAN DENTAL PULP STEM CELLS ON ENZYMATICALLY CROSSLINKED GELATIN HYDROGELS

## 1. INTRODUCTION

Teeth are hard organs that are susceptible to damage caused by mechanical trauma, chemicals, periodontal disease, caries and pulpitis disease and bacterial infections. Tooth loss can have ever-increasing social and economic impact, especially in the elderly [16]. Currently, damaged dental tissues are replaced by synthetic materials, such as titanium alloy, amalgam, composite resin, gutta percha and zirconia ceramic. However, such therapies are incapable of fully restoring the biological function of the lost tissue, thus reducing the mechanical properties and vitality of the teeth [17-19]. The advances in tissue engineering techniques present a prospect for the biologic regeneration of the damaged dental tissues. Similar to the construction of other tissues, dental tissue engineering also requires an appropriate cell source (DPSCs), a scaffold that can mimic the natural extracellular matrix (ECM) and bioactive molecules [20-22]. With the recent isolation of postnatal human dental pulp stem cells (DPSCs), they have become an attractive potential source for odontogenesis [23-26] since they are more ethically acceptable and easily obtained unlike embryonic stem cells. It has been shown previously that DPSCs can be induced by Dex to differentiate along an odontogenic lineage and induce mineralization in vitro [27] to form regular-shaped dentin pulp complex [28, 29]. However, steroids should be avoided as they can cause adverse side effects such as hyperglycemia and weakened immune system [30].

The selection of scaffold material is critical and is determined by the properties of the cell-scaffold interactions that affects cell proliferation, attachment and differentiation. The performance of a scaffold structure would benefit from mimicking the characteristics of natural ECM and allowing cells to influence their own microenvironment [4, 31]. Young et al. showed that DPSCs from third molar seeded onto polymer scaffolds and implanted into

rats, yielded recognizable dentin, odontoblasts, cementoblasts and enamel after 20-30 weeks [32]. Poly-glycolic acid (PGA), poly-L-lactic acid (PLA), or a copolymer of PGA and PLA (PLGA) have been used as scaffolding materials to regenerate dentin or dentin-pulp complexes [32-34]. Dex and bone morphogenetic protein (BMP-7) induced odontogenic differentiation has been observed on PLA scaffolds in vitro and in vivo after 8 weeks [17, 35]. In vitro and in vivo hard tissue formation on hydroxyapatite/tricalcium phosphate ceramic scaffolds (HA/TCP) and titanium scaffolds was also seen when DPSCs were induced by Dex [24, 36]. However, all these synthetic scaffold materials have certain disadvantages because of their acidic degradation products which around the tissue after in vivo implantation can cause severe inflammation [37]. The synthetic scaffolds also lack cell recognition signals. Yang et al. tried to overcome this problem by using a blend of electrospun poly (ε-caprolactone) and gelatin with hydroxyapatite (HA). They also induced DPSCs with Dex towards odontoblasts differentiation. Collagen type I (Col I) is the most abundant extracellular protein in dentin and has been used in 3-dimensional form or as a surface coating for primary and reparative dentin formation [38-40]. Gelatin also known as denatured collagen has also been used to successfully regenerate dentin-pulp complex but always as a blend in combination with other scaffolds such as PCL/nano HA [41] and chondroitin/hyaluronan [42]. Such blends still use synthetic polymers and may not be stable over long periods of time. Gelatin can also be chemically cross-linked to improve mechanical properties. However, this might pose potential problems of cytotoxicity owing to cross-linking agents such as formaldehyde or glutaraldehyde [43].

Therefore, the rationale of our current study is to investigate the in vitro differentiation of DPSCs into odontoblasts on enzymatically crosslinked gelatin hydrogels of variable stiffness without Dex induction. In this chapter, we focus on the differentiation of DPSCs with and without Dex on enzymatically crosslinked gelatin hydrogels of variable stiffness. We quantify the odontoblastic behavior of cells in vitro by means of RT-PCR and Alizarin Red staining and document the biomineralization by SEM and EDS. We hypothesize that our hydrogels are not only adequate to support DPSCs proliferation and differentiation leading to an early biomineralization, but they are also capable of self- mineralization. Furthermore, the biggest outcome of our study is the Dex independent nature of our DPSCs differentiation and biomineralization.

## 2. MATERIALS AND METHODS

### 2.1 *PREPARATION OF ENZYMATICALLY CROSSLINKED GELATIN HYDROGELS*

Hydrogels were formed by first dissolving gelatin (300-bloom, Porcine Type A, Sigma Aldrich, MO, USA) in DPBS (1X pH 7.4 GIBCO, Invitrogen Co., Carlsbad, CA, USA) at 70-80$^{o}$C at a gelatin concentration of 0.1g/ml (10%(w/v)) followed by sterile filtration through 0.22 µm SteriFlip (Millipore) media filters before thermally setting at room temperature for 24 h. These physically-crosslinked hydrogels are not permanent and are thermally reversible. Microbial transglutaminase (mTG) was used as a cross-linker at a stock concentration of 0.1g/ml (10 %( w/v)). Hard, medium and soft gelatin-mTG gels were made by mixing 1.125 mL, 1.442mL and 1.488 mL of a 10% gelatin solution in DPBS with 0.375 mL(3:1(v/v) gelatin:mTG), 0.058mL (25:1(v/v) gelatin:mTG) and 0.012 mL (125:1(v/v) gelatin:mTG) of a sterile filtered stock solution of mTG (10%, Ajinomoto LLC, NJ, USA) respectively, to obtain total of 1.5 mL hydrogel solution. Stock mTG solution was made by first dissolving mTG powder in DPBS and then sterile filtering through 0.22 µm Millex (Millipore) syringe filters. The crosslinking reaction took place in a cell culture incubator at 37$^{o}$C for 24hrs. After 24hr, the hydrogels were heated at 65$^{o}$C for 5-7 minutes to deactivate mTG. The hydrogels were made in 6 well/ 12 well/ 35mm TCP (BD Biosciences, Franklin Lakes, NJ) depending on the assay to be carried out.

### *2.2 DYNAMIC RHEOLOGICAL CHARACTERIZATION*

Oscillatory shear rheometry tests were carried out on the gelatin-mTG hydrogels with rotational rheometer (Bohlin HR Nano, Malvern Instruments Ltd., Germany) using a standard steel parallel- plate geometry of 20mm diameter. During each test method, all 35 mm TCPS containing the hydrogels were fixed to the bottom plate with a double-sided tape. The top plate was then lowered to a gap of 1mm from the bottom of the 35mm TCPS. The stress sweep was done by holding the temperature (37$^{o}$C) and frequency (1 Hz) constant while increasing the shear stress from 1 to 5000 Pa. In the oscillatory stress sweep (or "controlled stress") tests, the stress was locally controlled in every cycle and the strain (and the corresponding G') was measured. The stress sweeps measures G' (storage/elastic modulus; index of stiffness) information on the structural behavior of the crosslinked network, the linear viscoelastic region (LVR) profiles and

its limit ("yield point" or "breaking stress") for all hydrogels by shearing them until the structure broke down. All samples were tested in triplicates.

### *2.3 CELL CULTURE AND CELL SEEDING*

Human DPSCs were obtained from the Department of Oral Biology and Pathology, School of Dental Medicine, Stony Brook University, NY, USA. The $3^{rd}$-$6^{th}$ passage DPSCs were cultured in alpha Minimal essential medium (α-MEM) (Catalog # 12571, GIBCO, Invitrogen, Carlsbad, CA, USA) supplemented with 10% fetal bovine serum (FBS) (GIBCO, Invitrogen) and 1% penicillin–streptomycin (GICO, Invitrogen) in a humidified incubator at $37^{o}$C with 5% CO2. The medium was changed every 2 days. The DPSCs monolayers were grown in tissue culture polystyrene (TCPS) dishes to nearly 80% confluence, harvested after treatment with 0.05% trypsin-EDTA (GIBCO, Invitrogen) solution, then centrifuged to obtain a pellet and finally re-suspended in α-MEM containing 10% FBS, 1% Pen-Strep, 10mM β-glycerol phosphate (Sigma Aldrich), 200μM L-ascorbic acid 2-phosphate (Sigma Aldrich) also known as the "base / non-induced media" for use in functional assays. 1500cells/$cm^2$ DPSCs were seeded onto crosslinked gelatin-mTG scaffolds, TCPS (control), mTG coated TCPS and gelatin coated TCPS in a 6 well TCP. Half of the samples were incubated at $37^{o}$C with 5% CO2 and cultured with the "base/ non-induced media" and the other half with the "induced media" (base media containing $10^{-8}$M Dex (Sigma Aldrich)) till 35 days. Hard gelatin-mTG hydrogel was also incubated with induced and non-induced media without DPSCs for a period for 35 days. Culture medium was refreshed every alternate day.

### *2.4 SHEAR MODULATION FORCE MICROSCOPY (SMFM)*

Cell stiffness was measured on the cross-linked hydrogels after day 1, 3and 7 of incubation in induced and non-induced media using an atomic force microscope (AFM, Dimension 3000; Digital Instruments, Co., Ltd. Santa Barbara, CA). AFM was operated in shear modulation force microscopy (SMFM) mode [44] using a silicon nitride tip on a cantilever with a bending spring constant of 0.06 N/m. During the measurement, a force of ~ 25nN was exerted by the cantilever on the cell's perinuclear region and a sinusoidal drive signal (1400Hz) was applied to the x-piezo controlling cantilever, inducing a small oscillatory motion of the tip parallel to the cell surface. When the drive signal amplitude was varied from 7.5mV up to 125mV, which corresponds to an

x-piezo displacement of 1.5–25nm, the cantilever response was recorded to estimate the stiffness of the cell surface [45]. The AFM set-up was calibrated such that a greater response amplitude indicated a more compliant surface and vice versa. The drive frequency of 1400Hz was chosen for the measurements since it lies in the flattest region of the cantilever's response curve. A total of nine experimental points (three points per cell and three cells per sample) were obtained for each hydrogel condition.

### *2.5 SCANNING ELECTRON MICROSCOPY (SEM)*

On day 1, 3, 7, 14, 21 and 35 after cell seeding, the hard and soft hydrogel were washed in DI water twice. The samples were cut into half and scooped out of the 6 well plates and placed on a piece of Si wafer to be left for air-drying at room temperature till they got dehydrated and shrunk. The specimens were sputtered with gold and examined with a LEO/Zeiss 1550 field emission SEM (Minnesota, USA) at 20KeV accelerating voltage using Robinson type backscattering electron detectors. The elemental contents on the surface of the scaffolds were measured by energy dispersive X-ray microanalysis (EDX) (Phoenix XEDS system). Hard hydrogel without cells was also examined the same way. mTG and gelatin coated TCPS were also evaluated after 21 days of incubation as controls.

### *2.6 CONFOCAL LASER SCANNING MICROSCOPY*

To determine actin cytoskeleton organization and the morphology, the cells were fixed with 3.7% (w/v) formaldehyde, permeabilized with a mild detergent (0.4% Triton, Sigma), stained for actin with Alexa Fluor-488 Phalloidin (Molecular Probes, Eugene, OR) with Propium Iodide (Molecular Probes, Eugene, OR) for the nucleus. The hard and soft gelatin-mTG samples were then imaged using a Leica TCS SP2 laser scanning confocal microscope (Leica microsystem Inc., Bannockburn, IL) after 21 days of incubation.

### *2.7 RT-PCR*

On day 1, 7, 14, 21 and 35 after cell seeding, the cross-linked hydrogels were washed with DPBS and then cell layer was extracted using 3mg/ml of collagenase type I (230u/mg, Worthington Biochemicals Corp., Lakewood, NJ). 1ml of collagenase was added to each

hydrogel sample followed by 1 hr. incubation at 37$^{o}$C. This was followed by another10min incubation at 37$^{o}$C in 0.05% trypsin –EDTA and centrifugation in non-induced media. The total RNA was extracted from hard and soft gelatin-mTG hydrogel and TCPS control using Qiagen RNEasy kit (RNEasy kit, Qiagen, Valencia, CA). 1µg of total RNA was reverse-transcribed using Superscript II Reverse Transcriptase (Invitrogen) into cDNA using Random Primers (Invitrogen). The obtained cDNA was used as a template in PCR. The odontogenic differentiation of cells was monitored by specific markers for- osteocalcin (OC), bone sialoprotein (BSP), dentin Sialophosphoprotein (DSPP) and alkaline phosphatase (ALP). The sequences of the specific primer sets are listed below: *ALP* (sense: 5'-ACGTGGCTAAGAATGTCATC-3'; antisense: 5'-CTGGTAGGCGATGTCCTTA-3');*dentinsialophosphoprotein* (DSPP) (sense: 5'- AATGGGACTAAGGAAGCTG-3'; antisense: 5'-AAGAAG CATCTCCTCGGC-3'); *osteocalcin* (OCN) (sense 5'-CATGAGAGCCCTCACA-3'; antisense 5'-AGAGCGACACCCTAGAC-3'); 18s (sense: 5'-AACCCGTTGAACCCCATT-3'; anti-sense: 5'-CCATCCAATCGGTAGTAGCG-3'). 18s was used as a housekeeping gene to normalize mRNA expression. Real-time PCR was performed using SYBR Green PCR kit (Qiagen, Valencia, CA) and controlled in a DNA engine Opticon 2 thermal Cycler with continuous fluorescence detection (MJ Research Incorporation, Union, NJ). DNA amplifications were performed under the following conditions: 95 $^{o}$C (15min), 94$^{o}$C (30 s), 55$^{o}$C (30 s), and 72 $^{o}$ C (30 s) for 40 cycles, with a final 10 min extension followed by data collection (Opticon Monitor 3analysis software, MJ Geneworks, Bio-Rad Laboratories Inc.). Each sample was assessed in triplicate. All mRNA expression was absolute and shown in units of Atta mole/20ng RNA. This work was done in collaboration with Aneel Bherwani at the School of Dental Medicine.

### *2.8 ALIZARIN RED STAINING*

After 35 days of incubation, the hydrogel constructs (both with and without cells) were rinsed twice with DPBS and then fixed with 10% (w/v) formalin for 1 day, washed with PBS and stained with 1mg/ml (0.1%w/v) alizarin red stain (Sigma Aldrich) for 30 sec. Stained samples were then washed with DI water 4 times, each wash being 1 min long. Pictures were taken using an optical microscope (CK40, Olympus).

### *2.9 EDUCATION*

"Education" is defined as the maintenance of differentiation markers including OCN/ALP/DSPP. To investigate if the DPSCs differentiation was long term, after 21 days of incubation, the cell layer was extracted from the cross-linked hydrogels with collagenase and trypsin using the procedure mentioned in RT-PCR section. The extracted cell layer was suspended in non-induced media for the non-induced samples and induced media for the induced hydrogel samples. This layer was broken down by pipetting to get a homogenous cell suspension. 1563cells/$cm^2$ was seeded on 6 well TCPS plates. Half of the samples were cultured in non-induced base media and other half in induced media for 21 days. SEM, EDAX analysis and RT-PCR were carried out after 21 days of incubation on all samples.

## 3. RESULTS

### *3.1 RHEOLOGICAL CHARACTERIZATION OF GELATIN-MTG HYDROGELS*

Logarithmic plot of G' and shear stress (FIGURE 1-1) represents the storage/elastic modulus, LVR profile and the breaking stress of the 24-h cured hydrogels with variable mTG concentration. FIGURE 1-1 clearly shows that the hard hydrogel has maximum stiffness of 8KPa followed by medium gel with 2KPa stiffness and soft gel with 0.15KPa stiffness. A typical stress sweep graph shows that at low stress amplitudes, G' maintains a constant linear plateau region (or, LVR) indicating the structural stability under those conditions. FIGURE 1-1 shows that the LVR is between 1-900 Pa, 1-1200 Pa and 1-1300 Pa for hard, medium and soft hydrogels. On increasing the stress amplitudes further, the bonds of the gel are stretched to maximum so as to reach the limiting value of the LVR. Beyond this limiting stress amplitude (or, breaking stress/yield point), G' begins to deviate noticeably from the LVR plateau indicating the irreversible structural change. The breaking stress documented for hard hydrogel is the least (0.8KPa), increasing as the stiffness decreases (medium gel: 1.1KPa, soft gel: 1.25KPa).

### *3.2 CELL STIFFNESS*

AFM, operated in the SMFM mode, was used for in situ measurement of AHDF modulus (an index of stiffness) after 1, 3 and 7 day of incubation. During our measurement, two simultaneous forces were exerted on the cells; first, a sinusoidal drive signal applied to the x-piezo that induced a small oscillatory motion on the cell surface, and second, a normal force of~ 2nN to maintain tip contact with the cell surface. The normal indenting force was applied to the perinuclear region between the cell nucleus and cytoplasmic edge to ensure reproducibility of the stiffness measurement. The lateral deflection (response) amplitude of the cantilever was measured and plotted against drive amplitude, with the response amplitude found to be proportional to drive amplitude, indicating that there was no slip during the cell-tip contact. Assuming a Hertzian model for this SMFM set-up, the response amplitude has been previously shown to be inversely proportional to 2/3 power of the lateral modulus of the specimen [46]. Using this calibration, we found that cell stiffness increased more than 2-fold over 7 days of incubation (FIGURE 1-1B). Cell stiffness was sensitive to substrate mechanics (FIGURE 1-1B), where an increase in cell stiffness was seen on the non-induced hard gel-mTG hydrogel (modulus of 8kPa) compared to soft hydrogel (modulus 0.15kPa) which documented lower cell stiffness. Similar kind of substrate dependent cell stiffness was seen Ghosh et al.[47]. In the induced gel-mTG samples, the hard and soft hydrogel recorded almost equivalent response in cell stiffness. No distinct correlation was seen between cell stiffness and the medium hydrogel modulus (2kPa) and a similar trend was seen on day 1, 3 and 7 (FIGURE 1-1). The cell stiffness was also found to be independent of Dex corresponding to a particular hydrogel on a particular day of incubation. This may be because the difference between the moduli of soft and medium hydrogel is not too large. Hard (8kPa) and soft (0.15kPa) hydrogel represent two extreme moduli where a correlation in cell stiffness response can be seen, hence, for further experiments we would consider only hard and soft hydrogels.

## *3.3 BIOMINERALIZATION OF THE ECM*

### *3.3.1 IN PRESENCE OF DPSCS*

SEM was used to analyze the presence of mineralized deposits on hard and soft gelatin-mTG hydrogels on day 1, 7, 14, 21 and 35. FIGURE 1-2 (panel a-e) show white mineralized deposits present on the induced hard hydrogel surface. The amounts of deposits were seen to be increasing with the increase in the number of incubation days. By day 35, most of the deposits

have formed clusters and they appear to cover the entire surface of the hydrogel. Morphology of the clusters appears to be similar on all days of incubation. FIGURE 1-2 (panel f-j) shows the corresponding EDAX spectra for the mineralized deposits from day 1-35 of incubation which indicates the presence of CaP mineral and formation of a hard tissue. This type of mineralized deposits in the Dex induced samples is consistent with past literature [48] where it was found that Dex promotes mineral nodule formation. FIGURE 1- 3 (panel a-j), FIGURE 1- 4 (panel a-j) and FIGURE 1- 5 (panel a-j) also display the SEM imaged mineralized deposits EDAX spectra for CaP in non-induced hard gel, induced soft gel and non-induced soft gel respectively.

Although, the amount of bio mineralized deposits was difficult to quantify, it was found to be present *without Dex* and was independent of *hydrogel stiffness.* Biomineralization appeared to increase in amount with the increasing incubation time. It was noteworthy to see that the biomineralization began as early as 1 day after cell seeding and without a chemical inducer (Dex).

### *3.3.2 IN ABSENCE OF DPSC'S*

FIGURE 1- 6 (panel a-e) shows the SEM images of the non-induced hard hydrogel without DPSCs on day 1, 7, 14, 21 and 35. Day1 (FIGURE 1- 6a) shows very few mineralized deposits on the hydrogel surface. These mineralized deposits increase gradually in amount and size as the incubation time increases. Compared to the SEM images of the non-induced hard hydrogel with DPSCs, the amount of these deposits on the same gel without cells is *very less*. Also, by day 35, clusters of mineralized deposits weren't found and they didn't cover the surface entirely as seen before in gels with DPSCs under the same conditions. FIGURE 1- 6 (panel f-j) depicts the EDAX spectra for the corresponding SEM images (panel a-e). EDAX spectra showed the evidence of calcification by indicating CaP peaks for the mineralized deposits present. Our results showed that the crosslinked hydrogel was capable of self -mineralization on a small scale but this biomineralization was rapidly enhanced when DPSCs were seeded onto the crosslinked gel.

### *3.3.3 GELATIN AND MTG ALONE CANNOT TRIGGER BIOMINERALIZATION*

It was important to see the effect of uncross-linked gelatin and mTG as promoters of biomineralization. So, after 21 days of incubation, SEM and EDAX were used to analyze the presence of any mineralized deposits. FIGURE 1- 7 (panel a-d) show the SEM images of the

induced and non-induced gelatin and mTG coated TCPS with DPSCs. FIGURE 1- 7(a) and FIGURE 1- 7(c) show a couple of white deposits on the surface of induced mTG and gelatin coated TCPS. Corresponding EDAX spectra (FIGURE 1- 7(e), FIGURE 1- 7(g)) for these SEM images show a low signal of CaP. This might be due to the DPSC induction by Dex. FIGURE 1- 7(b) and FIGURE 1- 7(d) also show one or two white deposits on the non-induced gelatin and mTG coated TCPS but the corresponding EDAX spectra (FIGURE 1- 7(f), FIGURE 1- 7 (h)) does not show any CaP peak indicating the absence of any calcification. These images indicate that gelatin and mTG alone without any chemical inducer (Dex) cannot promote biomineralization and their crosslinking is important to produce that effect of biomineralization.

### *3.4 ECM MINERALIZATION OF DPSCS ON CROSSLINKED HYDROGELS*

SEM and EDAX indicated that the crosslinked gels showed enhanced biomineralization in presence of DPSCs. We wanted to see the pattern of this biomineralization, therefore, alizarin red (AZ) stain was performed on the crosslinked hydrogels with and without DPSCs after 35 days of incubation. Via alizarin red staining, we observed remarkable differences in the ECM mineralization in crosslinked hydrogels with DPSCs and without DPSCs (FIGURE 1- 8 (a)-(h)). There was no distinction between hard and soft hydrogel and both induced (FIGURE 1- 8 (a-b)) and non-induced (FIGURE 1- 8 (e-f)) hard and soft crosslinked hydrogel showed distinct patterns of Ca deposits in presence of DPSCs. The samples without DPSCs (controls) (FIGURE 1- 8 (c-d, g-h)) did not show any distinct patterns of Calcified deposits. No effect of induction was clearly seen as the calcification patterns were also present in the non-induced samples. These results further confirm the role of DPSCs in the biomineralization.

### *3.5 CELL MORPHOLOGY*

After 21 days of confluence, confocal laser scanning microscopy was applied to visualize the cells on the crosslinked hydrogel surface to know the effect of Dex and hydrogel stiffness on the cells in a bio mineralizing environment. The results shown in FIGURE 1- 9(a-d) display the morphology of DPSCs seeded on hard and soft gelatin-mTG gel after 21 days. At a 63x magnification, the cells mostly appeared fibroblast-like. The actin filaments were well developed stress fibers and cells looked healthy. There was no visible change seen in the morphology of the

cells on the hard or soft / induced or non-induced hydrogel surfaces emphasizing even more that Dex is not required for DPSCs on these surfaces.

### *3.6 EXPRESSION OF DIFFERENTIATION MARKERS (RT-PCR)*

Expression levels of mRNA for OCN, BSP, ALP and DSPP from DPSCs seeded on induced and non-induced hard and soft gelatin-mTG gels and TCP were compared on day 1, 7, 14, 21 and 35 to investigate the Odontogenic differentiation. As shown in FIGURE 1- 10a, there is an upregulation of OCN post 21 days of incubation on all the crosslinked hydrogels. On day 35, we notice a down regulation of OCN on all the hard and soft crosslinked hydrogels. The upregulation also seems to be independent of Dex as non-induced hard gel had the highest OCN expression. There was no distinct dependence seen on the stiffness of the hydrogel as well since in induced samples, hard gel had lower expression than the soft whereas, in the non-induced samples, soft gel had lower expression than the hard gel. It is interesting to see that at 21 day of incubation, the cells expressed six-nine fold more OCN on the induced crosslinked gels than the TCP (+) control. On the non-induced crosslinked hydrogels, this difference is 11-16 folds higher than the TCP (-) control. There was no significant change in the mRNA expression of BSP (FIGURE 1- 10b) and overall mRNA expression of BSP was very low (FIGURE 1- 10b) on all the surfaces. Huge error bars were recorded due to very low levels of BSP. Low expression of BSP indicates that the differentiation is not osteoblastic but more towards odontogenic.

Expression of ALP (FIGURE 1- 10c) increases increased over time on all the surfaces showing the highest expression levels on day 35 of incubation. Cells had overall higher ALP activity on the crosslinked gels compared to the control (TCP). Dex increases the mRNA expression of ALP on all the samples which is consistent with the literature [49, 50]. However, in crosslinked hydrogels, the ALP activity seems to be independent of Dex as non-induced hard gel recorded the highest ALP expression. Without Dex, the crosslinked hydrogels had threefold higher ALP expression than control. Both non-induced and induced hard hydrogels had slightly higher ALP expression than soft gels. The DSPP expression (FIGURE 1- 10d) also increased with incubation time, indicating the highest expression on day 35 of incubation on all the crosslinked hydrogel samples. Non-induced hard and soft gels had slightly higher DSPP expression than their induced counterparts showing that Dex wasn't required for the odontogenic differentiation. Induced crosslinked hydrogels had fourfold higher DSPP expression than the induced control (TCP+)

whereas; the non-induced crosslinked hydrogels had fivefold higher expression than the non-induced control (TCP-). Higher DSPP expression in contrast to lower BSP and OCN expression on day 35 of incubation clearly shows that the DPSCs are differentiating towards odontogenic lineage.

### *3.5 LONG TERM DIFFERENTIATION*

After 21 days of differentiation, the cells were removed from the induced and non-induced hard and soft gels and were re-plated on the TCP and incubated for 21days in ± dex.

#### *3.5.1 MINERALIZATION AFTER 21 DAYS OF INCUBATION*

FIGURE 1- 11 (panel a-d) shows the SEM images of the cells that were re-plated on TCP and fed with induced media. H+ (+)/S+ (+) denotes that the cells were removed from induced hard/ soft gel re-plated on TCP in an induced medium. H-(+)/ S- (+) denotes that the cells were removed from non-induced hard /soft gel and re-plated on TCP in an induced medium. FIGURE 1- 11 (panel e-h) shows the corresponding EDAX spectra for H+(+)/H-(+)/ S+(+)/S-(+). SEM images depict the mineralized deposits present on these surfaces in the induced media. The morphology of the clusters appears to be similar on all the surfaces. However, S+ (+) and S- (-) have less amount of mineralized deposits than H+ (+) and H- (-). Corresponding EDAX spectra shows the CaP peaks indicating that the mineralized deposits are hydroxyapatite. FIGURE 1- 12 (panel a-h) shows the SEM images and the corresponding EDAX spectra of the cells that were re-plated on TCP and fed with non-induced media (H+(-)/H-(-)/ S+(-)/S-(-)). All surfaces show same morphology of the mineralized deposits. However, H+ (-) and H- (-) show the presence of more mineralized deposits than S+ (-) and S- (-), indicated that the hard gels were more calcified than the soft gels. An EDAX spectrum (panel e-h) corresponding to those SEM images, indicates the presence of Ca P in the mineralized deposits.

#### *3.5.2 EXPRESSION OF DIFFERENTIATION MARKERS*

FIGURE 1- 13 shows the mRNA expression of OCN on H+/H-/S+/S-(+) and H+/H-/S+/S-(-) after 21 days of incubation and compares it to the mRNA OCN expression on TCP (+) and TCP (-). The figure shows that the cells expressed higher levels of OCN than TCP control. Cells extracted from H + expressed almost eightfold higher OCN than TCP in the induced medium whereas H-

/S +/ S- had almost fourfold higher OCN expression than TCP (+). In the non-induced medium, cells extracted from H+ expressed almost thirteen fold higher OCN expression than TCP(-). Cells extracted from H-, S+ and S- also had almost nine fold, six fold and twofold higher OCN expression than TCP (-) respectively. All these results indicate that the cells grown on hydrogels maintained differentiation when plated on TCP and those grown on H+/H- compared to S+/S-, expressed more OCN, ALP following growth in TCP, both in the induced and non-induced medium. This may be due to difference in the population or difference in the expression.

In the induced media, the ALP mRNA expression (FIGURE 1- 13b) of cells extracted from H+ and H- is almost six fold and fourfold higher than ALP expression of cells on TCP+ respectively. In the non-induced media also, cells extracted from H+/H- had almost six fold higher expressions than cells on TCP- In non-induced and induced media both, cells extracted from S+/S- had 1.5 fold higher ALP expressions than cells on TCP+ and TCP-. This also shows cells extracted from hard gels remain educated even when plated on a different surface and without Dex.

DSPP mRNA expression (FIGURE 1- 13c) of cells extracted from both H- and S- had fourfold higher expression than cells on TCP in the induced media. Cells extracted from H+ had three fold higher DSPP expressions than TCP+, while the DSPP expression of S+ and TCP+ was the same in the induced media, indicating that hard gel was more educated than soft. In the non-induced media, the cells extracted from S+ and S- documented almost threefold higher DSPP expression than the control TCP- . However, the cells extracted from H+ and H- showed fivefold and sevenfold higher DSPP expression than control TCP-. This also shows that the cells extracted from hard gels were more educated and were better able to retain the memory of prior differentiation and differentiate further after being plated on TCP.

## 4. DISCUSSION

Regeneration of pulp tissue essentially requires a proper scaffold which can support cell adhesion, proliferation, migration, differentiation and mimic the natural ECM environment to promote tissue regeneration. Traditional materials used to restore the damaged pulp are unable to restore the normal function and structure of the dental tissue exposed to harmful stimuli [51].

Various hydroxyapatite based scaffolds despite of having good biocompatibility and osteoconductivity, have also had limitations including brittleness [23, 29, 36, 52]. Collagen and

chemically or UV crosslinked gelatin scaffolds have also been used widely as a naturally derived scaffold for regenerating pulp [39, 40, 53]. Many studies have shown that collagen had an unstable healing effect and an insufficient regeneration of dentin-like tissue [54, 55]. Chemically crosslinked gelatin can have potential cytotoxic effects and UV crosslinked gelatin scaffolds failed to express DSPP, an important marker for pulp regeneration [53]. The aim of our study was to investigate the efficacy of enzymatically crosslinked gelatin hydrogel for the regeneration of dentin-like hard tissue. Enzymatically crosslinked gelatin is stable, biocompatible, and biodegradable, has improved tunable mechanical properties, can be easily fabricated without any harmful chemicals, and promotes cell adhesion, proliferation and migration. Most importantly, it presents with no cytotoxic effects on the cells which makes it as a potential scaffold for tissue regeneration. This was confirmed by our in vitro studies where DPSCs grew very well for a period of 35 days, differentiated along odontogenic lineage and biomineralized to produce dentin-like hard substance.

SEM images showed the formation of calcified deposits on both hard and soft substrates and EDAX spectra indicated the presence of Ca P in those mineralized deposits. Mineralization which is a key goal of dentin regeneration was seen as early as day 1 of incubation and it increased with the increase in the incubation time. The mineralized deposits seen grew in size, formed clusters and covered the entire gel surface by day 35. The odontogenic differentiation of DPSCs was confirmed by the RT-PCR analysis which showed a higher mRNA expression of DSPP on the crosslinked hydrogels (more in hard than soft) at day 35 compared to the TCP control. DSPP is used as a specific marker of odontoblast differentiation. It is highly expressed by odontoblasts and is essential for dentinogenesis [56, 57]. DSPP is the initial translational product of DSPP mRNA which is then cleaved to dentin sialoprotein (DSP) and dentin phosphoprotein (DPP) [56]. Both DSP and DPP play important roles in the ECM mineralization and dentinogenesis. DSPP mRNA is upregulated in a time-dependent manner when DPSCs are cultured in the induction medium containing glycerophosphate, ascorbate-2-phosphate, and Dex [58]. ALP is usually regarded as an early marker of hard tissue formation or odontogenic differentiation and is required for deposition of minerals in tooth and bone. OCN, a vitamin K-dependent non-collagenous ECM protein is also used as a late marker of osteogenic differentiation but it plays an important role in dentin regeneration and therefore, it’s used as a confirmation marker for odontogenesis. BSP is an extremely specific marker for bone and is

produced in very small amounts in dentin but in large amounts during bone formation. Our results showed an upregulation of osteocalcin by day 21 on all crosslinked hydrogels (more on hard, less on soft) and a down regulation by day 35of incubation. BSP was expressed in extremely low amounts whereas; ALP was upregulated on all crosslinked hydrogels by day 35. Downregulation of OCN (FIGURE 1- 10a), very low expression of BSP (FIGURE 1- 10b), upregulation of DSPP (FIGURE 1- 10c) and ALP (FIGURE 1- 10d) by day 35 are all indicative of odontoblast differentiation.

It was interesting to note that the cells differentiated along odontogenic lineage and that DSPP was upregulated on the crosslinked gels even in the absence of Dex, a chemical inducer normally required for DPSCs to differentiate in vitro into odontoblasts [27]. In fact, OCN, ALP and DSPP were up regulated the most on the H- gel. Non-induced soft gel (S-) also showed a high expression of these genes. Dex has been considered as an important inductive factor for stimulation of DPSCs into odontoblasts [27] which has been used in culture compositions for various scaffolds and explant DPSCs cultures [17, 23, 36, 41, 52, 53, 59]. In this study, we have shown that DPSCs can differentiate into odontoblasts even without Dex, producing abundant bio-mineralized CaP deposits and upregulating OCN, ALP and DSPP. The reason of this differentiation is the interaction of DPSCs with the gelatin-mTG crosslinked gel. Non-induced hard gel (H-) showed higher OCN, ALP and DSPP expression than soft (S-) gel, indicating that the crosslinked gel gives the required mechanical and biochemical stimuli to the DPSCs for odontogenic differentiation, thus, completely avoiding the use of Dex. SEM and EDAX results of the hard gel without DPSCs and without any culture media on day 0 shows no biomineralization at all (FIGURE 1- 14). However, when incubated in the non-induced culture medium without DPSCs, the hard gel (H-) starts showing trace amounts of CaP mineralization (FIGURE 1- 6) progressing from day 1 to day 35. This mineralization was also seen in gels with variable gelatin (fixed mTG) concentrations which had been cultured for 2 days in non-induced media without DPSCs (FIGURE 1- 15(panel a-j). This indicates that the crosslinking of gelatin mTG is unique in nature to provide the crucial binding sites for the adsorption of proteins or minerals required for odontogenic differentiation and biomineralization. The enzymatic crosslinking produces a change in the structure of gelatin such that spontaneous biomineralization can be seen when incubated in the base culture media. This bio-mineralization gets enhanced further when the DPSCs come in contact with the hydrogel surface. This

phenomenon has not been seen before and cannot occur by using gelatin or mTG independently (FIGURE 1- 7). This further highlights the application of this hydrogel scaffold for in-vivo for regeneration of dentin-pulp complex. Our hydrogel scaffold also overcomes the limitations of previous based scaffolds where there was very low expression of DSPP during the 21 days of incubation [53].

Finally, once the DPSCs were differentiated on these gelatin-mTG scaffolds, they were able to retain their odontogenic phenotype and continued to differentiate into odontoblasts when re-plated on a different substrate (TCP). SEM and EDAX results showed the formation of mineralized CaP deposits both in induced and non-induced culture medium (FIGURE 1- 11, FIGURE 1- 12). Hard gels irrespective of Dex were more "educated" than the soft gels. Their differentiation was more long term as cells had upregulation of OCN, ALP and DSPP (FIGURE 1- 13(a-c)).

## 5. CONCLUSION

In this study, we investigated the reaction of DPSCs on hard and soft enzymatically crosslinked gelatin gels towards odontogenesis. We found that gelatin-mTG hydrogel supported the attachment, growth and odontogenic differentiation of DPSCs and formation of dentin-like mineralized tissue, demonstrating its potential for dental tissue regeneration. The odontogenic differentiation and abundant biomineralization was achieved without Dex. The crosslinking scaffold itself played an important role by not only self-mineralizing but also promoting enhanced biomineralization with DPSCs. Moreover, the cells retained the odontogenic lineage and continued to differentiate into odontoblasts on a different substrate, indicating the presence of long term differentiation.

## 6. FIGURES

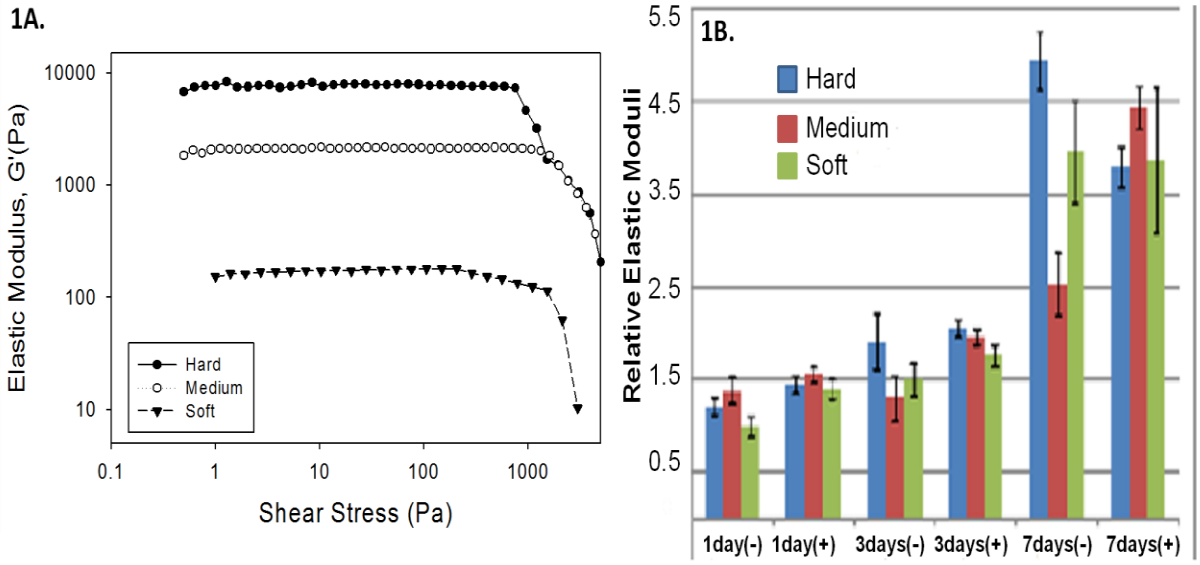


FIGURE 1-1: OSCILLATORY SHEAR STRESS SHOWING THE STIFFNESS OF HARD, MEDIUM AND SOFT HYDROGEL (B) CELL STIFFNESS FROM DAY 1 TO DAY 7 IN INDUCED AND NON-INDUCED HARD AND SOFT HYDROGELS.

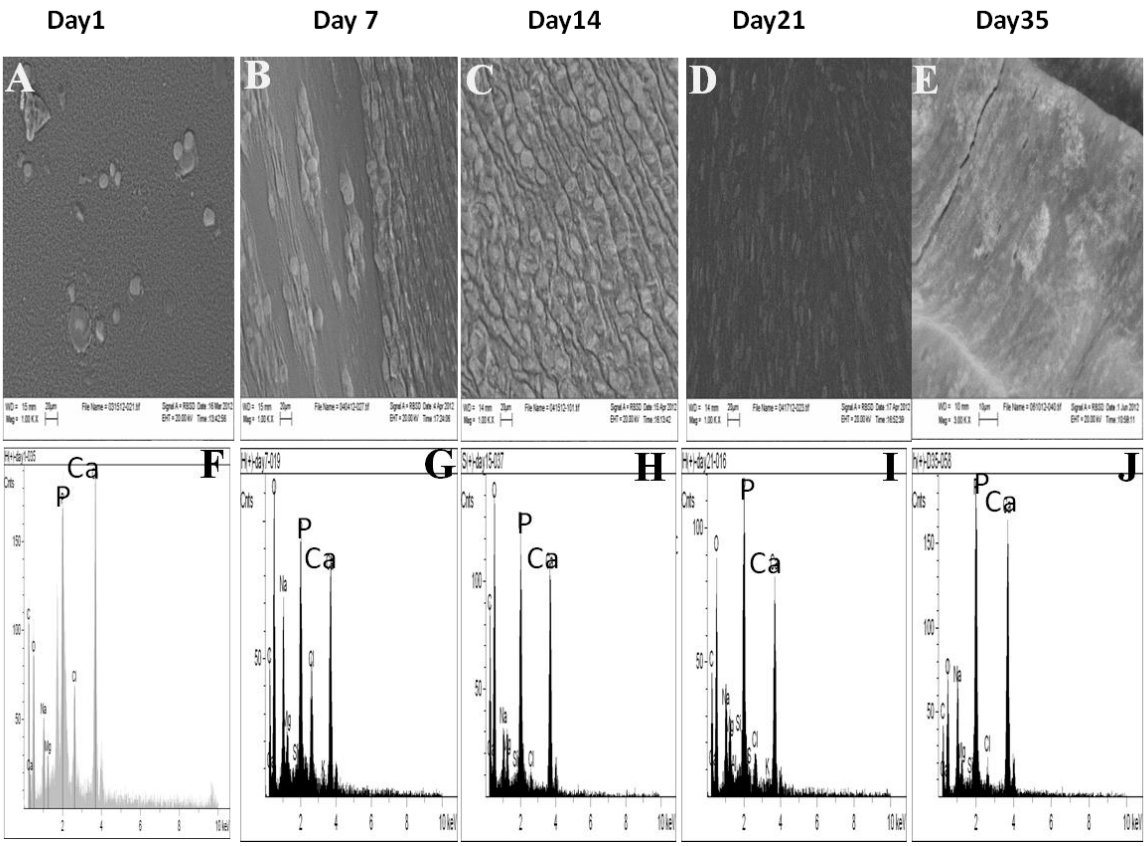


FIGURE 1-2: SEM MICROGRAPHS OF INDUCED HARD GEL (H+) WITH DPSCS, SHOWING BIOMINERALIZED DEPOSITS ON (A) DAY1 (B) DAY 7 (C) DAY 14 (D) DAY 21 (E) DAY 35. EDAX SPECTRA SHOWING PEAKS FOR CALCIUM PHOSPHATE ON (F) DAY 1 (G) DAY 7 (H) DAY 14 (I) DAY 21 (J) DAY 35. MAGNIFICATION= 1KX; SCALE= 20µM

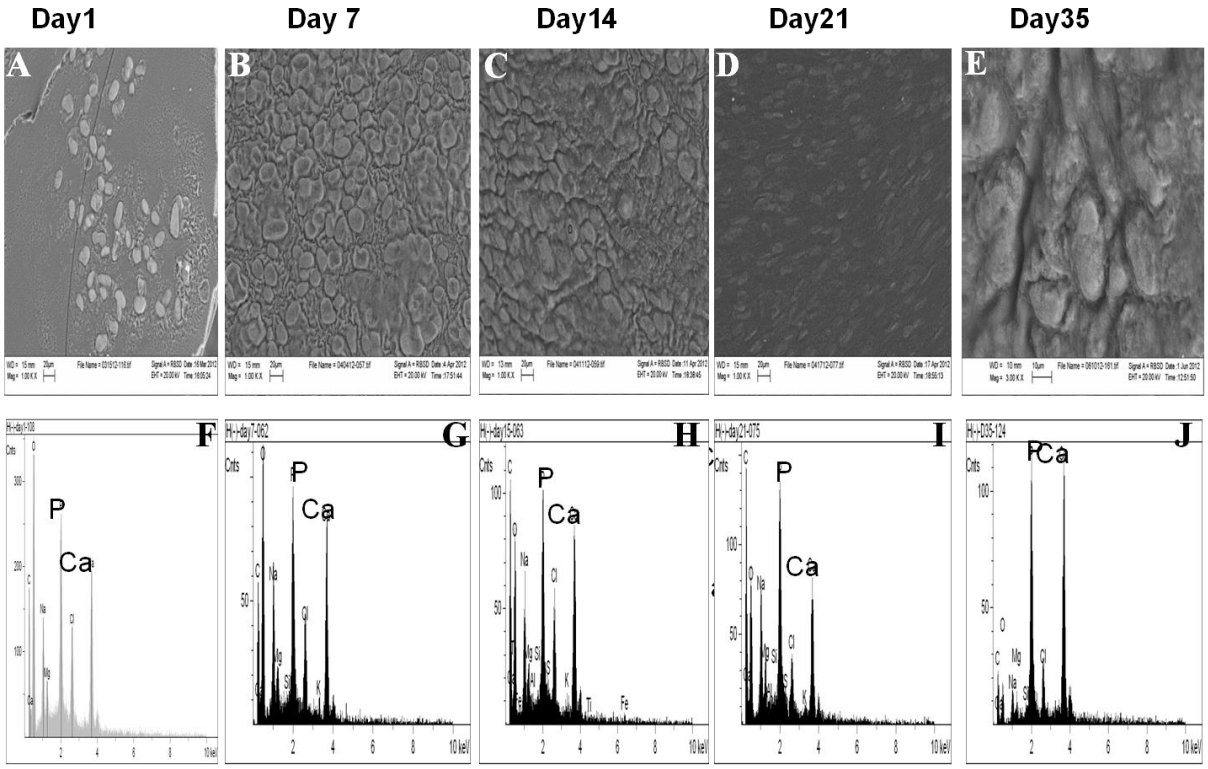


FIGURE 1- 3: SEM MICROGRAPHS OF NON-INDUCED HARD GEL (H-) WITH DPSCS, SHOWING BIOMINERALIZED DEPOSITS ON (A) DAY1 (B) DAY 7 (C) DAY 14 (D) DAY 21 (E) DAY 35. EDAX SPECTRA SHOWING PEAKS OF CALCIUM PHOSPHATE ON (F) DAY 1 (G) DAY 7 (H) DAY 14 (I) DAY 21 AND (J) DAY 35. MAGNIFICATION= 1KX; SCALE= 20µM

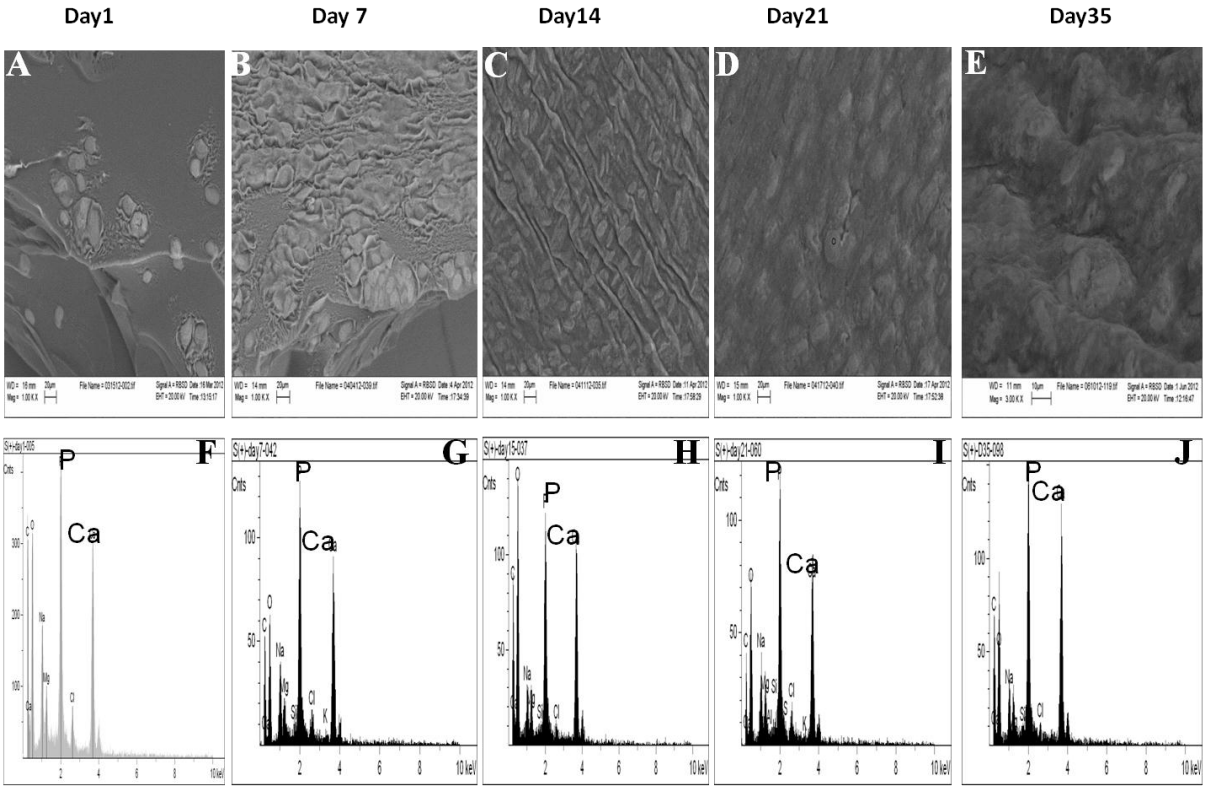


FIGURE 1- 4: SEM MICROGRAPHS OF INDUCED SOFT GEL (S+) WITH DPSCS, SHOWING BIOMINERALIZED DEPOSITS ON (A) DAY1 (B) DAY 7 (C) DAY 14 (D) DAY 21 (E) DAY 35. EDAX SPECTRA SHOWING PEAKS OF CALCIUM PHOSPHATE ON (F) DAY 1 (G) DAY 7 (H) DAY 14 (I) DAY 21 (J) DAY 35. MAGNIFICATION= 1KX; SCALE= 20µM

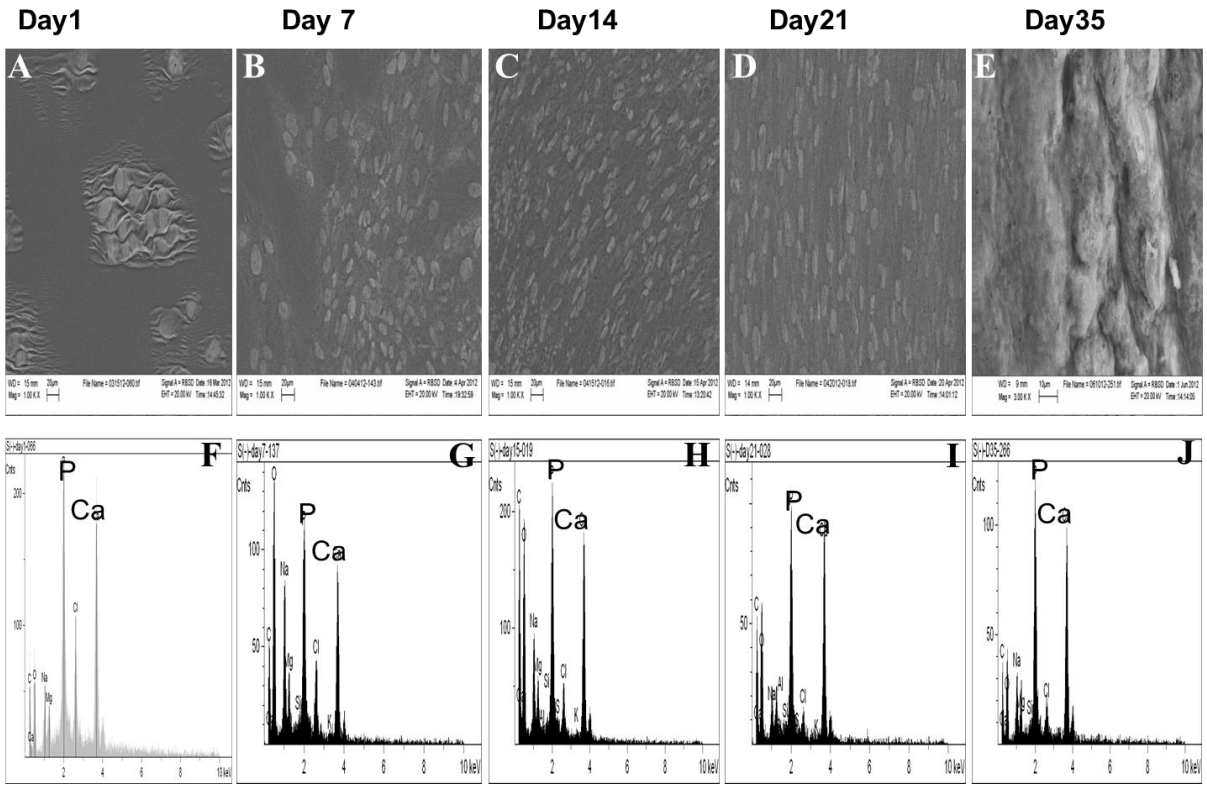


FIGURE 1- 5: SEM MICROGRAPHS OF NON-INDUCED SOFT GEL (S-) WITH DPSCS, SHOWING BIOMINERALIZED DEPOSITS ON (A) DAY1 (B) DAY 7 (C) DAY 14 (D) DAY 21 (E) DAY 35. EDAX SPECTRA SHOWING PEAKS OF CALCIUM PHOSPHATE ON (F) DAY 1 (G) DAY 7 (H) DAY 14 (I) DAY 21 (J) DAY 35. MAGNIFICATION= 1KX; SCALE= 20µM

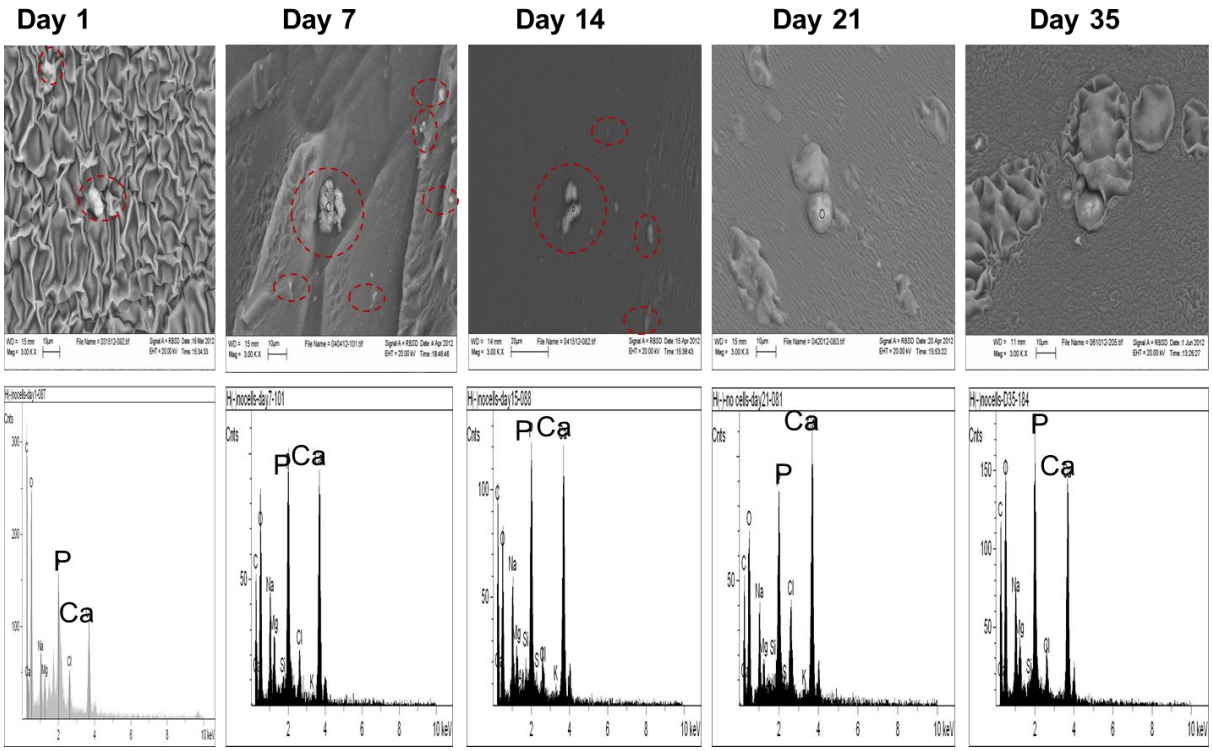


FIGURE 1- 6: SEM MICROGRAPHS OF NON-INDUCED HARD GEL (H-) WITHOUT DPSCS, SHOWING BIOMINERALIZED DEPOSITS ON (A) DAY1 (B) DAY 7 (C) DAY 14 (D) DAY 21 (E) DAY 35. EDAX SPECTRA SHOWING PEAKS FOR CALCIUM PHOSPHATE ON (F) DAY 1 (G) DAY 7 (H) DAY 14 (I) DAY 21 (J) DAY 35. MAGNIFICATION= 3KX; SCALE= 20µM.

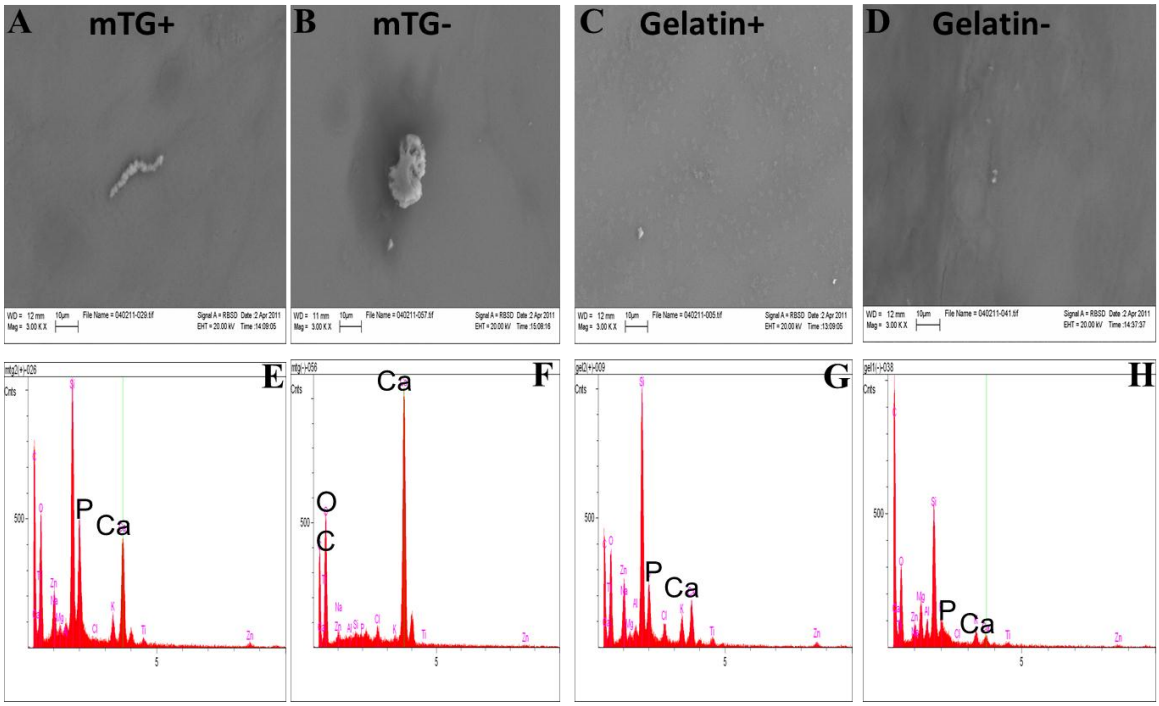


FIGURE 1- 7: SEM MICROGRAPHS AFTER 21 DAYS OF INCUBATION OF DPSCS ON TCP COATED WITH (A) INDUCED MTG (MTG+) (B) NON-INDUCED MTG (MTG-) (C) INDUCED GELATIN (GELATIN+) (D) NON-INDUCED GELATIN (GELATIN-). EDAX SPECTRA AFTER OF DPSCS ON TCP COATED WITH (E) INDUCED MTG (MTG+) (F) NON-INDUCED MTG (MTG-) (G) INDUCED GELATIN (GELATIN+) (H) NON-INDUCED GELATIN (GELATIN-) AFTER 21 DAYS OF INCUBATION. MAGNIFICATION= 3KX; SCALE= 10µM.

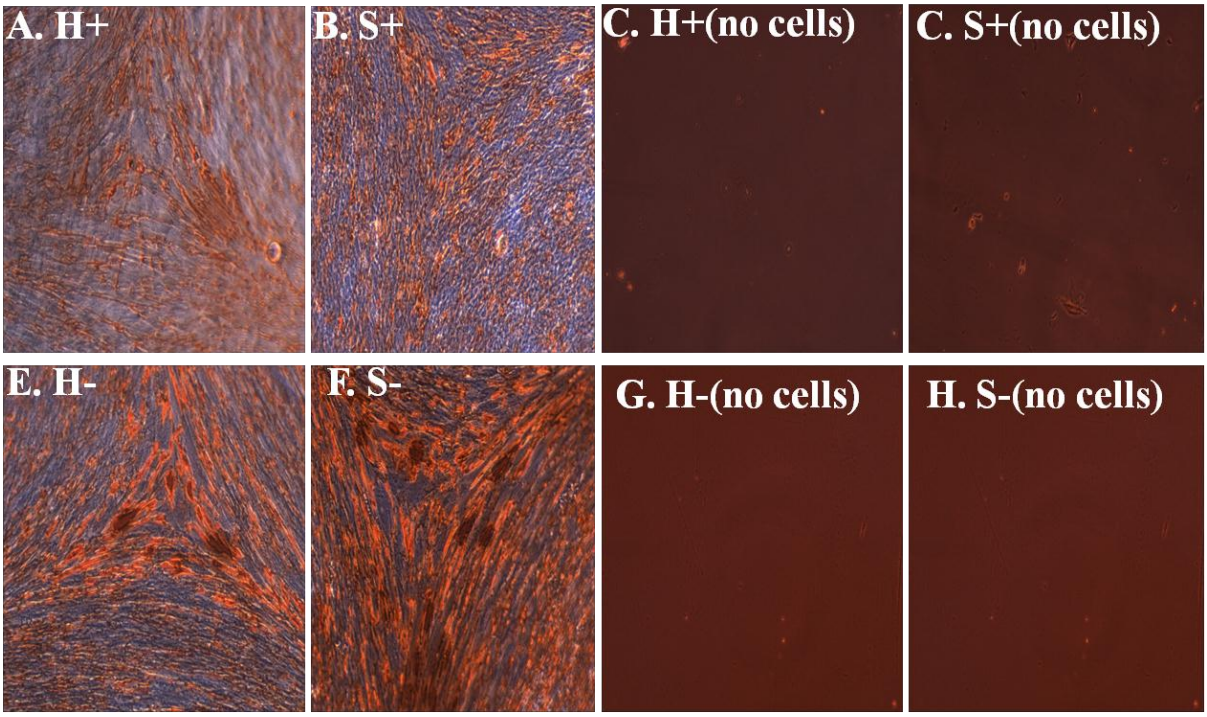


FIGURE 1- 8: MINERALIZATION SHOWN THROUGH ALIZARIN RED STAINING AFTER DAY 35 OF INCUBATION ON: INDUCED (A) HARD GEL (H+) WITH DPSCS (B) SOFT GEL (S+) WITH DPSCS (C) HARD GEL (H+) WITHOUT DPSCS (D) SOFT GEL (S+) WITHOUT DPSCS, NON-INDUCED (E) HARD GEL (H-) WITH DPSC (F) SOFT GEL (S-) WITH DPSC (G) HARD GEL (H-) WITHOUT DPSC (H) SOFT GEL (S-) WITHOUT DPSC. MAGNIFICATION=10X

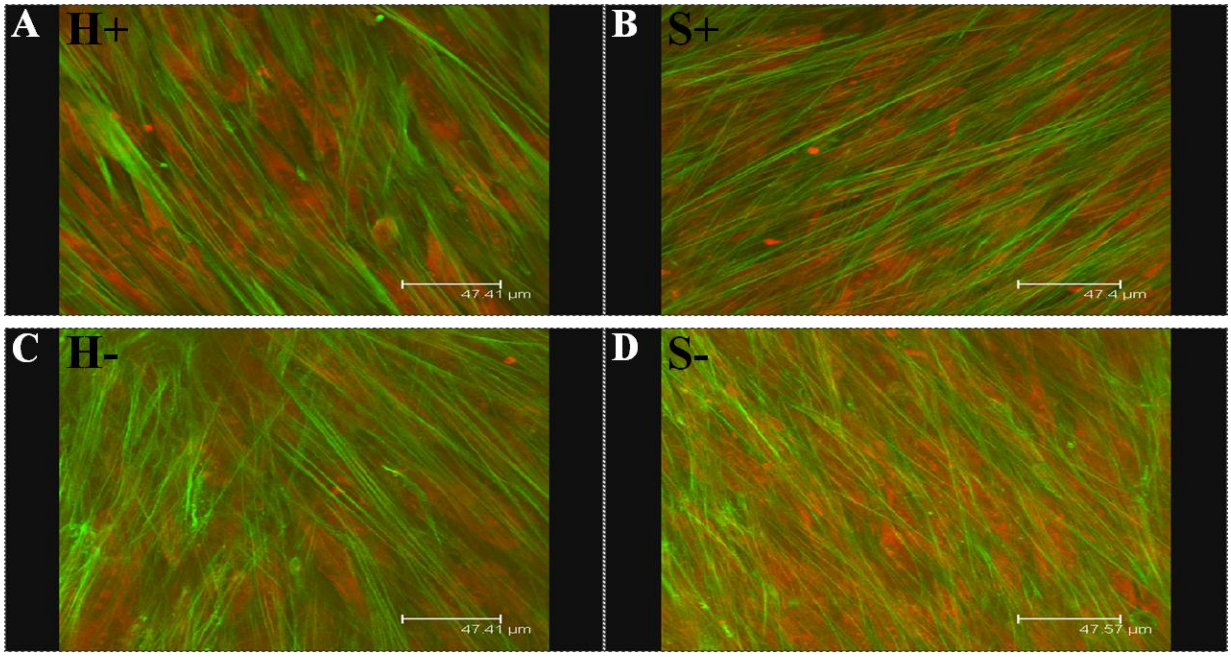


FIGURE 1- 9: MORPHOLOGY OF THE DPSCS AFTER 21 DAYS OF INCUBATION ON INDUCED (A) HARD GEL (H+) (B) SOFT GEL (S+), NON-INDUCED (C) HARD GEL (H-) (D) SOFT GEL (S-). ACTIN FILAMENTS WERE STAINED BY ALEXA FLOUR 488 (GREEN), NUCLEUS WAS STAINED BY PROPIUM IODIDE (RED). MAGNIFICATION= 63X; SCALE = 47.41µM.

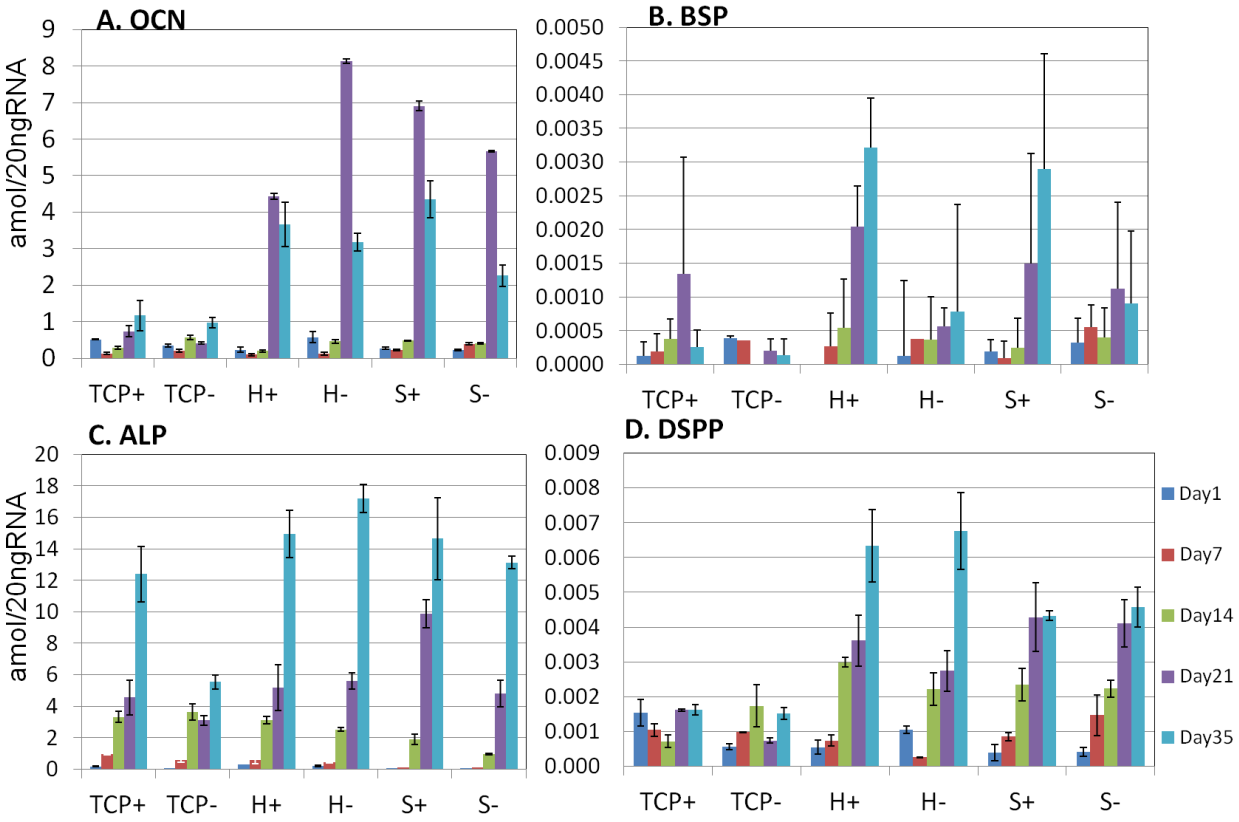


FIGURE 1- 10: mRNA EXPRESSION OF (A) OSTEOCALCIN (OCN) (B) BONE SIALOPROTEIN (BSP) (C) ALKALINE PHOSPHATASE (ALP) (D) DENTIN SIALOPHOSPHOPROTEIN (DSPP) FROM DAY 1 TO DAY 35 ON CONTROLS (TCP+, TCP-), H+, H-, S+, S-.

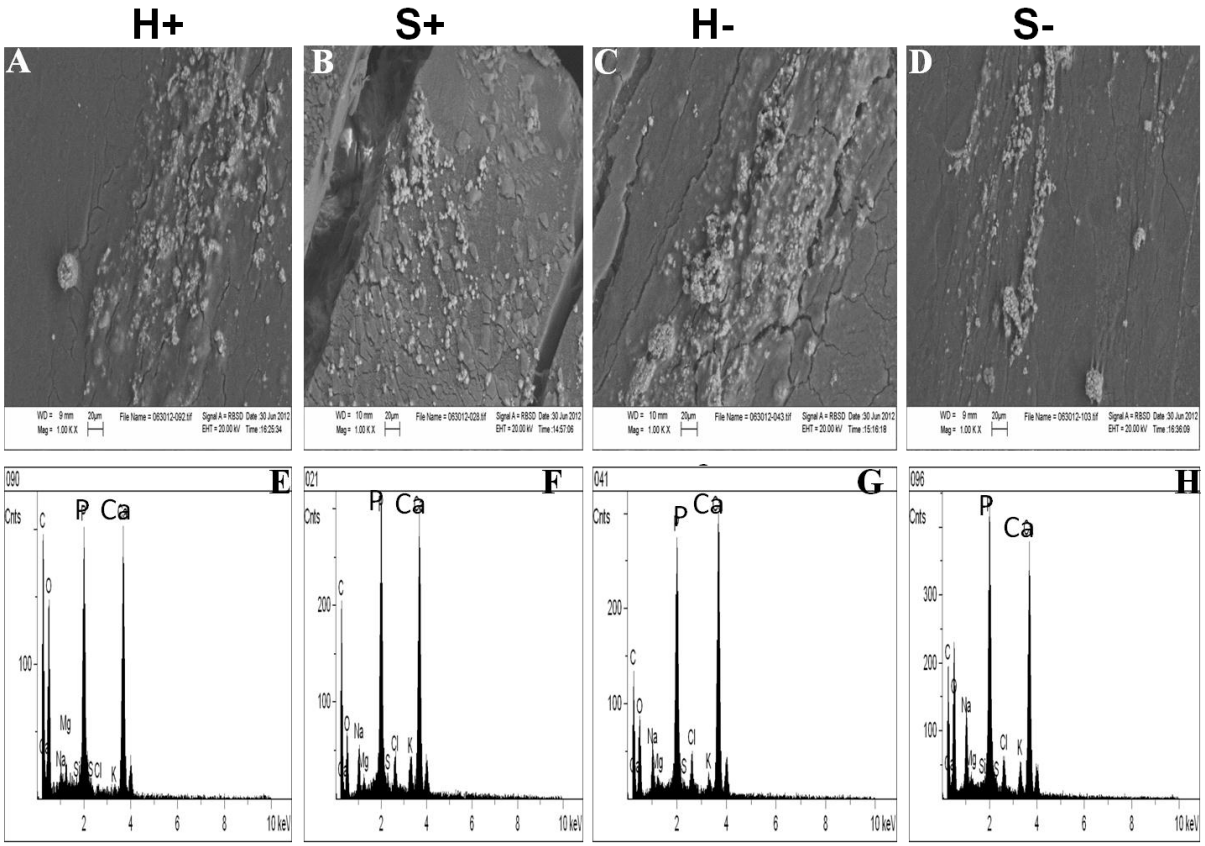


FIGURE 1- 11: SEM MICROGRAPHS SHOWING BIOMINERALIZED DEPOSITS OF INDUCED "EDUCATION SAMPLES" WHERE THE DPSCS WERE RE-PLATED ON TCP FOR 21 DAYS AFTER GETTING EXTRACTED FROM (A) INDUCED HARD GEL (H+(+)) (B) INDUCED SOFT GEL (S+(+)) (C) NON-INDUCED HARD GEL (H-(+)) (D)NON-INDUCED SOFT GEL (S-(+). CORRESPONDING EDAX SPECTRA SHOWING CALCIUM PHOSPHATE PEAKS OF INDUCED "EDUCATION SAMPLES" WHERE THE DPSCS WERE RE-PLATED ON TCP FOR 21 DAYS AFTER GETTING EXTRACTED FROM (E) INDUCED HARD GEL (H+(+)) (F) INDUCED SOFT GEL (S+(+)) (G) NON-INDUCED HARD GEL (H-(+)) (H) NON-INDUCED SOFT GEL (S-(+). MAGNIFICATION= 1KX; SCALE=20µM.

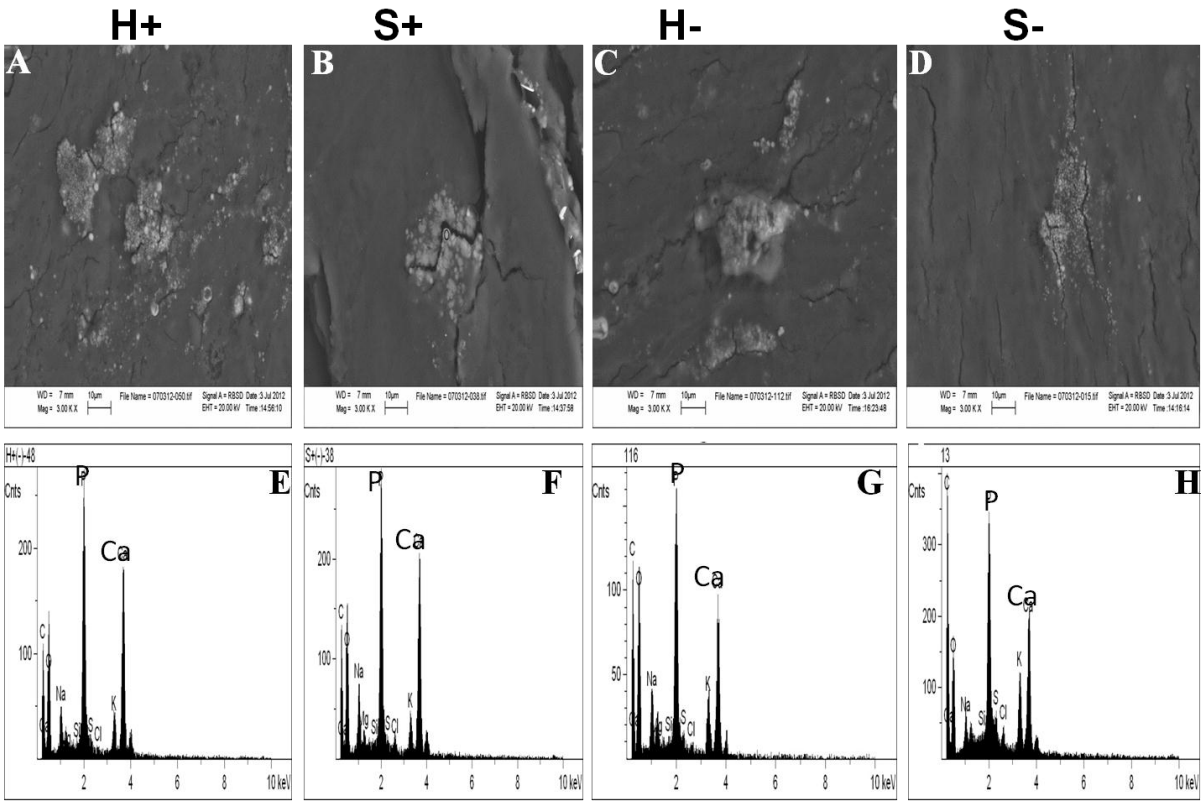


FIGURE 1- 12: SEM MICROGRAPHS SHOWING BIOMINERALIZED DEPOSITS OF NON-INDUCED "EDUCATION SAMPLES" WHERE THE DPSCS WERE RE-PLATED ON TCP FOR 21 DAYS AFTER GETTING EXTRACTED FROM (A) INDUCED HARD GEL (H+(-)) (B) INDUCED SOFT GEL (S+(-)) (C) NON-INDUCED HARD GEL (H-(-)) (D) NON-INDUCED SOFT GEL (S-(-)). CORRESPONDING EDAX SPECTRA SHOWING CALCIUM PHOSPHATE PEAKS OF INDUCED "EDUCATION SAMPLES" WHERE THE DPSCS WERE RE-PLATED ON TCP FOR 21 DAYS AFTER GETTING EXTRACTED FROM (E) INDUCED HARD GEL (H+(-)) (F) INDUCED SOFT GEL (S+(-)) (G) NON-INDUCED HARD GEL (H-(-)) (H) NON-INDUCED SOFT GEL (S-(-). MAGNIFICATION= 1KX; SCALE=20µM.

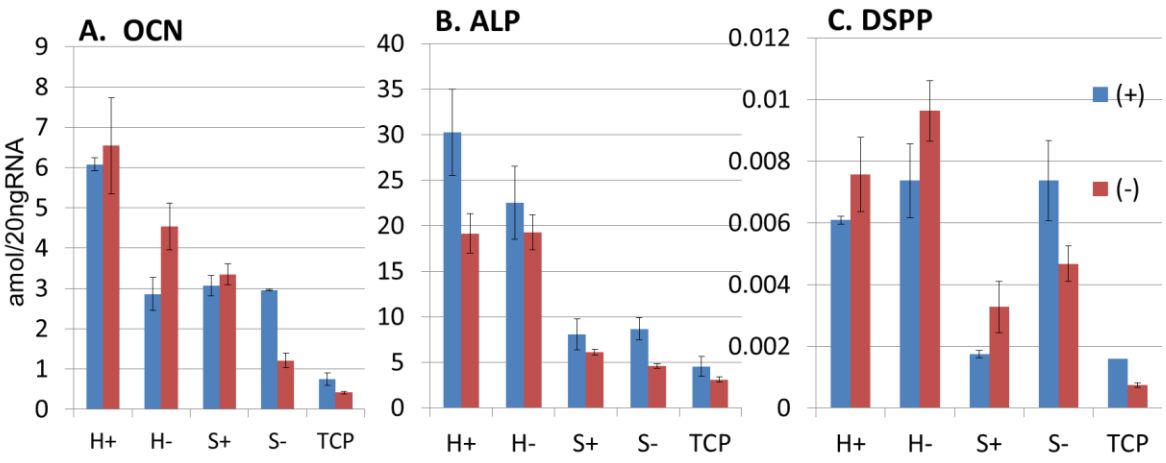


FIGURE 1- 13: COMPARISON OF 21 DAY mRNA EXPRESSION OF (A) OSTEOCALCIN (OCN) (B) ALKALINE PHOSPHATASE (ALP) (C) DENTIN SIALOPHOSPHOPROTEIN (DSPP) ON H+(+), S+(+), H-(-) AND S-(-) EDUCATION SAMPLES AND TCP(+), TCP(-) CONTROLS.

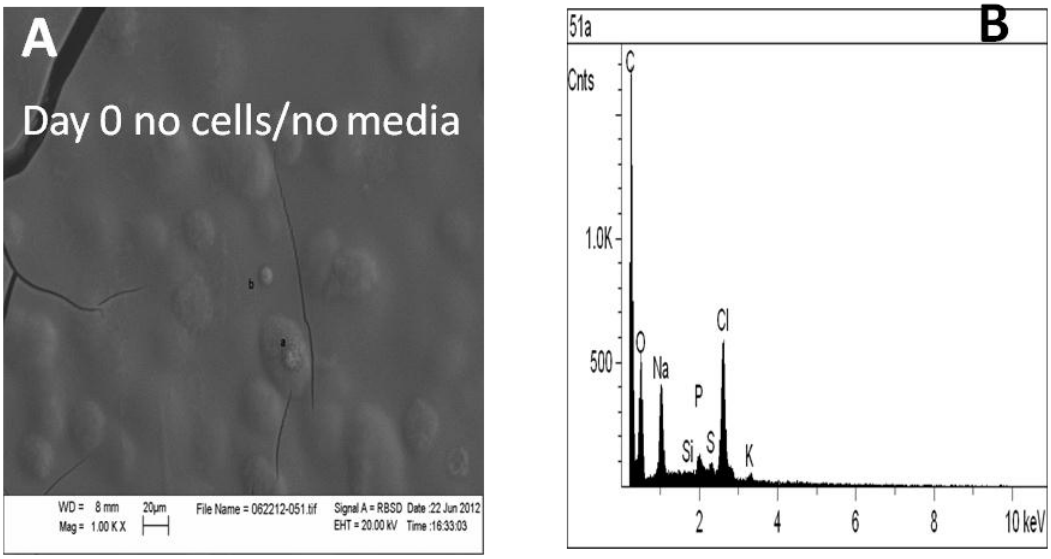


FIGURE 1- 14: HARD GELATIN-MTG GEL ON DAY 0 WITHOUT CELLS AND WITHOUT INDUCED/NON-INDUCED MEDIA (A) SEM MICROGRAPH SHOWING THE SURFACE WITH NO MINERALIZED DEPOSITS (B) CORRESPONDING EDAX SPECTRA SHOWING ABSENCE OF CALCIUM PHOSPHATE PEAKS. MAGNIFICATION=1KX; SCALE =20µM.

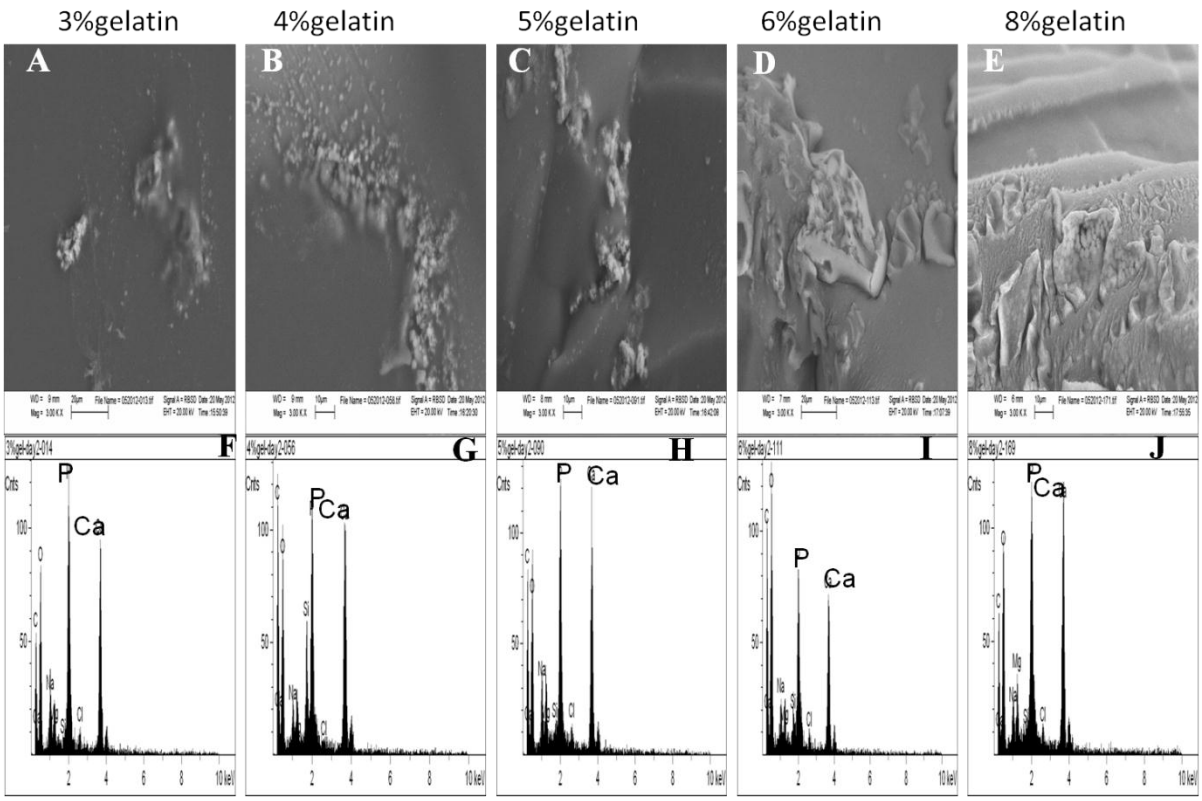


FIGURE 1- 15 BIO-MINERALIZED DEPOSITS (SEM MICROGRAPHS) AFTER DAY1 OF INCUBATION ON NON-INDUCED GELATIN-MTG GELS WITHOUT DPSCS. THESE GELS ARE MADE WITH VARIABLE AMOUNT OF GELATIN AND FIXED AMOUNT OF MTG (A) 3%(W/V) GELATIN (B) 4%(W/V) GELATIN (C) 5%(W/V) GELATIN (D) 6%(W/V) GELATIN (E) 8%(W/V) GELATIN. CORRESPONDING EDAX SPECTRA SHOWING CALCIUM PHOSPHATE PEAK ON GELATIN-MTG GELS WITH (F) 3%(W/V) GELATIN (G) 4%(W/V) GELATIN (H) 5%(W/V) GELATIN (I) 6%(W/V) GELATIN (J) 8%(W/V) GELATIN. MAGNIFICATION=3KX; SCALE=20µM.

# CHAPTER 2

# HYALURONIC ACID AND GELATIN CLAY COMPOSITE HYDROGELS: SUBSTRATES FOR CELL ADHESION AND CONTROLLED DRUG DELIVERY

## 1. INTRODUCTION

In tissue engineering, there is great interest in designing scaffolds that are not only biocompatible and physically robust, but also biodegradable. Hydrogels made from thermally-cooled gelatin and cross-linked hyaluronic acid (HA) are one of the most commonly used matrices for mammalian cell growth [60]. The advantage of gelatin and HA hydrogels is mainly due to their ability to closely mimic the native environment of mammalian cells since gelatin is the basic building block of collagen, a major component of the extracellular matrix (ECM) [12, 60, 61] and HA is a linear polysaccharide (FIGURE 2- 1A) that can be found extensively in the extracellular matrix (ECM) of virtually all mammalian connective tissues [62]. The employment of these natural biopolymers thus offers a growth medium that is highly biocompatible and biodegradable. However, these physically cross-linked gelatin hydrogels melt at physiological temperature and are prone to degradation by proteolytic enzymes such as gelatinase and collagenases [60]. On the other hand, pure non-modified HA has poor biomechanical properties as it does not promote cell adhesion and degrades naturally in vivo by hyaluronidase [63]. Thus, both gelatin and HA must be cross-linked if they have to be used as a biomaterial for tissue engineering and drug delivery.

While there are multiple ways to chemically cross link gelatin [64-70], the cross-linkers often exhibit cytotoxic side-effects [71-76]. Hence the use of gelatin for cell encapsulation can pose a

challenge. The situation is even more complex in the case of HA. To improve the mechanical properties of HA and to make it more cell compatible, several chemical modifications such as those with hydrazide derivatives, annealing, crosslinking of thiol-functionalized HA (HA-DTPH) with poly (ethylene glycol) diacrylate (PEGDA) [77-83] and FN functional domains (FNfds) [63] or photocrosslinkable moieties [84] have successfully been employed. Although many of these hydrogels were stable and had complete biocompatibility and potential for drug delivery [85-87], they were difficult to synthesize and produce in sufficient quantities for larger scale tissue engineering.

Another way of crosslinking biopolymers is to use inorganic clays as cross linkers to form a physically crosslinked polymer composite hydrogel. Hectorite clay falls in the class of smectite-phyllosilicates which are considered to be Generally Recognized as Safe (GRAS) by FDA. Hectorite clays have been used previously to crosslink many synthetic polymers such as poly(ethylene oxide) (PEO)[88-91], poly(acryl amide) [92] and poly(vinyl alcohol) [92] but little attention has been paid to biopolymer–clay composite hydrogels. Recently, the field of biopolymer–clay mineral composites attracted much interest in biomedical and pharmaceutical applications. Montmorillonite clays (MMT) have been used to prepare gelatin-chitosan and chitosan-clay composite hydrogels for improved mechanical and cell adhesive properties [93, 94]. Bhavesh et al. recently used MMT crosslinked alginate hydrogels for drug delivery [95]. The excellent properties of the biopolymer–clay mineral composites such as easy degradation, biocompatibility and tunable mechanical properties are essential for controlled drug delivery and tissue engineering [96].

In this paper, we have engineered a matrix of HA and gelatin cross-linked with Laponite XLG clay where HA and gelatin were intercalated into Laponite by ion exchange. Laponite, an

inorganic synthetic hectorite clay, when suspended in water forms disk like particles [FIGURE 2-1B] with a thickness of 1 nm, a diameter of about 30 nm, and a negative surface charge density of 0.014*e*1/*A*2, which stabilizes dispersions in water. Laponite is most effective because of its high degree of swellability, and exfoliation, high purity, gelation properties, sufficiently small platelet size and good interaction with biopolymers [97, 98]. Furthermore, by varying the content of the clay cross-linker, we were able to design HA-clay, gelatin-Clay and HA-gelatin-Clay scaffolds of variable stiffness in a time span of few seconds. To compare the mechanical stiffness (G', shear storage moduli) of our hydrogels, we carried out oscillatory shear rheometry, operated in stress and frequency sweep modes at a physiological temperature.

An important application of these hydrogel constructs is to support cell growth, enable encapsulation, and to serve as an efficient drug delivery system. Recently, Laponite crosslinked PEO and chitosan hydrogels have been used for better dermal fibroblasts adhesion and proliferation while maintaining the mechanical stability and injectability of the hydrogels [99, 100]. Therefore, in this study, we also investigated the cell attachment of AHDFs on the hydrogel substrates for a period of 3 days. Hydrogels were prepared with different cross-linking densities to provide harder and softer environment to the cells. Therefore, we also investigated the modulus of live AHDFs to determine if cell stiffness was altered to adapt to substrate mechanics. It is known that high glucose levels could inhibit the ability of a hydrogel to support fibroblast migration [101] and that HA is structurally affected by high glucose levels [102-104]. Since, glucose is used in physiological conditions or drug delivery vehicles; we felt that it was important to understand its effect. Therefore, we also looked at the effect of increasing glucose concentration on the stiffness of the HA-Clay hydrogels.

Lastly, to examine the application of our gel as a topical drug delivery system we investigated the controlled time release of Salicylic acid encapsulated in HA-Clay hydrogel. Diffusing a drug out of a gel can ease the access to the absorbing membrane, i.e. the skin and can also help to directly administer the drug to the pathological site [105]. Brown et al. have shown the topically applied localized delivery of a drug (3% diclofenac) in 2.5% hyaluronic acid gel formulation to the epidermis. They also showed that the skin hydration properties of HA can enhance the topical delivery of applied drugs across the skin barrier. Furthermore, Laponite based polymer composite hydrogels exhibit reliable barrier properties thus making these gels useful in sustained drug delivery applications [98]. Thus, a biocompatible and biodegradable drug delivery system of this sort can enhance the healing process by penetrating the skin and providing sustainable drug release. Thus, we were not only able to successfully design cost- effective hydrogel constructs with variable stiffness but also constructs which can support cell growth while maintaining their mechanical strength as well as serve as efficient drug delivery vehicles.

## 2. MATERIALS AND METHODS

### *2.1 RAW MATERIALS*

Fermentation-derived hyaluronan (HA, sodium salt, Mw 1.19 M Da) was provided by Lifecore Biomedical (Chaska, MN); courtesy Professor Mary Cowman from Polytechnic Institute of New York University, NY. The inorganic clay Laponite XLG was provided by Rockwood, Ltd., UK; $[Mg_{5.34}Li_{0.66}Si_8O_{20}(OH)_4]Na_{0.66}$ ; layer size =30 nm diameter x 1 nm thickness; cation-exchange capacity: 104 mequiv per 100g. Dulbecco's modified Eagle's Medium (DMEM), Penicillin streptomycin (Pen strep, PS), 0.05% Trypsin-EDTA solution (1X) and distilled Phosphate buffered Saline (1X PBS, pH 7.4) were obtained from GIBCO Invitrogen Co. (USA). The deionized water used for this preparation was treated with Millipore-Q water purification system.

D-(+)-Glucose (Dextrose; geq 99% (GC)) used to prepare glycated HA-Clay hydrogels was obtained from Sigma-Aldrich (St. Louis, MO). Gelatin -type A (Porcine Skin; Bloom 300) was provided by Sigma-Aldrich, USA. Fetal bovine Serum (FBS, heat inactivated) to prepare the cell culture media was obtained from HyClone Laboratories (Logan, Utah, US). Sterile Bovine Fibronectin (FN) solution was purchased from Sigma-Aldrich (St. Louis, MO, US). Salicylic Acid (ACS certified) and Ethyl Alcohol (190 Proof, 95% pure, ACS/USP grade) used for drug delivery were obtained from Fischer Scientific (Fair Lawn, NJ, US) and Pharmco AAPER (Brookfield, CT, US) respectively.

## *2.2 PREPARATION OF THE HYDROGELS*

### *2.2.1 HA-CLAY, GELATIN-CLAY AND HA-GELATIN-CLAY HYDROGELS*

A 0.5% (w/v) (0.005gms/ml HA/gelatin in SF-DMEM) HA and gelatin stock solutions were prepared in Serum -Free DMEM (DMEM supplemented with 1% PS). A 3% (w/v) (0.03gms/ml clay in DI water) clay solution was prepared in deionized water (DI) using an ultrasonic bath where clay in DI water was sonicated for atleast 30minutes to get a clear exfoliated solution. The stock solutions were filtered using 0.22um filter under sterile conditions. For HA-Clay hydrogels, 0.5% (w/v) HA solution was added to 3% (w/v) clay solution in various ratios [Table1] and swirled around to mix and form a hydrogel in few seconds. Gelatin-Clay hydrogels were prepared in a similar way using 0.5% (w/v) of gelatin instead of HA [Table 1]. For HA-Gelatin-Clay hydrogels, a 50-50 uniform solution of gelatin and HA [0.5% (w/v)] was added to 3% (w/v) clay solution [Table 1]. The nomenclature used to identify the type of hydrogel depends on the volume to volume ratio of the polymer and clay mixed. For example, 1:20 HA-Clay gel indicates the volume to volume ratio of HA: clay to form a hydrogel (for every 2ml of the gel, 0.095ml HA solution was mixed with 1.905 ml of clay solution). Hydrogels were made

in 35mm tissue culture plates (TCPS) for rheology and in 6 well TCPS for cell culture. They were incubated at 37$^{o}$C for 24 hrs. The resulting gels were homogeneous and transparent.

### *2.2.2 HA-CLAY HYDROGEL SUBSTRATES WITH GLUCOSE*

To prepare glycated HA-Clay hydrogel, different amounts of glucose (0.25mg/ml, 0.5mg/ml, 0.75mg/ml, 1mg/ml, 2mg/ml, 3mg/ml, and 5mg/ml) was added to 3% (w/v) (0.03gm/ml) clay to get 7 different solutions. These solutions were then sonicated for atleast 30minutes to get a clear exfoliated clay solution with required concentration of glucose. Clay-glucose solutions were filtered using a 0.22m filter. Eventually, glycated HA-Clay hydrogels were prepared in 35mm TCPS by adding sterile 0.5%(w/v) HA solution to 3%(w/v) clay-glucose solution in a ratio of 1:20(v/v) (HA:Clay) and swirled around quickly to mix completely. All samples were prepared under sterile conditions and incubated at 37$^{o}$C for 24hrs.

### *2.3 DYNAMIC RHEOLOGICAL CHARACTERIZATION*

Oscillatory shear rheometry tests were performed on the HA-Clay, Gelatin-Clay, HA-Gelatin-Clay and glycated HA-Clay hydrogels with rotational rheometer (Bohlin HR Nano, Malvern Instruments Ltd., Germany) using a standard steel parallel- plate geometry of 20mm diameter. During each test method, all 35 mm TCPS containing the hydrogels were fixed to the bottom plate with a double-sided tape. The top plate was then lowered to a gap of 1mm from the bottom of the 35mm TCPS. A dynamic rheological test involves applying a sinusoidal shear stress on the sample and measuring the resulting strain. The applied stress, $\tau$, is

$$\tau(t) = \tau_A(t).\sin\omega t \qquad (1)$$

where, $\tau_A(t)$ is the variable stress amplitude, $\omega$ is the frequency of oscillation, and t is time.

The resulting strain, $\gamma$, is then

$$\gamma(t) = \gamma_A(t).\ \sin(\omega t+\delta), \qquad 0 \leq \delta \leq \pi/2 \qquad (2)$$

Based on Hooke's law, we assumed that if stress is applied to the hydrogels, the strain can be measured at a force corresponding to that stress and G' and G" can be calculated

$$\tau(t) = G'\ \gamma_A(t)\ \sin\omega t + G''\ \gamma_A(t)\ \cos\omega t \qquad (3)$$

where G' is the elastic (storage) modulus and G" is the viscous modulus. The two moduli characterize the elastic (G') and viscous (G") behavior of the material. The storage modulus measures the elastic response or deformation energy stored during the shear process, whereas the viscous modulus measures the viscous response or the deformation energy dissipated during the shear process of the material[106].

The tests employed were oscillatory shear stress sweep and frequency sweep. The stress sweep was done by holding the temperature ($37^oC$) and frequency (1 Hz) constant while increasing the shear stress from 1 to 1000 Pa. In the oscillatory stress sweep (or "controlled stress") tests, the stress was locally controlled in every cycle and the strain (and the corresponding G') was measured. The stress sweeps provides G' (storage/elastic modulus) information on the structural behavior of the crosslinked network, the linear viscoelastic region (LVR) profiles and its limit (or "breaking stress") for all hydrogels by shearing them until the structure broke down.

We also subjected all the hydrogels to a frequency sweep at 50% of their respective ultimate stress levels (corresponding to the point of dip on the LVR profile). At this fixed shear stress and temperature (37 °C), the oscillatory frequency was increased from 0.1 to 100 Hz and the *G*' and G" were recorded. Plots of G' versus shear stress and G' and G" versus frequency were obtained directly from the software controlling the rheometer. All samples were done in triplicate.

## *2.4 CELL CULTURE*

Primary adult human dermal fibroblasts (AHDFs) were obtained from ATCC. The cells were routinely cultured in DMEM supplemented with 10% fetal bovine serum (FBS) and a 1% antibiotic mix of penicillin, streptomycin and L- Glutamine (FULL DMEM), in a 37$^{o}$C, 5% $CO_2$, 95% humidity incubator. The AHDF monolayers were grown in tissue culture polystyrene (TCPS) dishes to nearly 80% confluence, harvested after treatment with 0.05% trypsin-EDTA solution, then centrifuged to obtain a pellet and finally re-suspended in SF-DMEM or FULL-DMEM for use in functional assays.

### *2.5 CELL ATTACHMENT*

Cell adhesion was seen over a period of 3 days. To avoid the use of FN for cell attachment, gelatin was used in HA-Gelatin-Clay hydrogel substrates as gelatin promotes cell adhesion. AHDFs were seeded on the 1:20 and 1:10 HA-gelatin-clay hydrogel surfaces at 5000cells/cm$^2$ and incubated at 37°C, 5% $CO_2$. Throughout the cell-culture process, the FULL-DMEM was replaced every 24hrs. Cell proliferation was documented by taking phase-contrast pictures using optical microscope (IX51, OLYMPUS; Center Valley, PA) with a 10x objective and a camera attached to it.

### *2.6 CELL STIFFNESS*

Cell stiffness was measured using an atomic force microscope (AFM, Dimension 3000; Digital Instruments, Co., Ltd. Santa Barbara, CA), which was operated in shear modulation force microscopy (SMFM) mode [44] using a silicon nitride tip on a cantilever with a bending spring constant of 0.06 N/m. AHDFs were seeded on HA-Gelatin-Clay hydrogels of different stiffness (1:10, 1:20) at 5000 cells/cm$^2$ and incubated for 24 h at 37$^{o}$C prior to measurement. During the measurement, a force of~25nN was exerted by the cantilever on the cell's perinuclear region and

a sinusoidal drive signal (1400Hz) was applied to the x-piezo controlling cantilever, inducing a small oscillatory motion of the tip parallel to the cell surface. When the drive signal amplitude was varied from 7.5mV up to 125mV, which corresponds to an x-piezo displacement of 1.5–25nm, the cantilever response was recorded to estimate the stiffness of the cell surface [45]. The AFM set-up was calibrated such that a greater response amplitude indicated a more compliant surface and vice versa. The drive frequency of 1400Hz was chosen for the measurements since it lies in the flattest region of the cantilever's response curve. A total of nine experimental points (three points per cell and three cells per sample) were obtained for each hydrogel condition.

### *2.7 SALICYLIC ACID DRUG DELIVERY*

Salicylic Acid (SA) was dissolved in ethanol to obtain 1% (w/v) (0.01gm/ml) SA stock solution. 0.05% (w/v) SA was encapsulated inside 1:20 (v/v) HA-Clay hydrogel by adding the required amount of SA while preparing the hydrogel in a 50 ml beaker. The SA encapsulated hydrogel (SA gel) was incubated at 37$^{o}$C over 24 hrs. 20 mL of PBS was added to the beaker after 24hrs for the diffusion of SA. The beaker was placed on a shaker at 37$^{o}$C, and was set to a slow speed (~200 rpm) so that the solution slightly revolved around the gel sample. This was done to mix the SA diffusing out of the gel throughout the entire 20 mL solution, ensuring homogeneity when aliquots were taken. 1.5 mL aliquots of solution were pipetted out at 0, 4, 6, 12, 24, 32, 48, 80, 96, 120 and 144hrs and simultaneously, 1.5 mL of fresh PBS at 37°C was replaced into the beaker. Aliquots were analyzed by UV-VIS Double Beam Research Spectrophotometer (Model Cary 1, path length=1cm; Varian Inc., Santa Clara, CA, US) to determine the absorbance of SA diffused at the different time intervals by recording the SA absorbance peak at a wavelength of 296nm. A calibration curve (with a best linear fit) was obtained using varied range of SA dilutions (0.005% - 0.06% (w/v)) in PBS to establish the mathematical relationship of the

absorbance and concentration. Concentration of the SA diffused at different time intervals was obtained using the Beer's Law:

$$A = \varepsilon.l.c \qquad (4)$$

where, ε is the molar absorptivity (slope of the calibration curve), l is the cell path length (1cm), c is the concentration of SA diffused and A is the absorbance measured at different time intervals.

## 3. RESULTS AND DISCUSSION

### *3.1 SYNTHESIS OF HA-CLAY HYDROGELS*

Polymer composite hydrogels are formed via physical interactions that are non-covalent in nature and often a result of hydrogen bonding, hydrophobic, and ionic interactions. Laponite clay is commonly used as layered silicates where stacks of layers are formed upon exfoliation of clay platelets. The negative charge is located on the surface of silicate layers, and hence, the polymer matrices can react more readily [107]. HA-Clay, Gelatin-Clay, HA-gelatin-Clay hydrogels were formed when entangled polymer chains of HA and gelatin are adsorbed and desorbed on the surface of Laponite particles [FIGURE 2- 2(A-C)]. The polymer chains interact at the clay-polymer surface and coat them, thereby, screening the internal charges to form a stable hydrogel within few seconds. This rapid gelation occurring at physiological pH and room temperature, advocates its proposed injectable in vivo use. Hydrogels of different stiffness were formed by varying the volume ratios [TABLE 2- 1]. The extent of crosslinking and the rate of formation of these hydrogels can alter the rheological properties of these HA-Clay/Gelatin-Clay/ HA-Gelatin-Clay hydrogels. Therefore, in this study we aimed to determine the effect of crosslinking on the rheological behavior of the hydrogels.

## *3.2 RHEOLOGICAL CHARACTERIZATION OF HA-CLAY/GELATIN-CLAY/HA-GELATIN-CLAY HYDROGELS.*

### *3.2.1 OSCILLATORY STRESS SWEEP*

The oscillatory stress sweep was performed to determine and compare their G' (elastic or storage modulus) under the same physical condition and to see if the percentage of modification of HA, Gelatin, HA-Gelatin mix and glucose effects the stiffness of the respective gels. According to the principle of small deformation rheology [108], the hydrogels must be tested within their respective linear viscoelastic ranges (LVR) , the length of which determines the structural stability. We, therefore, first determined the LVR profiles and the limiting value of the LVR (breaking stress) for the 1:20, 1:10, 1:7 and 1:5 HA-Clay, Gelatin-Clay, HA-Gelatin-Clay hydrogels by subjecting them to stress sweep until structure breakdown. Rheological properties such as the LVR profile and frequency response of *G*' (in the following section) were determined at a fixed curing time of 24 h. Logarithmic plots depicted in FIGURE 2- 3(A), (B) and (C) represents the LVR profile and the breaking stress of the 24-h cured HA-Clay, Gelatin-Clay and HA-Gelatin-Clay hydrogels respectively. A typical stress sweep graph shows that at low stress amplitudes, G' maintains a constant linear plateau region (or, LVR) indicating the structural stability under those conditions. FIGURE 2- 3(A-C) show that the LVR is between 1-35 Pa, 1-50 Pa and 1-55 Pa for HA-Clay, gelatin-Clay and HA-gelatin-clay hydrogels. The stress value within this region is safe to be used for other oscillatory tests. On increasing the stress amplitudes further, the bonds of the gel are stretched to maximum so as to reach the limiting value of the LVR. Beyond this limiting stress amplitude (or, breaking stress) as indicated in Table1, the G' begins to deviate noticeably from the LVR plateau indicating the irreversible structural change.

FIGURE 2- 3(A-C) clearly show that, with increasing polymer-clay ratio (1:20(polymer: Clay)), the structure breakdown occurred at higher shear stress levels and G' also increased. 1:5 ratios in all hydrogels recorded the lowest stiffness and lowest breaking point while 1:20 ratios showed the highest stiffness and larger breaking stress [FIGURE 2- 3D, TABLE 2- 1]. G' and the breaking stress increased from 1:5 to 1:20, a trend that was followed in all types of gels. FIGURE 2- 3(A-C) also illustrates that G' of HA-Clay, gelatin-Clay and HA-gelatin-Clay is dependent on the type of polymer used. HA-Gelatin-Clay hydrogels showed~ 1.5 fold higher stiffness than HA-Clay gels. Overall, the following conclusion can be drawn about individual hydrogels. HA crosslinked with clay produced a gel which was the softest, although the increase in clay concentration increased the stiffness. On other hand when gelatin is crosslinked with clay, it produces hydrogels which exhibit higher rigidity and higher breaking stress than HA-Clay at respective concentrations. However, when HA and gelatin both are crosslinked with clay together, the hydrogel formed exhibits highest rigidity and breaking stress indicating highest structural stability. This phenomenon can be explained based on the model depicted in FIGURE 2- 2. HA is a long chain polymer and its flexible and loose chains when adsorbed on the clay surface, forms a softer cross-linked network. Gelatin is a short chain polymer and in the given polymer clay ratios, has 12 times more chains than HA. When short gelatin polymer chains adsorb on the clay surface, they form a significantly harder network. In Ha-gelatin-clay hydrogel, the number of polymer chains increases. While chains of HA provide an outward tension, the gelatin chains at the same time provide an inward tension thus tightening the HA-gel-clay network and making it the stiffest among all three types of gels.

### *3.2.2 OSCILLATORY FREQUENCY SWEEP*

Frequency sweep tests are widely used to obtain information about the stability of the gel networks and to verify if their structures correspond to the rheological definition of a gel. Consequently, we subjected our hydrogels to a frequency sweep from 0.1 to 100 Hz. The shear stresses applied to hydrogels were 10% of their respective ultimate stress levels (breaking stress). FIGURE 2- 4(A), (B), (C) shows a logarithmic plot of G'(elastic modulus)/G" (viscous modulus) versus variable oscillatory frequencies for HA-Clay, Gelatin-Clay and HA-Gelatin-Clay hydrogels. The characteristics at low frequencies represent the behavior at low changes of shear stresses while higher frequencies display the characteristics at high changes of stress[109]. As seen in FIGURE 2- 4(A-C), G' exhibited a pronounced plateau in the frequency range of 0.1-10Hz that is indicative of a stable, crosslinked network. 1:5 ratios in all the gels failed to plateau within 10Hz, indicating poor stability of the gel. The observed difference in G' (FIGURE 2- 4 (A-C)) with different polymer clay ratios correlates well with the obtained stress sweep tests indicating that 1:20 has the highest stiffness. G' and G" also varied depending on the type of polymer used with HA-gelatin-Clay being the stiffest.

Recently, Almdal and coworkers [110] defined the term 'gel' which is to be used to describe the systems that (a) consist of two or more components one of which is a liquid (b) are soft, solid, or solid-like materials and, (c)where, the storage modulus, G′, exhibits a pronounced plateau extending to times at least of the order of seconds and a loss modulus, G″, is considerably smaller than the storage modulus in the plateau region. Our gels satisfied the above mentioned characteristics, most importantly a constant G'>corresponding G", indicating the formation of a stable real viscoelastic 'gel'. We observed that at higher frequencies (10-100Hz), all hydrogels showed an increase in G' where the rate of increase was highest for the 1:20 gels and lowest for 1:5 gels. This trend was followed in all HA-Clay, gelatin-clay and HA-gelatin-clay gels. FIGURE

2- 4(A-C) also showed that HA-gel-clay gels have higher G' than HA-clay has lower G', corroborating the oscillator stress sweep tests.

### *3.3 EFFECT OF GLUCOSE ON THE RHEOLOGICAL PROPERTIES*

These hydrogels have numerous potential applications in the tissue engineering and drug delivery. In physiological conditions, presence of high amount of glucose (diabetic range is >2mg/ml) can affect the modulus of the hydrogels[111], therefore, we have examined the effect of glucose on the rheological properties of HA-Clay hydrogel so that they can be used effectively in normal and diabetic conditions. Oscillatory stress sweep mode was used to obtain shear storage modulus (G'), LVR and the breaking stress of the glycated HA-Clay gels in terms of severity of glycation. The G' values relate to the stiffness of the matrix as a function of glucose concentration. FIGURE 2- 5A shows the variation of G' as a function of concentration of glucose. We observed that the stiffness of HA-Clay hydrogel increases drastically with the increase in the concentration of glucose from 0 to 0.5mg/ml, reaching the maximum stiffness at 0.5mg/ml. However, further increase in the glucose concentration to 0.75mg/ml decreases the stiffness which further decreases dramatically at 2mg/ml (critical diabetic concentration) to approximately the same value of G' as control (0mg/ml). As the glucose concentration reaches the diabetic blood sugar level of 3mg/ml, we noticed a sudden 20% decrease in the stiffness of the hydrogel, indicative of a collapse of the gel[101], seen in polymer systems when separation of fluid element from solid element occurs. We also noticed the similar behavior of the breaking stress as G' as shown in FIGURE 2- 5B. The breaking stress for HA-Clay gels with 0.5mg/ml glucose was around 84 Pa while for 3mg/ml glucose sample; it was around 10 Pa corroborating the above result.

Our group has previously studied the effect of glucose on Pluronic copolymer gels[111] where they described about a competing phenomenon of glucose and hydrogel for water. Using the similar explanation, theoretically, glucose may be promoting crosslinking of the HA-Clay matrix, making it stiffer with increasing concentrations of glucose. HA-Clay gel is composed of HA, hydrophilic clay and glucose predominantly where both glucose and the hydrogel have affinity for water. In the hydrogel system, polymer and clay form bonds with water molecules but with the addition of glucose, those water molecules have to be shared with glucose molecules too. Addition of glucose up to a certain concentration makes the HA-Clay-Glucose network harder till all the water molecules are bonded together either by glucose or by the HA-Clay mesh. On increasing the concentration of glucose, more and more glucose molecules compete for water molecules and bind with it leaving the HA-Clay network deprived of water. This could have led to a decrease in the modulus as well as the breaking stress. Another hypothesis could be that, with the addition of more glucose, the network of HA-Clay and glucose became so hard and brittle that even on the application of a small stress (10Pa), the network collapsed and rheological measurements were of the liquid component of the system and not of the network alone.

### *3.4 IN-VITRO SALICYLIC ACID RELEASE*

Controlled drug release could be very valuable since HA-clay hydrogel has potential applications in wound healing as well as for preventing post- surgical adhesions. To evaluate the ability of HA-clay hydrogel for drug delivery, we loaded the HA-clay hydrogel with salicylic acid (SA). Fig. 5C shows the release profile of salicylic acid with time. The initial burst release of 14%, 34.2%, 47.5% was observed in the first 12 hrs. At PBS pH=7.4, the release of SA was~71.4% within 12 hrs. and~82.3% within 24hrs. Therefore, 82% of the drug was released by 24hrs and a

release plateau was reached. These results indicate that this HA-clay has excellent potential for controlled drug release at wound sites.

### *3.5 IN VITRO CELL CULTURE TESTING*

In addition to the study of rheological properties, HA-gelatin-clay hydrogels were also analyzed for biological compatibility. This parameter is the most important considering the potential applications of these hydrogels for tissue engineering, wound healing or cell delivery. Hence, AHDFs were seeded on 1:20 and 1:10 composition of the hydrogel for a period of 3 days. Lower polymer ratios such as 1:5 were avoided for cell attachment studies since the stiffer matrices seemed to support better cell adhesion. The cells were investigated by microscopic observation of their attachment and spreading till 3 days of incubation. FIGURE 2- 6(A), 6(B) show the day 3 phase contrast pictures of the cells attached to 1:10 and 1:20 HA-Gelatin-Clay hydrogel surfaces respectively. The cells showed good viability in the presence of the scaffolds. This leads to the conclusion that both the materials and the preparation conditions of the hydrogels are not toxic for the AHDFs. In this study, we found gelatin to be important for the cell adhesion in these scaffolds so as to avoid the use of FN. Nevertheless, HA is important for providing mechanical stability and for facilitating the use of these hydrogels for wound healing, cell and drug delivery.

### *3.5 MEASUREMENT OF CELL STIFFNESS*

Human dermal fibroblasts were plated on 1:20 and 1:10 HA-gelatin-Clay hydrogels for 24 h to allow sufficient adhesion and spreading of the cells. AFM was operated in the SMFM mode and used for measuring the cell modulus which is an index of its stiffness. While taking the measurements, a sinusoidal drive signal was applied to the x-piezo that induced a small oscillatory motion on the cell surface. Simultaneously, a normal force of~2nN was also applied

to maintain tip contact with the cell surface [112]. The normal indenting force was applied to the perinuclear region between the cell nucleus and cytoplasmic edge to ensure reproducibility of the stiffness measurement. The response amplitude of the cantilever was measured and plotted against drive amplitude (FIGURE 2- 6 D). It was found that the response amplitude was proportional to drive amplitude, indicating that there was no slip during the cell-tip contact. Assuming a Hertzian model for this SMFM set-up, the response amplitude has been previously shown to be inversely proportional to 2/3 power of the lateral modulus of the specimen[45]. Using this calibration, we found that cell stiffness was sensitive to substrate mechanics (Figure 6E), where a 1.5-fold increase in hydrogel stiffness (from 7KPa to 12K Pa) produced a 200% increase in cell moduli, with the stiffness on the 1:20 and 1:10 hydrogels showing significant difference.

## 4. CONCLUSION

In this work we presented the preparation of physically crosslinked and mechanically stable biopolymer (HA and gelatin)-composite hydrogels based on crosslinking using a sodium clay. The in-depth comparison of the physical properties of different hydrogels (HA-clay, gelatin-clay and HA-gelatin clay) was successfully done through the oscillatory stress and frequency sweep tests. These rheological tests indicate that HA-gelatin crosslinked with clay forms the most stable networks while HA-clay hydrogels are relatively soft and gelatin-clay hydrogels are intermediate. 1:20 polymer-clay ratio in all hydrogels exhibited the maximum stiffness and breaking stress whereas 1:5 polymer-clay ratios were the weakest indicating that the clay concentration plays an important role in the mechanical stability of these hydrogels.

The rheological measurements of the effect of glucose on the HA-clay hydrogels also showed the large increase in the modulus of the hydrogels with increasing glucose concentration. This increase of modulus and breaking stress is followed by a sharp decline as the glucose concentration approaches the diabetic level. At the diabetic blood sugar level of 3mg/ml, the hydrogel collapses and has a 20% decline in its modulus. These results suggest that careful considerations of glucose concentrations must be made in order to use these hydrogels under physiological environment. Biological testing with AHDFs showed good biocompatibility and cell survival in the presence of all hydrogels discussed for up to 3 days. Adhesion of cells was observed to be more prominent in the presence of gelatin and stiffer matrices were found to support cell adhesion better than softer matrices. Drug release from the HA clay hydrogel showed that it could maintain a slow, sustained release rate for the hydrophobic SA. Therefore, the HA-clay hydrogel has significant potential to act as a valuable, natural, non-toxic delivery vehicle for sustained release of drugs at wound sites. Our findings have the potential to guide the development of natural, biocompatible, mechanically stable scaffolds that can facilitate drug or cell delivery and tissue repair.

## 5. FIGURES

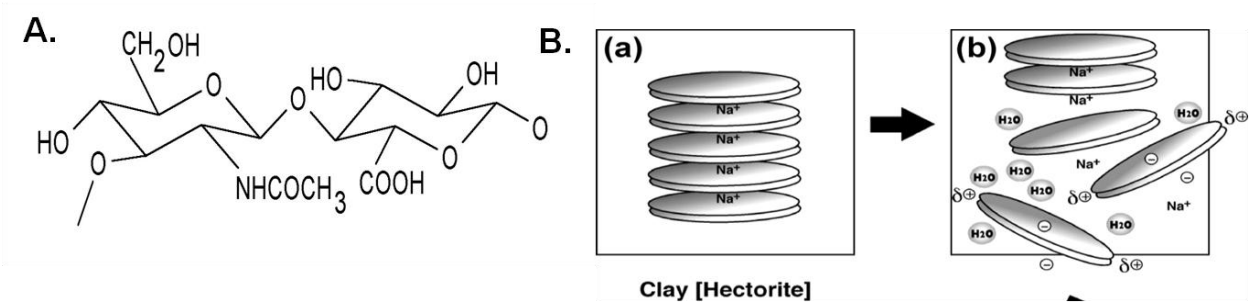


FIGURE 2- 1: (A) SCHEMATIC SHOWING STRUCTURE OF HA MOLECULE. (B) (A) STRUCTURE OF HECTORITE CLAY (B) EXFOLIATED CLAY IN DI WATER [39]

| **Type of Hydrogel** | **Polymer and Clay concentration (w/v)** | | | **Polymer Clay ratio(v/v)** | | | **Storage Modulus, G'(Pa)** | **Breaking Stress (Pa)** |
|---|---|---|---|---|---|---|---|---|
| | *HA* | *Gelatin* | *Clay* | *HA: Clay* | *Gelatin: Clay* | *HA-Gelatin: Clay* | | |
| *HA-Clay hydrogel* | 0.5% | | 3% | 1:5 | | | 1257 | 38.7 |
| | 0.5% | | 3% | 1:7 | | | 2274 | 64.6 |
| | 0.5% | | 3% | 1:10 | | | 4696 | 87.5 |
| | 0.5% | | 3% | 1:20 | | | 6775 | 133.3 |
| *Gelatin-Clay* | | 0.5% | 3% | | 1:5 | | 1529 | 50 |
| | | 0.5% | 3% | | 1:7 | | 3020 | 74 |
| | | 0.5% | 3% | | 1:10 | | 6406 | 116.5 |
| | | 0.5% | 3% | | 1:20 | | 8496 | 177.8 |
| *HA-Gelatin-Clay* | 0.5% | 0.5% | 3% | | | 1:5 | 2059 | 58 |
| | 0.5% | 0.5% | 3% | | | 1:7 | 3864 | 83.4 |
| | 0.5% | 0.5% | 3% | | | 1:10 | 7810 | 133.3 |
| | 0.5% | 0.5% | 3% | | | 1:20 | 11455 | 237.1 |

TABLE 2- 1: PREPARATION OF HA-CLAY, GELATIN-CLAY, HA-GELATIN-CLAY HYDROGELS WITH THEIR STORAGE MODULI AND BREAKING STRESS.

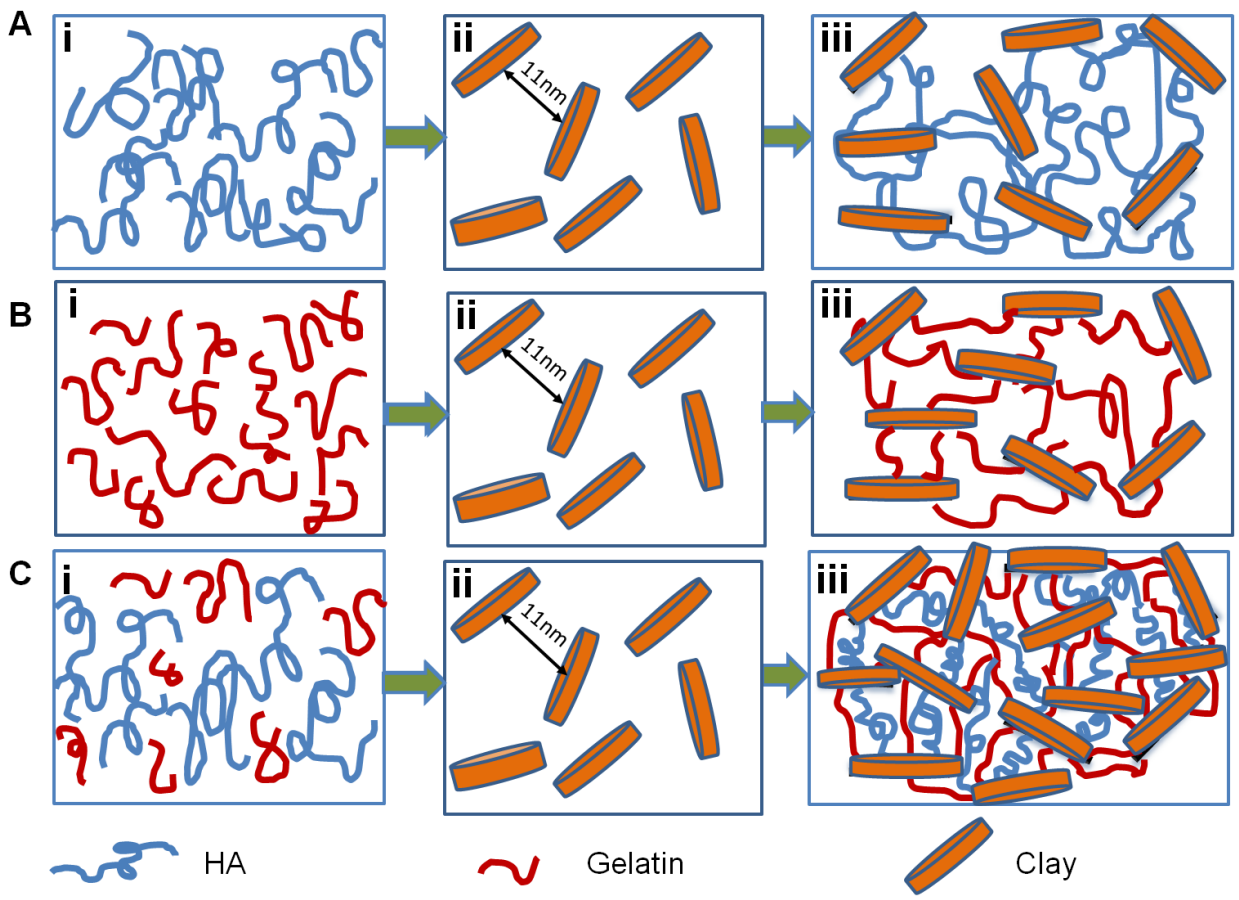


FIGURE 2- 2: SCHEMATIC REPRESENTATION OF THE MECHANISM OF FORMATION OF HYDROGELS (A) HA-CLAY (B) GELATIN-CLAY (C) HA-GELATIN-CLAY

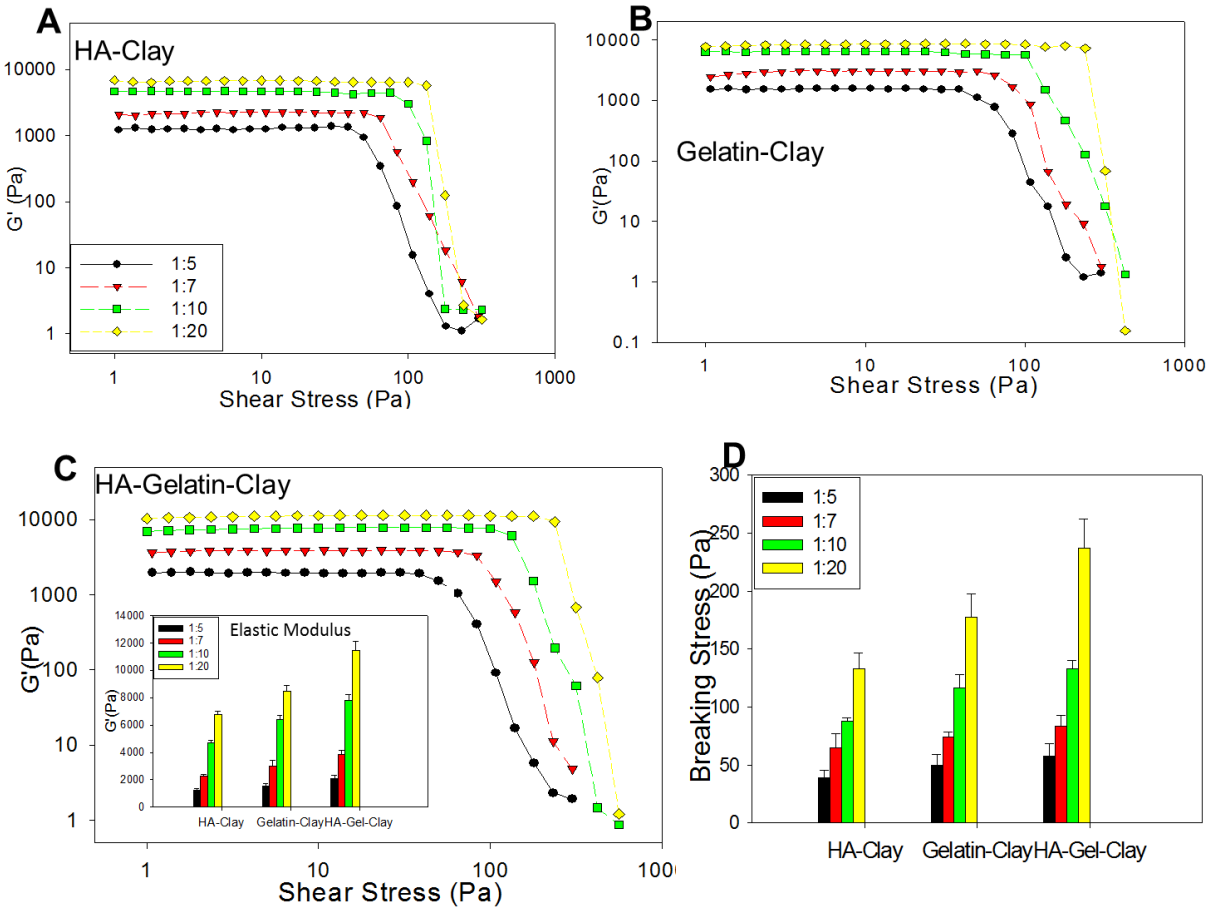


FIGURE 2- 3: OSCILLATORY STRESS SWEEP ON DIFFERENT TYPES OF HYDROGELS (A) HA-CLAY (B) GELATIN-CLAY (C) HA-GELATIN-CLAY (D) PLOT OF THE BREAKING STRESS FOR DIFFERENT TYPES OF HYDROGELS.

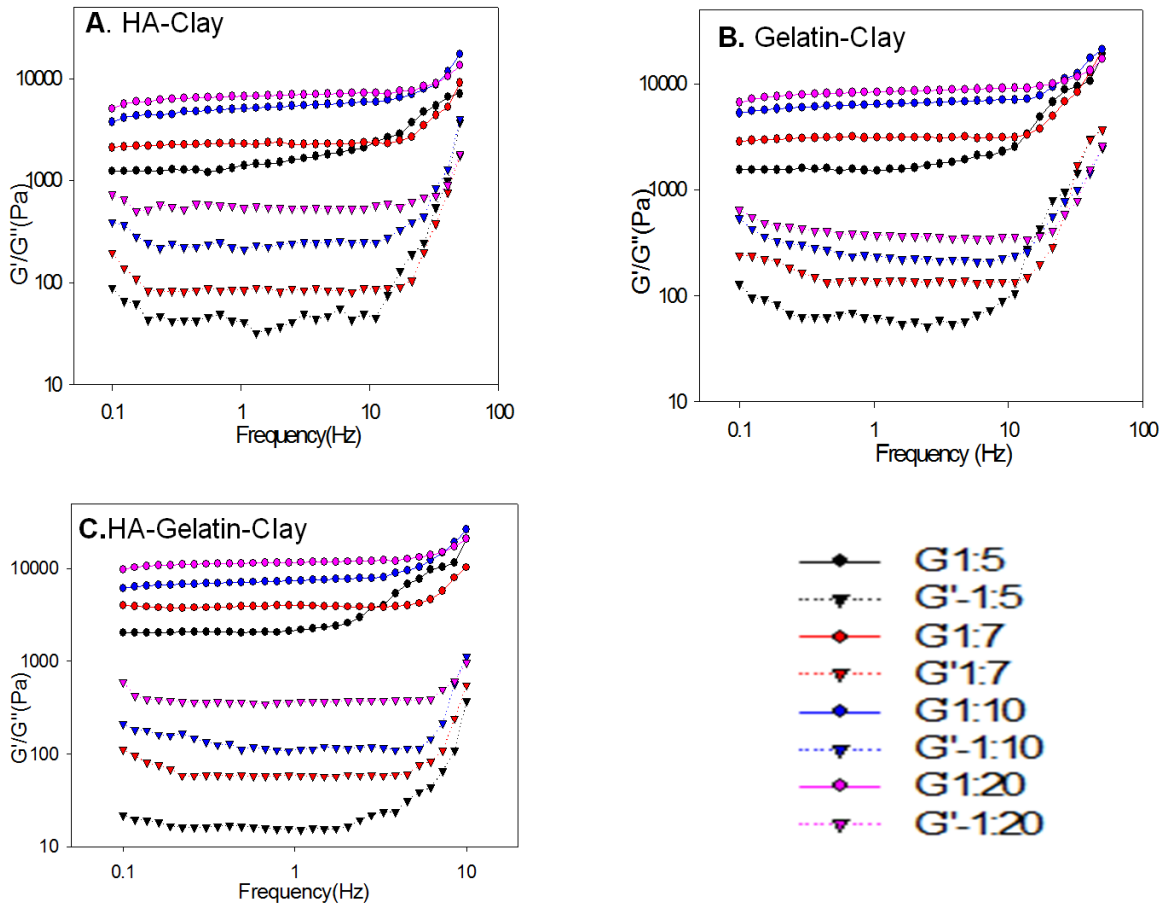


FIGURE 2- 4: OSCILLATORY FREQUENCY SWEEP OF DIFFERENT HYDROGELS TO DETERMINE G' AND G" (A) HA-CLAY (B) GELATIN-CLAY (C) HA-GELATIN-CLAY.

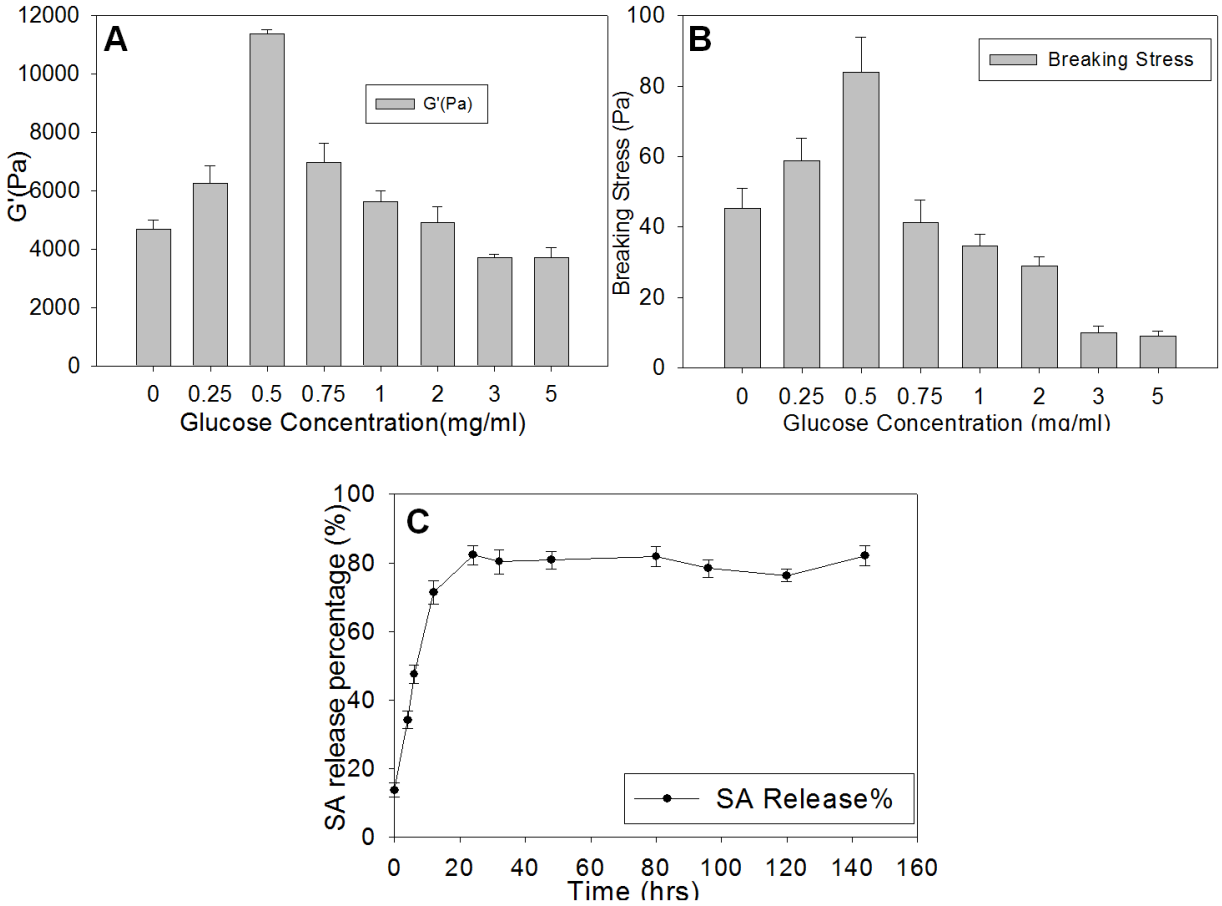


FIGURE 2- 5: 1:20(V/V) HA:CLAY HYDROGEL (A) PLOT OF G'(PA) VS DIFFERENT GLUCOSE CONCENTRATIONS (MG/ML) (B) PLOT OF BREAKING STRESS VS DIFFERENT GLUCOSE CONCENTRATIONS (C) CONTROLLED TIME RELEASE OF SA.

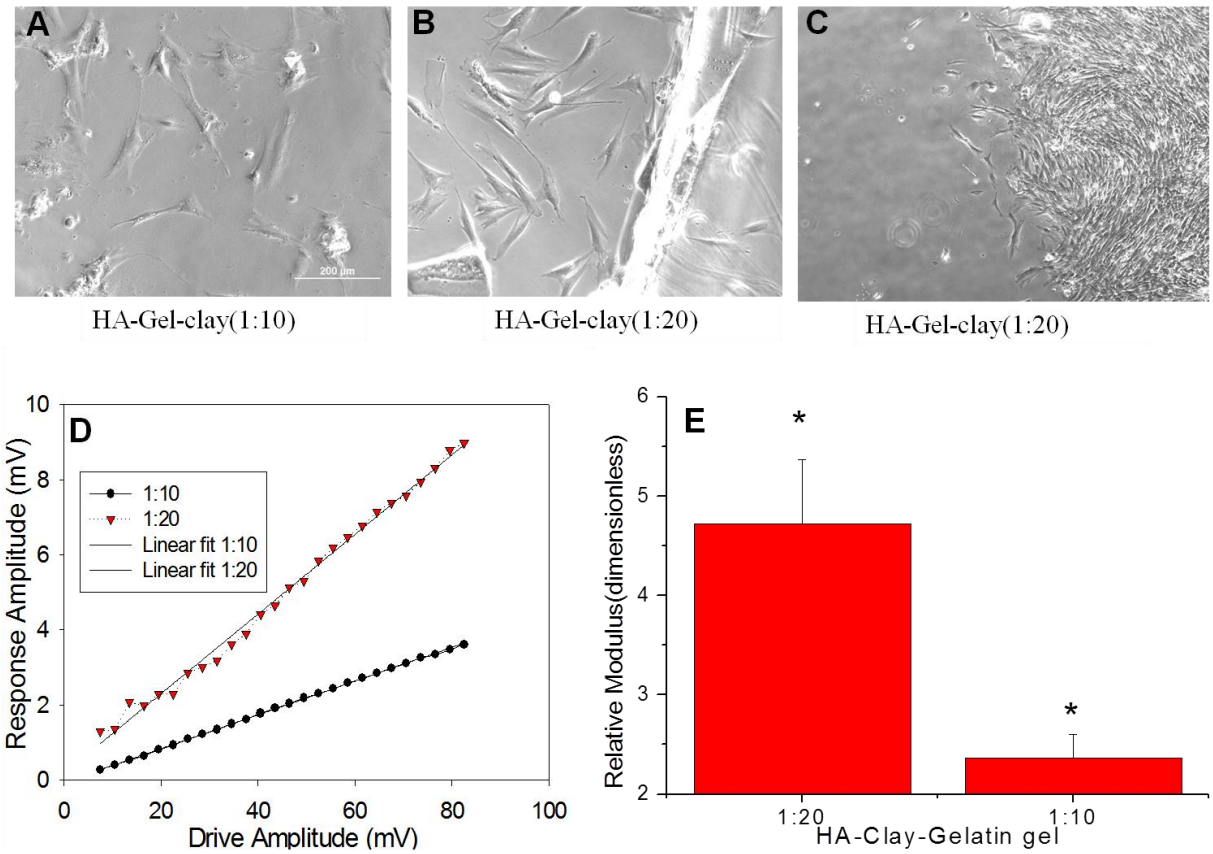


FIGURE 2- 6: PH PICTURE OF CELLS ON HA-GELATIN-CLAY HYDROGEL AFTER 3 DAYS OF INCUBATION(A) 1:10 (B) 1:20 (C) AGAROSE DROPLET WITH CELLS ON 1:20 GEL (D) LINEAR RELATIONSHIP BETWEEN DRIVE AND RESPONSE AMPLITUDE (E) CELL MODULUS ON 1:20 AND 1:10 HA-GELATIN-CLAY AFTER DAY 1 (* INDICATES $P<0.05$)

# CHAPTER 3

# NON-INVASIVE ANALYSIS OF THE EFFECT AND DURATION OF TREATMENT WITH BOTULINUM TOXIN TYPE A USING DIGITAL IMAGE SPECKLE CORRELATION

## 1. INTRODUCTION

Following its introduction into clinical use in the early 1980s, the neuromuscular blocking agent Botulinum toxin type A (BTX-A) has assumed a number of therapeutic roles, including the cosmetic relaxation of wrinkles. BTX-A causes a transient dose-related muscle weakness by blocking acetylcholine release at the synaptic cleft, resulting in neuromuscular paralysis of the facial muscles [113]. This effectively releases the underlying muscular tension to reduce wrinkling of the skin. The surface of the skin is covered by intersecting grooves and ridges, producing characteristic skin surface patterns. It has been suggested that these folds provide a reserve of tissue that allow the skin to stretch during normal muscle movements [114]. Muscle contraction produces skin creases that lie perpendicular to the underlying muscular force vector [115]. Wu et al. [116] simulated the correlation of muscular tension and skin wrinkling and demonstrated that wrinkles form due to deformation of the dermis and the hypodermis layers of skin following muscle contraction. They were able to show that the wrinkle appears perpendicular to the direction of muscle movement and the height of the wrinkle bulge is dependent upon contraction amplitude; thus release of muscular tension should result in dissipation of skin wrinkles. BTX-A was first shown to have this effect in 1992 when Carruthers successfully treated glabellar frown lines by inducing muscle paralysis [117].

Despite its immense popularity in the non-operative treatment of facial rhytids, little is known about the time course of muscle paralysis and its relationship to the reappearance of the overlying wrinkles. Currently, clinical trials establishing aesthetic outcomes of BTX-A are based on patient-reported data such as the eleven-item Facial Line Outcomes (FLO) questionnaire (Allergan, Irvine CA) and physician observation using the Subject Global Assessment (SGA). FLO-11 has previously been used to measure BTX-A treatment efficacy [118, 119]. The questionnaire asks the patient to consider a particular treatment area (forehead, glabellar, or crow's feet) or the upper face in total, and rank her agreement with a series of eleven statements regarding her perception of her facial lines. A score is then calculated, with higher values corresponding to higher levels of satisfaction. While the highly subjective FLO-11 has utility in determining pre-treatment self-assessment as well as subsequent improvement in attitude about facial lines, it does not quantify the degree of BTX-A effect on facial musculature, nor is sensitive enough to detect the precise onset and offset of paralysis. Other techniques, such as the Facial Wrinkle Scale (a 3 point wrinkle severity scale in which 0=none, 1= mild, 2= moderate and 3= severe), provide a more quantitative measure of the appearance of the wrinkles [120, 121].

Very few methods have been explored to study the response of facial muscles to BTX-A. Heckman et al. [122] analyzed patient photographs to determine the degree of paralysis by geometrically measuring the extent of brow motion with respect to selected landmarks. This method fails to capture the correlation of individual muscle groups, which are vital in universal quantification of muscle paralysis. Hanin et al. [123] proposed a technique specifically aimed at measuring muscle contraction involving polymer impressions made of the face during motion, which is invasive and difficult to implement practically and consistently. Other invasive

measures such as electromyography or facial muscle biopsy are not practical in the cosmetic setting.

A systematic review performed by T.C. Flynn et al. integrated patient reported outcomes from published clinical trials of the cosmetic use of Botulinum toxin in order to show that patients can expect treatments to last ≥3 months but often as many as 4–5 months depending on the facial area, dose, and formulation. Their data demonstrated great variability in the existing literature with respect to the observed duration of treatment effects, across studies and even among patients within studies [124]. Although such subjective evaluations may be useful in determining patient satisfaction and self-image [118], they fail to objectively quantify the degree or duration of Botulinum toxin effect on the musculature and the extent of initial observed paralysis of each treated muscle group.

BTX-A injection locus is another important parameter influencing the cosmetic success of the procedure. There is great individual variability in the anatomic positioning of the muscles, the tension generated and the intensity of movement. Quantitative, objective data and useful metrics are lacking for identifying physiologically ideal injection locations. Consequently, it would be important to develop a spatially resolved, minimally invasive, in-vivo method that can measure the loci of applied stress on facial skin. This technique could then be used to predict injection site as well as monitor subsequent muscular paralysis and recovery and correlate it directly with subjective patient outcomes data.

In this paper, we investigate the clinical application of Digital Image Speckle Correlation (DISC), a non-invasive and non-contact technique which we have previously shown to be useful to measure the mechanical properties of skin [125]. Afriat et al. demonstrated that for face,

where the skin is directly attached to the muscles through the superficial musculoaponeurotic system (SMAS), DISC can be extrapolated to the contraction of the underlying musculature [15]. DISC analyzes two photographic images taken before and after the skin deformation during facial expression in order to quantitatively evaluate the dynamics of the skin as well as the underlying musculature. It detects the lines of tension generated by activated muscle groups and calculates their strength of contraction. Here, we extend DISC to direct clinical application by presenting data from six patients cosmetically treated with BTX-A and using DISC to analyze for both temporal and spatial correlation between the muscular contraction and the onset/offset of muscle paralysis. Results from DISC were also compared to the subjective results obtained from FLO-11 and SGA questionnaires. In addition to providing precise quantitative data, DISC enables the treating physician to decode the patient's facial muscle "fingerprint" and better determine the duration of effect, injection location and dosage of BTX-A to achieve optimal results.

## 2. METHODS

### *2.1 DISC METHOD*

First proposed in the 1980s, DISC [126] (known in earlier studies as digital image correlation) [127-130], has been used in experimental stress analysis studies of metals, rubbers and fracture dynamics [131-133]. Applied to biological systems, DISC uses the natural texture of the skin for tracking the facial motions. The distribution of skin pores on the face provides a highly dense texture, which can be exploited for capturing fine-scale facial movements. DISC works on a simple principle of matching two digital images taken before and after skin deformation produced by natural facial movements (blinking, smiling, frowning, raising eyebrows). By

tracking an individual's skin pores during a facial expression, DISC measures direction and magnitude of underlying facial tension [134] and calculates contraction strength of activated muscle groups, precisely quantifying facial paralysis. The basic setup of DISC involves a digital camera and a computer. As depicted in FIGURE 3- 1A, a photo is taken of the patient's face at rest and again during a small motion (FIGURE 3- 1B) of the above described natural facial movements, thus producing reference and deformed images respectively. DISC selects planar (x, y) coordinates in the baseline photo that corresponds to the pores on the skin and correlates them to the same pixels in the second picture (x', y') (FIGURE 3- 1C).

DISC matches the two images subset by subset and the coordinate difference between the two matched subsets gives the average displacement vector corresponding to skin deformation. If the coordinates of the reference image are (x, y), and of the deformed image are (x*, y*), the similarity of the deformed and reference subset centered at these points can be evaluated using a cross-correlation function (S), defined as:

$$S\left(x, y, u, v, \frac{\partial u}{\partial x}, \frac{\partial u}{\partial y}, \frac{\partial v}{\partial x}, \frac{\partial v}{\partial y}\right) = 1 - \frac{\sum I(x,y) * I^*(x^*, y^*)}{\sqrt{\sum I(x,y)^2 * \sum I^*(x^*, y^*)^2}}, \qquad (1)$$

Where I (x. y) and I*(x*, y*) are the intensity at the corresponding points and the summation within the correlation function is over the entire subset. If (x, y) and (x*, y*) are at exactly the same point, the value of the cross-correlation function (S) is equal to zero (or to be realistic, reaches its minimum), and

$$x^* = x + u, \qquad y^* = y + v;$$

in which u and v are the displacement components along the horizontal and vertical direction, respectively.

## *2.2 EXPERIMENTAL PROTOCOL*

Six female patients age 30-60 (mean age 47.5) with mild to severe upper facial rhytids were prospectively recruited under an Institutional Review Board-approved pilot study. Individuals treated with Botulinum toxin within last 6 months or who have had previous facial surgery were excluded from the study. Prior to treatment, patients completed baseline FLO-11, SPA, and SGA assessments. Each subject positioned her chin on a specially-designed head stabilizer, standardizing face position and camera distance. Photographs were taken prior to the BTX-A injections using a 6.3 megapixel CMOS sensor based Canon DS6041 camera with the face at rest and engaging the desired muscle group by frowning (glabellar complex), raising the eyebrows (forehead), and closing the eyes (crow's feet).

A single treating Board-certified plastic surgeon subjectively assessed patients' facial muscle mass to determine injection amount and number to achieve cosmetic effect based on the updated Plastic and Reconstructive Surgery Supplement Consensus Recommendations, outlined in Table I[135].

Injection locations were also chosen based on the Consensus Recommendations, determined by facial anatomic landmarks. The treating surgeon determined baseline wrinkle severity using the Facial Wrinkle Scale (FWS), as shown in Table II. Three treatment areas were defined: the forehead (frontalis), the glabellar region (corrugator supercilii, procerus, depressor supercilii, orbicularis oculi), and crow's feet (lateral part of the orbicularis oculi). 100-Unit vials of the Botulinum toxin product (*Botox Cosmetic*®, Allergan, Irvine, CA) were diluted to 5 U/0.1 mL for all patients. The exact locations and amounts of the injections were recorded in each subject (Table III), with per-patient totals averaging 64 U with a range of 50-75 U.

The patients were then photographed at rest and during animation as described above immediately post BTX-A injections, and at specific intervals of 1 week, 2 weeks, 4 weeks, 8 weeks, 12 weeks, 16 weeks, 20 weeks and 24 weeks. At each follow-up visit, subjects were also asked to complete the FLO-11, SPA and SGA questionnaires. Additional photographs were taken using standardized cosmetic office digital photography with a Nikon D90 SLR digital camera and Canfield Scientific® lighting equipment (Canfield Imaging Systems, Fairfield, NJ). Using these reference photographs, a second Board-certified plastic surgeon subjectively assessed improvement or worsening of wrinkle appearance, completing the SGA for each time point. Pair of reference and deformed speckle images was created and analyzed using DISC, and displacement maps were generated with incremental displacements at each time point. Changes in muscle contraction were then calculated and corresponding force vector maps were generated.

This study has been approved by Stony Brook University Institutional Review Board (IRB) and Stony Brook Human Subjects Committee IRB (CORIHAS-A; CORIHS#: 2010-0912-R1, study reference #: 152109-5). For this study, Declaration of Helsinki protocols was followed and the participants gave their written and informed consent.

# 3. RESULTS

## *3.1 VECTOR AND VERTICAL DISPLACEMENT MAPS*

FIGURE 3- 2 (A-D) and FIGURE 3- 3 (A-D) display the DISC-generated vector maps for patient 1, corresponding to the motion in the glabellar complex and forehead regions respectively. Vector diagrams illustrate the direction of lines of maximal tension during frowning or raising eyebrows, revealing where the overlying skin is under greatest tension and wrinkles are likely to form. In order to quantify the displacement, which is proportional to the contraction of the underlying muscle, the data for glabellar complex and forehead regions were plotted as

color displacement maps of patient 1 in FIGURE 3- 4 and FIGURE 3- 5 respectively. Contraction strength is quantified in units represented as a color field in two dimensions, the plane of which corresponds to the subject's face. These maps represent the magnitude of muscle contraction. The color intensity scale to the right of each figure ranges from 50 to -50 in the glabellar complex and 50 to -44 in the forehead area. The shades of the color scale are specific to the individual patient (who exhibits a unique muscle contraction profile), but the quantitative units of measurement are absolute and comparable among subjects. Color 'green' in each contour map corresponds to 'zero muscular displacement' or 'no deformation'. Colors corresponding to increasing numbers indicate increasing muscle motion and deformation. 'Red' and 'Navy Blue' correspond to areas of maximum deformation. FIGURE 3- 2 (A) and FIGURE 3- 3 (A) illustrate activation of the glabellar complex by frowning and the forehead region by raising the eyebrows, with color fields representing the muscle contraction strength.

### *3.2 QUANTIFICATION OF MUSCLE CONTRACTION USING DISC*

We quantified the intensity of the muscle contraction and paralysis as a function of time and relative to individual pre-treatment response. The magnitude of displacement distributions (represented by solid black curves) was averaged along the horizontal as shown in FIGURE 3- 6. The data integrated from the glabellar and forehead regions for the six patients is plotted as the percent change of the average intensity of deformation from the baseline over a period of six months, as shown in FIGURE 3- 7 and FIGURE 3- 8 respectively.

FIGURE 3- 7 shows the percent change in the degree of paralysis ("Red line") through which we can track the onset of paralysis and subsequent recovery of muscle function. 'Baseline' is defined at day 0 prior to BTX-A administration. A substantial drop in muscle contraction strength, indicating initial paralysis is seen at 1 week post-treatment. The degree of paralysis

further progresses with maximum decrease in muscle contraction by 94%, 88% and 72% from the baseline in patients 1, 2 and 3 at week 2 respectively. For patients 4, 5, and 6, the maximum paralysis occurs at week 4, at which point muscle activity decreases by 29%, 48% and 80% from baseline. FIGURE 3- 8 shows a decrease in muscle contraction strength of 68%, 68%, 82%, 77%, and 76% from the baseline for patients 1, 3, 4, 5 and 6 respectively at week 2. Patient 2 experienced maximum paralysis at week 1 with 73% decrease relative to the baseline.

Compared to the onset of paralysis, the recovery period for muscle contraction strength is slower, varying in duration from 2-6 months. As seen in FIGURE 3- 7, the majority of patients recovered 100% of glabellar complex contraction by week 12, except for patients 1 and 6 who regained only 80% of initial muscle contraction by that time. In fact, only 80% muscle recovery persisted for patient 6 until week 22. Similarly, FIGURE 3- 8 shows 100% forehead muscle contraction recovery for patients 1, 3 and 4 between 12-16 weeks. Patient 2 recovered the fastest in 8 weeks while patient 6 recovered between 14-22 weeks. Patient 5 was an exception, regaining only 70% of muscle contraction even by the study conclusion at 24 weeks.

We observed in FIGURE 3- 7 and FIGURE 3- 8 that in almost all patients, 100% muscle contraction recovery was followed by a period of either constant muscle contraction or increased contraction, possibly indicating the onset of hyperkinesis [136, 137]. In the glabellar region, the increase in contraction from the baseline ranged from 50% in patient 5 to 400% for patient 2 and remained constant for patient 3. In the forehead region, this increase ranged from 80% in patient 1 to 220% in patient 3 while remained constant in patient 2 for two weeks prior to the end of the study.

## *3.3 FLO-11 AND SGA*

FIGURE 3- 7 and FIGURE 3- 8 also plot the observing plastic surgeon's assessment score (SGA), and the patients' self-reported outcomes (FLO-11 questionnaire) taken during the same follow-up visit. SGA and FLO-11 scores are plotted as the percent change in wrinkle perception from baseline with increasing values indicating fewer wrinkles. Similar trend between DISC and the SGA scores is observed for patients 1, 5 and 6 in the glabellar complex and for patients 5 and 6 in the forehead regions, confirming the correlation between the disappearance/reappearance of wrinkles and the relaxation/recovery of muscular re-innervation. The recovery of muscle contraction precedes the wrinkle reappearance by 4-8 weeks for patients 1-5 in glabellar complex (FIGURE 3- 7) and for patients 1, 3-6 in the forehead region (FIGURE 3- 8). Patient 6 (FIGURE 3- 7) shows a nearly perfect correspondence between DISC and SGA while this lag is 10 weeks for patient 2 in the forehead region. FLO-11 scores remain high over the 6-month period , a trend observed throughout the literature [118] while SGA scores return to the baseline. In most cases, return of visible facial rhytids corresponds to >70% muscle recovery in the glabellar complex and >60% in the forehead region.

### *3.4 DETERMINATION OF THE SITE OF MAXIMUM MUSCULAR TENSION*

A DISC-generated vector map can provide insight into the areas where stress is directed and how it dissipates following the BTX-A treatment, predicting the ideal injection site, as shown in FIGURE 3- 9 (A-B). We compared the locus of injection marked by the physician (black crosses) and predicted by DISC (red dots), by superimposing the baseline vector maps on patients' face for the glabellar (FIGURE 3- 9 (A)) and forehead (FIGURE 3- 9 (B)) areas. The sites marked by DISC are along the lines of maximum magnitude of deformation and where there is a confluence of opposing forces. The value of maximum magnitude can be determined by the color maps.

## 4. DISCUSSION

Certain regions of face are always under constant tension, correlating resting tone to the existence of wrinkles [15]. Every individual has different muscular anatomy, muscle mass, recovery rate and personal perception of the wrinkles appearance. This leads to variability in retreatment frequency as well as optimal site of injection, which could result in undesired outcomes such as drooping eyelids and unsatisfactory aesthetic results. In order to avoid such complications and improve on the efficacy of BTX-A, one should aim to precisely determine (a) the optimal injection location, which can vary among individuals and (b) the time sequence of the muscular paralysis and re-enervation following injection and (c) its correlation to the appearance/disappearance of wrinkles. Since BTX-A treatment is an elective cosmetic procedure, it is important to establish a non-invasive, easily reproducible technique such as DISC that can precisely quantify muscle contraction and is practical for office-based use.

DISC measures the in-vivo displacement patterns in response to natural facial movement (FIGURE 3- 1). The DISC generated vector maps (FIGURE 3- 2 and FIGURE 3- 3) and the corresponding contour maps (FIGURE 3- 4 and FIGURE 3- 5) show the spatial distribution of skin deformation, as well as the direction and magnitude of the applied tension due to the underlying facial musculature. The lines of increased tension also coincide with the position of the prominent wrinkles and may correspond to ideal injection sites (FIGURE 3- 9).

A clinically observed phenomenon directly measured by DISC is that of alternative muscle recruitment in order to carry out facial expressions normally executed by the paralyzed muscle groups. This is seen by comparing the vector diagrams resulting from activation of frontalis muscles in weeks 0 and 1 (FIGURE 3- 3A-B). FIGURE 3- 3 (B) illustrates that at week 1, when the patient is unable to activate the paralyzed frontalis muscle while attempting to raise her

eyebrows, she compensates by activating the orbicularis oculi, zygomaticus major and nasalis muscles. This alternative recruitment starts to diminish by week 4 (FIGURE 3- 3(C)) and completely diminishes by week 16 (FIGURE 3- 3(D)) upon 100% muscle recovery. Similar behavior was seen in all the other patients following complete paralysis.

DISC can precisely quantify the degree of muscle contraction of different muscle groups following BTX-A injection and also monitor the recovery of different muscle groups over time (FIGURE 3- 7, FIGURE 3- 8). DISC can be sensitive to displacements as small as 0.5mm. This makes it more efficient in detecting the onset/offset of facial muscle paralysis compared to the existing subjective measures such as FLO-11 and SGA. The rate of change of SGA and FLO-11 is proportionally much smaller than that of DISC, and does not appear to go below the baseline while DISC can detect the increased muscle contraction (hyperkinesis) following 100% muscle recovery. Even though this behavior is observed for both glabellar and forehead regions, there does not seem to be a correlation between the rates of paralysis and recovery of the two regions. For example, patient 6 only recovered 80% of contraction in the glabellar region while full recovery is observed in the forehead region, whereas patient 5 recovered fully in the forehead region and only 70% in the glabellar region by the end of the study.

In most patients the forehead region (FIGURE 3- 7) experiences faster rate of muscle paralysis and recovery compared to the glabellar complex (FIGURE 3- 8). Hence, patients may require retreatment in one region sooner than another. By tailoring to individual facial muscle profiles, DISC could further optimize the unit dosage and number of office visits, potentially curtailing both discomfort and cost.

The data presented here represent the results of a 6-patient pilot study. The small sample size and subject heterogeneity limited our ability to perform detailed statistical analysis of our results. However, this study sufficiently demonstrates the ability of DISC to add a quantitative dimension to our understanding of cosmetic outcomes measures. Consequently, DISC can address previously unanswered questions about the immediate and longitudinal effects of BTX-A on the facial musculature and contribute greatly to what is already known about the cosmetic use of BTX-A.

## 5. CONCLUSION

DISC can precisely quantify the degree of contraction of different muscle groups following BTX-A injection and monitor the recovery of different muscle groups over time. It is more sensitive than existing subjective measures in detecting the onset/offset of facial muscle paralysis, and by using vector analysis it determines lines of maximal stress that may correspond to ideal injection sites.

DISC analysis has the potential to contribute greatly to what is already known about the cosmetic use of BTX-A, by adding a quantitative dimension to our understanding of cosmetic outcomes measures and addressing previously unanswered questions about the immediate and longitudinal effects of BTX-A on the facial musculature. It has countless applications in the cosmetic arena, and its ease of use facilitates its translation to the clinic. The setup requires only a digital camera and a computer equipped with DISC software, and the technique is entirely non-invasive and non-contact. The clinical adaptation of DISC can revolutionize cosmetic BTX-A injections by tailoring treatment to a patient's facial muscle profile, potentially minimizing injection amount and frequency while optimizing cosmetic benefit.

## 6. FIGURES AND TABLES

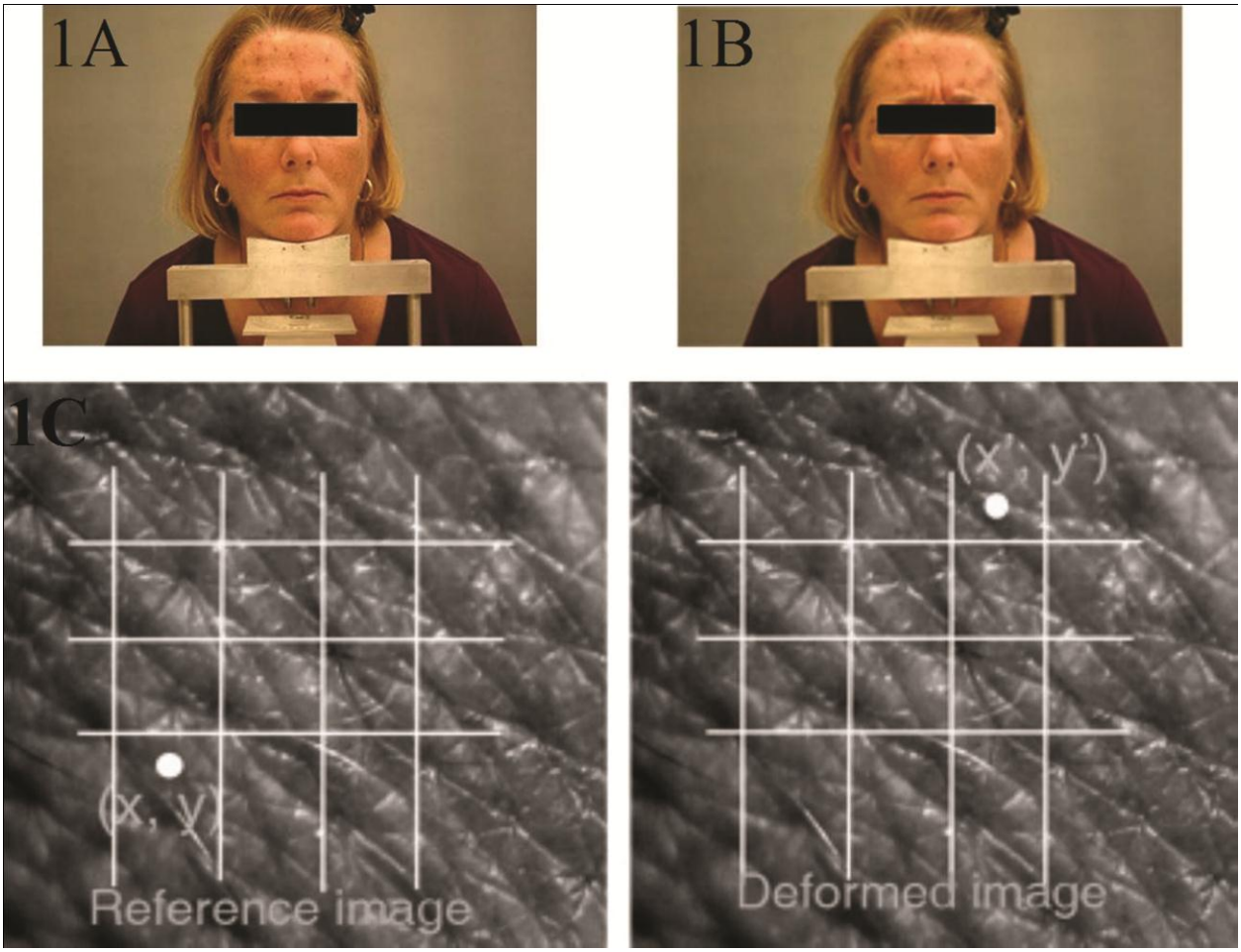


FIGURE 3- 1: [BOTULINUM TOXIN TYPE-A] REFERENCE AND DEFORMED IMAGES: (1A) PATIENT'S FACE AT REST (REFERENCE IMAGE); (1B) PATIENT FROWNING (DEFORMED IMAGE); (1C) A SCHEMATIC DIAGRAM OF THE DIGITAL IMAGE CORRELATION ALGORITHM [13].

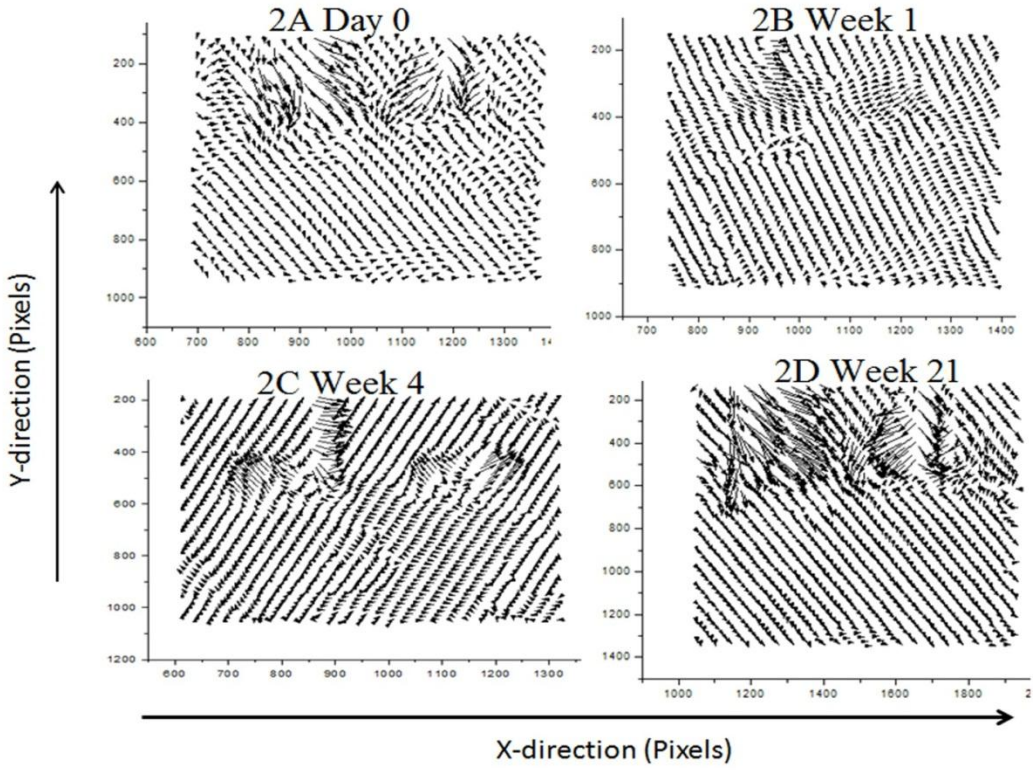


FIGURE 3- 2: [BOTULINUM TOXIN TYPE-A] VECTOR DIAGRAMS GENERATED BY DISC FOR GLABELLAR AREA OF THE PATIENT WHILE FROWNING. PRE-TREATMENT (2A) DAY0; POST-TREATMENT (2B) WEEK1 (2C) WEEK2 (2D) WEEK 21

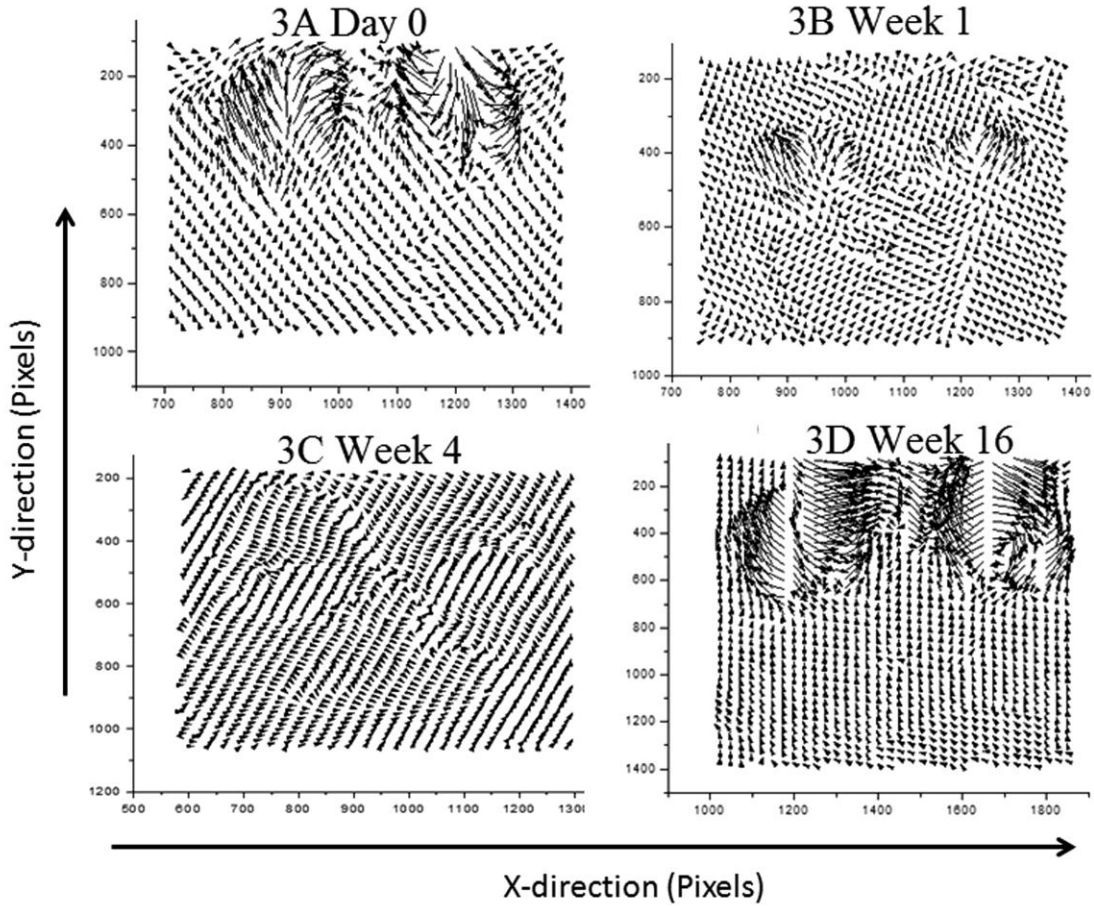


FIGURE 3- 3: [BOTULINUM TOXIN TYPE-A] VECTOR DIAGRAMS GENERATED DISC FOR FOREHEAD REGION WHILE RAISING EYEBROWS. PRE-TREATMENT (3A) DAY0; POST-TREATMENT (3B) WEEK1 (3C) WEEK2 (3D) WEEK 16.

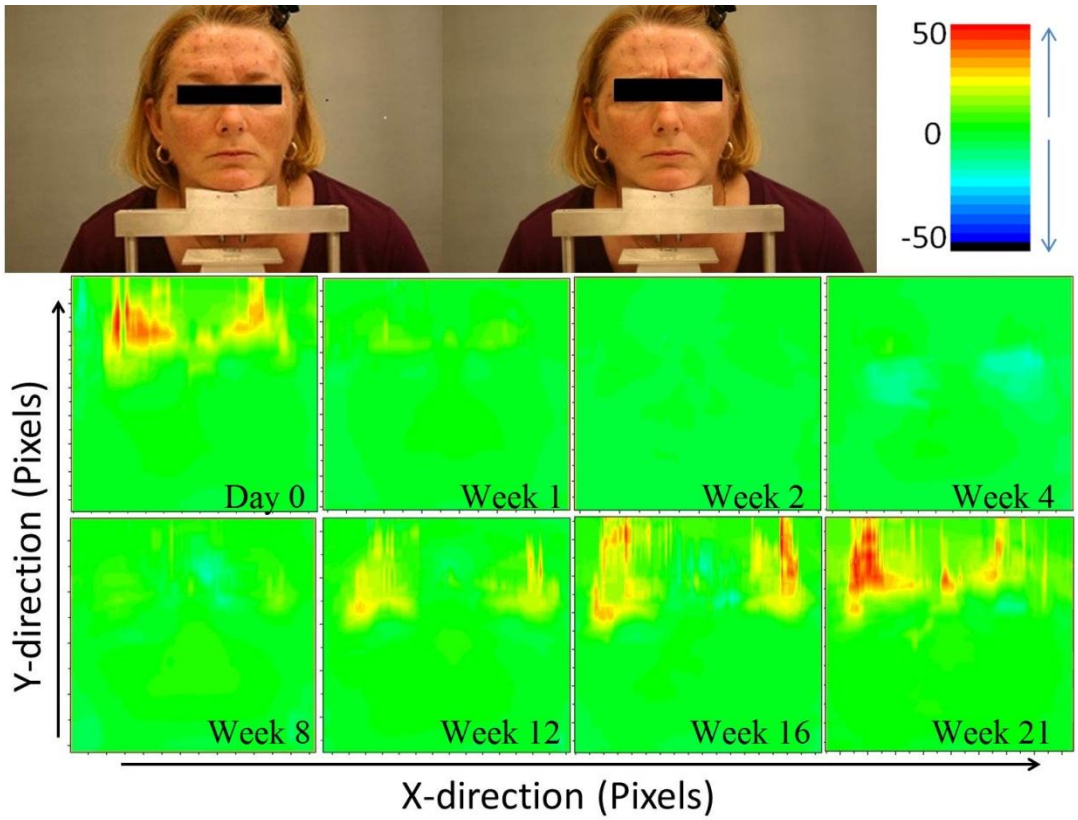


FIGURE 3- 4: [BOTULINUM TOXIN TYPE-A] VERTICAL PROJECTION OF DISPLACEMENT MAPS IN THE GLABELLAR REGION OF THE PATIENT PRIOR TO THE TREATMENT AND AT SPECIFIC FOLLOW UP TIME POINTS. UNIT: PIXEL. THE COLOR DESIGNATES THE RELATIVE DISPLACEMENT AMPLITUDE. SCALE OF COLOR INTENSITY BAR: 50 TO -50. GREEN: ZERO/NO DISPLACEMENT. RED AND NAVY BLUE: AREAS OF MAXIMUM STRESS/DEFORMATION. NOTICE THE SUDDEN DECAY OF THE DISPLACEMENT AMPLITUDE IN WEEK 1 AND THEN GRADUAL RECOVERY AFTER WEEK 4 TO FULL RECOVERY BY WEEK 21.

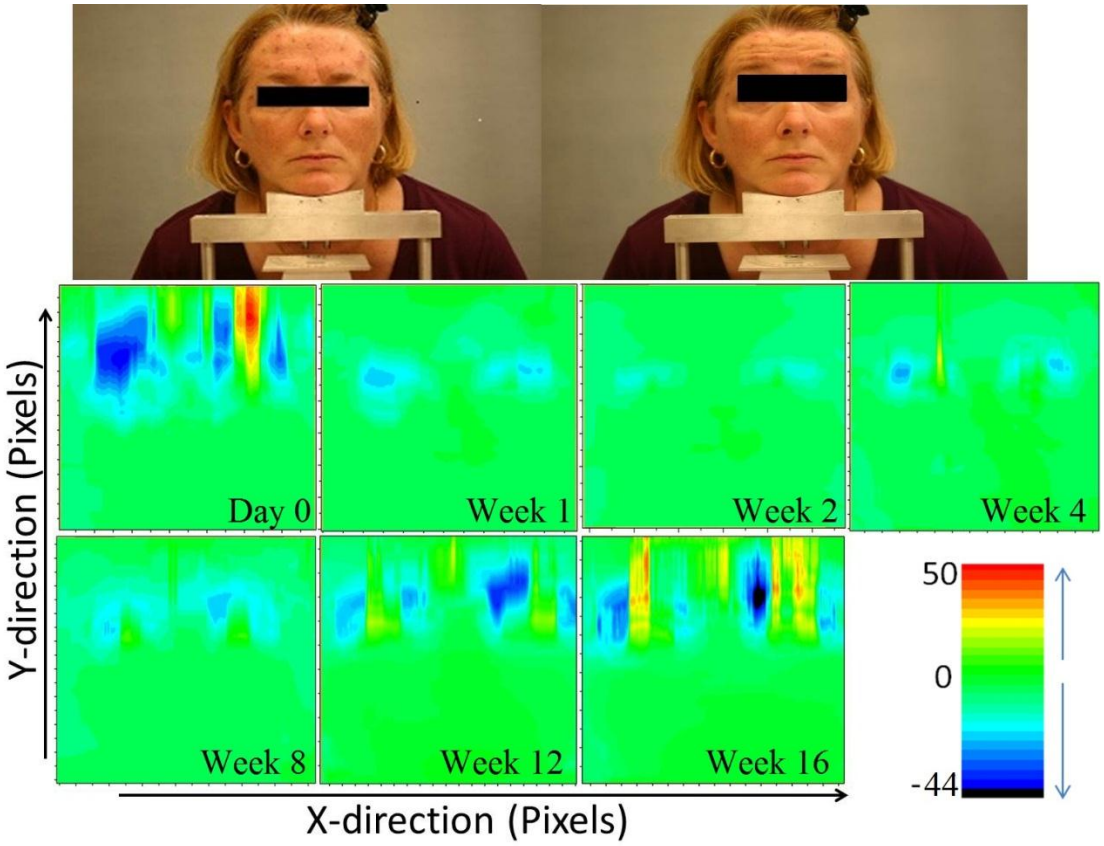


FIGURE 3- 5: [BOTULINUM TOXIN TYPE-A] VERTICAL PROJECTION OF DISPLACEMENT MAPS IN THE FOREHEAD REGION OF THE PATIENT PRIOR TO THE TREATMENT AND AT SPECIFIC FOLLOW UP TIME POINTS. UNIT: PIXEL. THE COLOR DESIGNATES THE RELATIVE DISPLACEMENT AMPLITUDE. SCALE OF COLOR INTENSITY BAR: 50 TO -44. GREEN: ZERO/NO DISPLACEMENT. RED AND NAVY BLUE: AREAS OF MAXIMUM STRESS/DEFORMATION. NOTICE THE SUDDEN DECAY OF THE DISPLACEMENT AMPLITUDE IN WEEK 1 AND THEN GRADUAL RECOVERY AFTER WEEK 4 TO FULL RECOVERY BY WEEK 16.

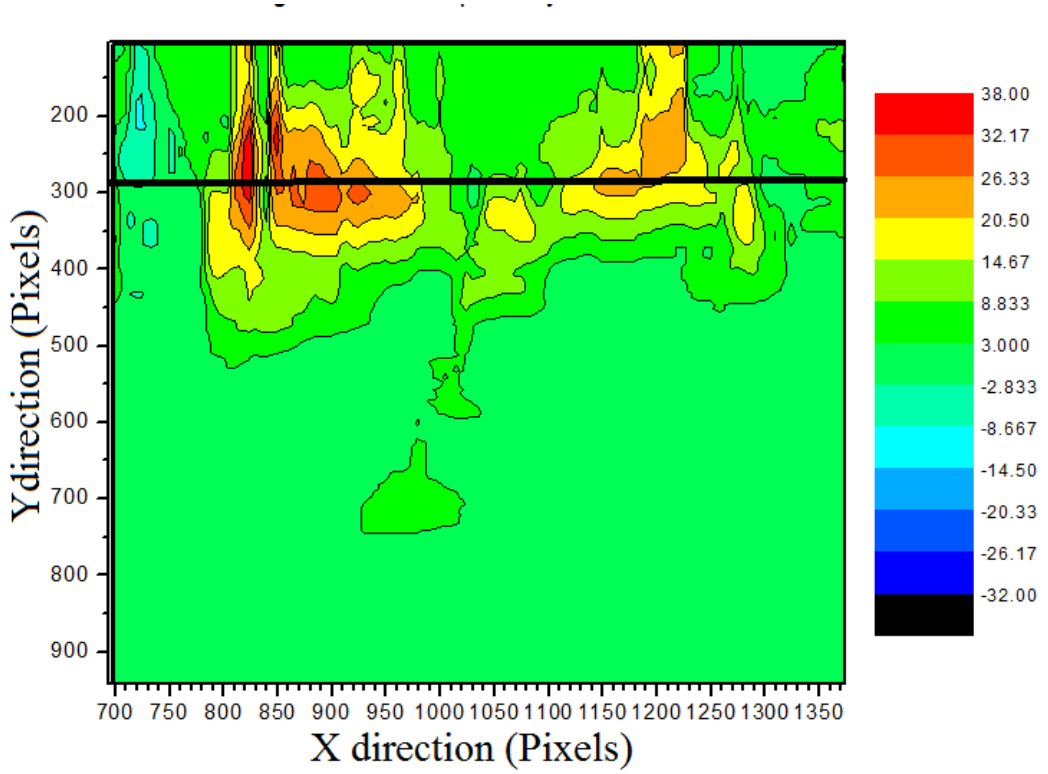


FIGURE 3- 6: [BOTULINUM TOXIN TYPE-A] AVERAGE OF INTENSITY OF DISPLACEMENT DISTRIBUTIONS ALONG THE LOCUS OF POINTS BY DRAWING A HORIZONTAL LINE.

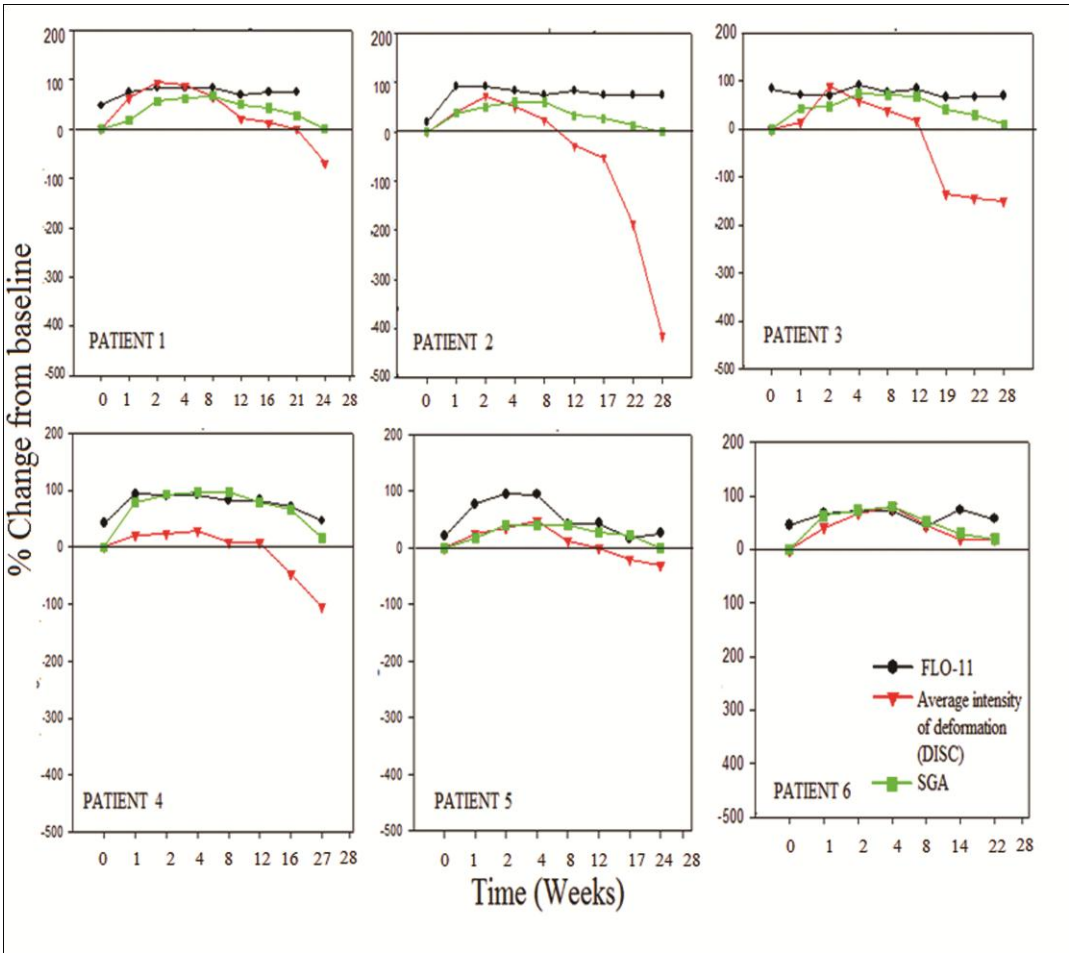


FIGURE 3- 7: [BOTULINUM TOXIN TYPE-A] (GLABELLAR COMPLEX) FLO-11, SGA AND AVERAGE INTENSITY OF DEFORMATION (DISC) PLOTTED AS PERCENTAGE CHANGE FROM THE BASELINE VERSUS TIME (IN WEEKS) FOR ALL THE SIX PATIENTS.

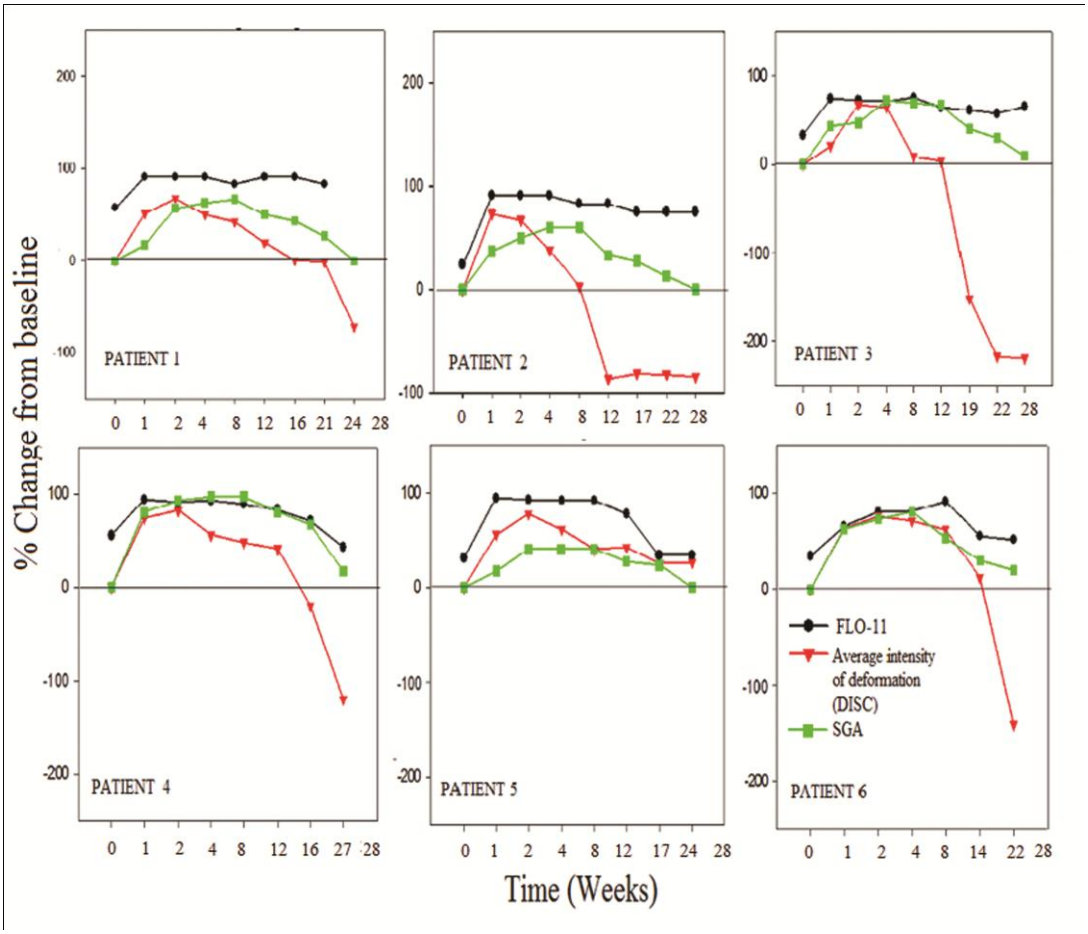


FIGURE 3- 8: [BOTULINUM TOXIN TYPE-A] (FOREHEAD REGION) FLO-11, SGA AND AVERAGE INTENSITY OF DEFORMATION (DISC) PLOTTED AS PERCENTAGE CHANGE FROM THE BASELINE VERSUS TIME (IN WEEKS) FOR ALL THE SIX PATIENTS.

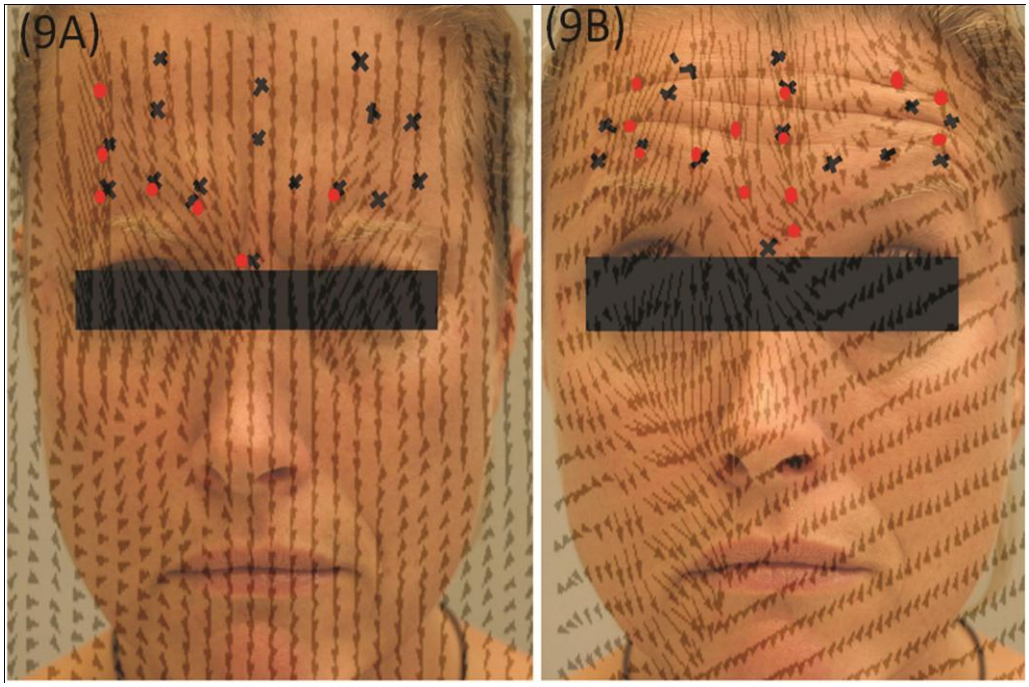


FIGURE 3- 9: [BOTULINUM TOXIN TYPE-A] (PATIENT4) VECTOR DIAGRAM OVERLAY ON THE FACE WHILE (9A) FROWNING (GLABELLAR) (9B) RAISING EYEBROWS (FOREHEAD). BLACK CROSSES ARE THE SITES WHERE BTX-A WAS INJECTED BY THE PHYSICIAN. RED CIRCLES INDICATE THE REGIONS WHERE THE DISC GENERATED VECTORS OF MAXIMAL TENSION PREDICT THE SITE OF INJECTION.

| Region | Muscles | Injection Number | Injection Volume |
|---|---|---|---|
| Glabellar Complex | Corrugator supercilii, procerus, depressor supercilii, orbicularis oculi | 5-7 | F: 10-30U<br>M: 30-50U |
| Forehead | Frontalis | 4-10 | F: 6-15U<br>M: 6->15U |
| Crow's Feet | Orbicularis oculi (lateral part) | 2-5(per side) | F: 10-30U<br>M: 20-30U |

TABLE 3- 1: TABLE I. [BOTULINUM TOXIN TYPE-A] INJECTION NUMBER AND LOCATION BASED ON THE 2008 PLASTIC AND RECONSTRUCTIVE SURGERY SUPPLEMENT CONSENSUS RECOMMENDATIONS [24]. (F=FEMALE, M=MALE, U=UNITS)

| | Age | Initial Facial Wrinkle Scale (FWS) Score | | |
|---|---|---|---|---|
| | | Glabellar Complex | Forehead Region | Crow's Feet |
| 1 | 51 | 1 | 1 | 1 |
| 2 | 49 | 1 | 1 | 1 |
| 3 | 53 | 1 | 2 | 1 |
| 4 | 42 | 2 | 2 | 1 |
| 5 | 30 | 1 | 1 | 1 |
| 6 | 60 | 3 | 3 | 3 |

TABLE 3- 2: [BOTULINUM TOXIN TYPE-A] SUBJECT DEMOGRAPHICS. INITIAL WRINKLE SEVERITY SUBJECTIVELY ASSESSED USING THE FACIAL WRINKLE SCALE (0=NONE, 1=MILD, 2=MODERATE, 3=SEVERE).

| Patient | Glabellar Complex | | Forehead Region | | Crow's Feet | | Total |
|---|---|---|---|---|---|---|---|
| | Muscle Mass | Injection Volume | Muscle Mass | Injection Volume | Muscle Mass | Injection Volume | |
| 1 | Medium | 20 | Medium | 25 | Small | 30 | 75 |
| 2 | Medium | 15 | Medium | 30 | Small | 15 | 60 |
| 3 | Medium | 15 | Medium | 35 | Medium | 25 | 75 |
| 4 | Medium | 17 | Medium | 27 | Small | 16 | 60 |
| 5 | Small | 15 | Small | 17 | Small | 18 | 50 |
| 6 | Large | 12 | Large | 23 | Large | 20 | 55 |

TABLE 3- 3: [BOTULINUM TOXIN TYPE-A] MUSCLE MASS (SMALL, MEDIUM, LARGE) AND INJECTION VOLUME (UNITS) PER LOCATION IN EACH PATIENT.

# CHAPTER 4

# AN ANALYSIS OF FACIAL NERVE FUNCTION IN PATIENTS WITH VESTIBULAR SCHWANNOMAS USING DIGITAL IMAGE SPECKLE CORRELATION

## 1. INTRODUCTION

Vestibular schwannomas (VS) represent an uncommon benign tumor arising from the nerve sheath of either the inferior or superior vestibular component of the 8th cranial nerve. The term "vestibular schwannoma" involves the vestibular portion of the 8th cranial nerve and arises from Schwann cells, which are responsible for the myelin sheath in the peripheral nervous system. The $8^{th}$ cranial nerve or the vestibulocochlear nerve (auditory vestibular nerve) is responsible for transmitting sound and equilibrium (balance) information from the inner ear to the brain. It consists of the cochlear nerve, carrying information about hearing, and the vestibular nerve, carrying information about balance. Over a century ago, unilateral hearing loss was identified as the most common presentation for these tumors (Malis). In large series of patients with VS, over 95% were found to have unilateral sensorineural hearing loss [138]. Symptoms such as tinnitus, vertigo, and disequilibrium were also present, but occurred much less frequently. [138]. Despite the close anatomic proximity of the facial nerve to VS within the internal auditory canal, less than 5% of all VS patients have documented loss of facial nerve function at the time of diagnosis [139]. Most facial nerve dysfunction with VS has been associated with large tumors (greater than 3cm) [138]. It has been proposed that the auditory nerve is more sensitive to early dysfunction, and thus tumors of more modest size, based upon segmental vascular compromise. The facial nerve, sub serving a broader range of function (i.e., facial movement, somatosensory and secretomotor function) is larger, has more myelinated fibers, and is therefore presumed to be more structurally immune to the compressive nature of VS than the auditory nerve.

At present, MRI scanning represents the gold standard for the identification of VS. It is definitively diagnostic, non-invasive, but expensive. Other non-invasive tests such as CT,

audiometry, electronystagmography, and auditory brainstem evoked responses, are helpful but lack specificity in terms of VS diagnosis. Facial electromyography (EMG) is a well-established technique to detect facial muscle activity in response to electrical or mechanical stimulation of the facial nerve [140-145]. Continuous facial EMG monitoring intraoperatively has proven to be of significant value in identifying and demonstrating the structural integrity of the facial nerve [141]. However, facial EMG's in the preoperative setting is an invasive and painful diagnostic method that furnishes qualitative information on facial function but lacks the ability to quantify the degree of facial nerve damage. Colletti et al. used an alternative technique called facial nerve antidromic potential (FNAP) to monitor the facial nerve and to determine postoperative facial function [146]. Although this technique is more sensitive in providing quantitative information and has some predictive value for post-operative facial function, it remains an invasive test.

In 1985, House and Brackman introduced a visual analog grading scale for facial motion which remains the current standard for post-operative assessment of facial nerve function [147]. The House-Brackman (H-B) scale is limited by inter-observer variability and has minimal applicability in the preoperative VS patient. Vrabec et al. [148] recently presented an updated version of the H-B scale known as facial nerve grading scale (FNGS) 2.0. Based upon visual observation, precise quantification of facial paralysis remains problematic as with the original H-B scale. The human eye cannot detect minute deficits in facial movement. Thus, there is a need for a non-invasive and consistent method of determining the degree of facial nerve impairment in individuals with VS. Precise quantification of facial nerve paresis in the VS population may be of importance in early diagnosis of VS as well as allowing for more precise post -operative monitoring of facial nerve function.

The primary objective of this article is to test the hypothesis that VS's influence facial nerve motor function on a level often undetectable by the human eye during routine clinical examination. These subtle changes to facial nerve motor function may be elucidated through a novel technique known as Digital Image Speckle Correlation (DISC). DISC is a non-invasive technique that tracks and characterizes displacement of a point/speckle on the specimen surface. Guan et al.[125] implemented this technique for clinical studies to measure the mechanical properties of rat skin. They used the skin pores as natural speckles, to evaluate the deformation field of skin and deduce its mechanical properties. In humans, the facial skin is directly attached

to the muscles through the superficial musculoaponeurotic system (SMAS). Afriat et al.[134] demonstrated that by tracking the vector displacement of the skin pores one could actually obtain a vector map of the underlying muscle motion [15]. Pamudurthy et al.[149], demonstrated that this vector field characterizing the deformation of face is sufficiently unique for each individual, such that, it was proposed as a more accurate method for identification than direct comparison of photographic images. In a recent study it was shown that DISC could be used to quantitatively determine and monitor the onset and recovery of facial paralysis inflicted by Botulinum toxin type A on face [150].

DISC analyzes two photographic images taken before and after skin deformation during facial expression (Smile, frown, blink) in order to quantitatively correlate the dynamics of individual facial pores to produce a vector map characteristic of facial motion. DISC can detect the lines of tension generated by activated muscle groups and calculate the strength of contraction. In this study we compare the quantitative facial nerve motor function of patients with VS's who are untreated, treated with surgery, or treated with radio surgery, to a control group of individuals with no neurologic dysfunction. In addition to providing precise quantitative data, this technology may have potential applications for medical diagnosis and prognosis in individuals with VS by comparing the patients "normal" functioning side of the face with the "affected side".

## 2. METHODS

### *2.1 EXPERIMENTAL PROTOCOL*

Twenty-nine (n=29) vestibular schwannoma patients, age 22-84 years who have been evaluated for vestibular schwannomas over the past aprox.10 years and who have had surgical resection or gamma knife radiosurgery for an vestibular schwannomas >1 year were prospectively consented and recruited. Individuals with history of stroke affecting the face; history of Bell's palsy; and history of facial surgery or trauma were excluded from the study. Fourteen (n=14) healthy volunteers, age 18-66 years , who in addition, also had no history of vestibular schwannomas diagnosis, were consented and included as a control("normal") population. A brief medical history was obtained and a review of the cranial nerves was performed by the physician for the patients and healthy volunteers. Each subject positioned their chin on a specially-designed head

stabilizer, standardizing face position and camera distance. Series of photographs were taken using a 6.3 megapixel CMOS sensor based Canon DS6041 camera with the face at rest and engaging the desired muscle group by smiling lightly. Each subject's photographs were coded with a subject identifier. Pairs of reference and deformed speckle images were created and analyzed using DISC, and displacement maps were generated with incremental displacements at each time point. Changes in muscle contraction were then calculated and the corresponding force vector maps were generated.

This study has been approved by Stony Brook University Institutional Review Board (IRB) and Stony Brook Human Subjects Committee IRB (CORIHAS-A; CORIHS#: 2009-0796-R2, study reference #: 80026-5). For this study, Declaration of Helsinki protocols was followed and the participants gave their written and informed consent.

## *2.2 THE DISC METHOD*

The DISC method, also known in earlier studies, as Digital Speckle Photography, is a well-established technique that has been used for past 30 years in the analysis of stress and fracture dynamics in materials [126-133]. The technique is based on the analysis of changes in the distribution patterns of a collection of light reflecting speckles attached to a material. The early papers were focused on micro/nano scale defects in metals and relied on spraying nanoparticles on surfaces which were then analyzed using lasers or electron microscopy [151, 152].

The basic setup of DISC consists of a digital camera (FIGURE 4- 1a), mounted on a track (FIGURE 4- 1b) at a fixed distance from a head and chin support (FIGURE 4- 1c), which allows the alignment of the camera with a specific region of the face. As shown in FIGURE 4- 2, two serial high resolution images are taken, one with the patient at rest/no motion (FIGURE 4- 2A) and the second after a slight smiling motion (FIGURE 4- 2B) producing a "reference" and a "deformed" image respectively. These images are divided into subsets of equal pixel content, represented by a set of planar (x, y) coordinates. The image contrast in each subset is provided by the density of skin pores. The intensities in the baseline/ reference and deformed images are compared and correlated in order to identify the translated region of each pixel subset in the second picture (x*, y*) (FIGURE 4- 2C). The two images are matched subset by subset and the

coordinate difference between intensities of the two matched subsets gives the average displacement vector corresponding to skin deformation [125, 149].

The cross-correlation function (S) is computed as:

$$S\left(x, y, u, v, \frac{\partial u}{\partial x}, \frac{\partial u}{\partial y}, \frac{\partial v}{\partial x}, \frac{\partial v}{\partial y}\right) = 1 - \frac{\sum I(x,y) * I^{*}(x^{*}, y^{*})}{\sqrt{\sum I(x,y)^{2} * \sum I^{*}(x^{*}, y^{*})^{2}}}, \qquad (1)$$

Where I (x. y) and I*(x*, y*) are the intensities at the corresponding points and the summation within the correlation function is over the entire subset and the baseline and shifted coordinates are related by,

$$x^{*} = x + u, \qquad y^{*} = y + v;$$

A quantitative color and vector map of the facial displacement can then be obtained by plotting the displacement vectors, or the vector coordinates, corresponding to each region of the face.

## *2.3 QUANTIFYING THE DISPLACEMENT OR DEFORMATION FIELD*

DISC generated displacement maps represent the way a subject's face deforms. We obtain magnitude ($r=\sqrt{x^2+y^2}$) and orientation (theta) fields from the vector displacement maps. Magnitude fields plotted as a color displacement map represent the magnitude of facial muscle deformation/contraction. FIGURE 4- 2D shows a typical color map where the red color indicates the increased motion or deformation corresponding to the activated muscle group (smile in our case) and green color indicates 'zero or no deformation'. The quantitative deformation can be calculated by averaging the area of deformation along the horizontal (black solid line drawn across the smile curves of the subject) on both right and left side of the face. This process is repeated for three sets of reference and deformed images to generate standard deviation and quantified average deformation on right and left side of an individual subject. Finally, to compare the deformation in healthy volunteers (control group) with no surgery (untreated group with tumor), gamma knife and resection population (treated group), the percentage area of deformation or muscle contraction between the right and left side (|R-L|/R) of the face can be measured for each subject. Mean percentage area of deformation between right and left side of the face (|R-L|/L) can be calculated for each group along with standard deviation.

## *2.4 STATISTICAL ANALYSIS*

Two-tailed P value was calculated with 95% confidence interval using an unpaired t-test (Graph Pad version 5) and column bar graphs of (|R-L|/R) were plotted between each group. Pearson's correlation test was performed to determine the significance of any correlation between the size of the tumor and the percentage area of deformation (|R-L|/R). Two tailed p value was also determined with 95% confidence interval (Graph Pad version 5). P value < 0.05 was considered significant.

## 3. RESULTS

### *3.1 ESTABLISHING THE DEGREE OF FACIAL ASYMMETRY IN THE CONTROL GROUP*

Multiple set of reference and deformed images were taken for each control subject. A color displacement map was generated from the first set of reference and deformed images and overlapped on the first deformed image (FIGURE 4- 3A). Corresponding to that color map, the average area of deformation for the right and left sides of the face were plotted (FIGURE 4- 3D). In order to probe the reproducibility of the method, a similar overlay of the color map (FIGURE 4- 3B, FIGURE 4- 3C) was done for the second and third set of images. Corresponding average area of deformation for the second and third set of images (FIGURE 4- 3E, FIGURE 4- 3F) was also plotted. The figures indicate that the average area of deformation between right and left side of an individual's face are nearly identical, and the error in the area calculations is small. FIGURE 4- 3G plots the average deformation/displacement on the right side versus the left side of the face. From FIGURE 4- 3G, we can deduce that in the control population the displacement between the left and right side of the face is related by a relationship, which corresponds to a straight line (y=mx+b) of unity coefficient. Hence, in control population, the motion of the left and right side of the face is relatively symmetric.

### *3.2 QUANTITATIVE DISC ANALYSIS OF UNTREATED (NO SURGERY) POPULATION*

Thirteen untreated patients (n=13), age 42-79 years; diagnosed with vestibular schwannomas tumors of variable sizes ranging from 1-12mm were designated as the 'no surgery' group. In FIGURE 4- 4A we show the overlay of the DISC generated color displacement map on the deformed image (slight smile) of a typical patient diagnosed with VS (3mm tumor, on the right side of her face). From the photographic image alone it is difficult to discern whether there is an impairment of motion. With the overlay of the DISC generated map (FIGURE 4- 4A), in contrast

to the control patient (FIGURE 4- 3A), one can clearly see that there is a large imbalance in the motion between the two sides of the face, which is otherwise undetectable by human eye. In FIGURE 4- 4(D) we plot the deformation on the left and right sides, where the large asymmetry becomes very clear. In FIGURE 4- 5(A) we compare the percentage area change in the muscle contraction between right and left side of the face, (|R-L|/R) , for the control and the untreated group of subjects, from which we can see that the asymmetry in untreated group is five times larger than the control, with a significance level of $p<0.01$.

It is also interesting to note that 9 out of the 13 patients exhibited lack of motion on the side *opposite* the tumor, while 3 patients had lack of motion on the *same* side as the tumor. This sample though is too small to draw conclusions, but it still does highlight the impact of tumor on the facial symmetry. In FIGURE 4- 5D, we also plot the average amplitude of the motion in control group and compare it to the average amplitude of the side with the maximum motion in the patients with neuroma. From the figure, we find that in the presence of a tumor, the untreated group presents with overall less motion compared to the control population. Hence, hypokinesia in addition to asymmetry may be associated with VS.

### *3.3 QUANTITATIVE DISC ANALYSIS OF GAMMA KNIFE RADIOSURGERY TREATED POPULATION*

Five (n=5) VS patients (age 61-65 years, tumor size 6-24mm) whose tumor was treated with gamma knife radiosurgery were studied and labeled 'gamma knife' group. The overlay of DISC generated color displacement map (FIGURE 4- 4B) on patient's (6mm tumor on left side) deformed image clearly shows the asymmetry of muscle contraction in patient's right and left side of the face. FIGURE 4- 4E shows a higher average area of deformation on the right side which is opposite to the side of tumor location. We see this increased muscle motion on the *opposite* side of the tumor in 4 out of 5 gamma knife treated patients. In FIGURE 4- 5B, we plot the percent muscle contraction area change between the right and left side for these patients and we observe that it is 15 times higher than the control population ($P<0.05$). In FIGURE 4- 5D, we observe that the amplitude of the maximum muscle activity is much smaller in the gamma knife treated patients than in the control group, or even in the untreated/pre-surgical group. These results indicate that treatment with gamma knife surgery may result in a reduction of motion and an increase in asymmetry ($p<0.05$).

### *3.4 QUANTITATIVE DISC ANALYSIS OF RESECTION TREATED POPULATION*

Eleven (n=11) VS patients (aged 22-84 years, tumor size 5-38mm) treated with surgical resection were considered as post-op 'resection' group. FIGURE 4- 4C shows the overlap of muscle contraction map on patient's deformed image (surgical resection of a 20mm tumor on right side of the face). The quantified average area of deformation is larger on left side of the face or the *opposite* side of tumor location (FIGURE 4- 4F). This increased muscle contraction on the *opposite* side of the tumor location was seen in 7 out of 11 patients whereas; the magnitude of muscle contraction was higher on the *same* side as the tumor location in the remaining 4 patients. FIGURE 4- 5C compares the percent muscle contraction area change between right and left side of the control and resection treated population. This change in the resection group is ~ 10 folds higher than the control group ($P<0.0001$). In FIGURE 4- 5D, we observe that the amplitude of the maximum muscle activity is the highest in the resection group compared to control, untreated or gamma knife population indicating that resection may result in an increased motion on one side of the face thus, increasing the asymmetry ($p<0.05$).

### *3.5 TUMOR SIZE*

FIGURE 4- 6 (A, B and C) show the correlation between the percent muscle contraction area change between the two sides of the face and the tumor size for the 'no surgery/untreated' group, the 'gamma knife surgery' treated group and the 'surgical resection' group respectively. No significant correlation ($p=0.4$ for 'no surgery/untreated'; $p=0.6723$ for the 'gamma knife radiosurgery'; $p=0.7262$ for the 'surgical resection' group; Pearson's correlation test) was observed with the tumor size for any of the groups.

## 4. DISCUSSION

DISC technique was recently shown [150] to be an effective, non-invasive method for detection of muscular enervation and paralysis. Here we show that this technique may also be used as a screen for VS, which frequently affects the facial nerve and results in abnormal muscular motion.

Facial movements result from a group of fairly complicated, coordinated set of displacements between multiple muscles. By applying DISC for the analysis of the facial movement involved in producing a slight smile, we were able to demonstrate that control (normal) individuals showed

marked consistency in movement of facial muscles bilaterally (FIGURE 4- 3). The intensity of displacement, as well as the specific groups of muscles involved can vary greatly between different individuals. However, the displacement corresponding to a given motion is unique to an individual and extremely reproducible (FIGURE 4- 3). In fact, Pamudurthy et al. [149] have shown that DISC could be used as an alternative method for facial recognition, which they showed to be more accurate than optical image analysis.

Our results strongly support the concept that even small vestibular schwannomas cause an alteration in facial nerve function which can be detected by an abnormal pattern of muscle motion. We found in our pilot study that untreated VS patients present with abnormalities in the muscle motion. 9 out of the 13(70%) untreated VS patients presented with hypo kinesis *on the opposite side* of the tumor, and a corresponding increase on the tumor side. This result was unexpected and indicates that paralysis of the facial nerve is not an initial symptom of the tumor. There are approximately 4000 individuals diagnosed annually with sensorineural hearing loss in the US[153], the majority of who undergo MRI scanning to rule out the potential of harboring a vestibular schwannomas. The radiologic yield is decidedly low, with less than 5 % revealing a tumor origin for their hearing loss. DISC represents the potential to be used as a screening test for these patients, eliminating in the majority, the need for costly and likely unnecessary MRI scanning. It is also possible with a larger cohort, that DISC may be able to define those tumors that are more likely to affect facial nerve function, thus directing decision making in the treatment of these patients. Following surgery, either resection or gamma knife, 11 out of the 16 patients presented with *reduced* motion on the *side of the tumor* and *increased* motion on the *opposing side*, when forming a smile. No correlation was found between the size of the tumor or the surgical method used to treat it and either the magnitude or the direction of the asymmetry.

Despite the large variation in magnitude of the muscular motion required to produce smile among the normal population, we found it useful to compare the average intensity of the motion on the side of the tumor and on the opposing side. From FIGURE 4- 5D we find that prior to surgery, the magnitude of motion is twofold (47%) lower on the opposing side than in the control group, and slightly lower (25%) than the control group on the side of the tumor ($p<0.05$). The largest differences are observed among the treated population. From the data, we can see that even on the opposite side of the tumor, where the motion is maximal, those who had

Gamma Knife treatment, have much less movement (fourfold less, 70%) than the control group, whereas those who had resection show a significantly larger degree of motion (1.5fold, 35%) than the control group. Patients treated with gamma knife showed significantly less motion on the side of the tumor post resection relative to the control group ($P<0.05$) . Thus, facial nerve recovery can be easily assessed and quantified in the patients who have undergone surgical resection or gamma knife radiation. These results clearly indicate that even though presence of VS results in abnormal muscular displacement patterns, the treatment alters the pattern but does not restore it to that observed in the control population. Furthermore, the nature of the alteration seems to be correlated to the type of treatment, providing more input to the patient and physician in selecting the nature of the treatment.

These facial muscle groups are also known to be involved in expressions involving the lower face, such as smiling. In the early stages, the abnormal motion in patients diagnosed with VS cannot be detected by human eye or physician's clinical observations, since impairment on one side can be compensated by enhanced motion on the other. However, since DISC is able to quantify the motion of different muscle groups on each side of the face separately, the resulting asymmetry in the muscular motion can easily be detected by asking the patient for form a simple facial movement such as a smile. It is possible that DISC will prove valuable in predicting to what degree and over what time course, facial nerve function will return in the treated population of VS individuals. DISC offers a novel, noninvasive, inexpensive means of assessing facial nerve function with the potential to aid in the diagnosis and treatment of vestibular schwannomas. It may ultimately prove beneficial in reducing the need for MRI scanning in patients with hearing impairment.

## 5. CONCLUSION

We have shown that the DISC technique can detect the presence of VS by observing asymmetric displacements in the facial muscles. The degree of asymmetry was not related to the size of the tumor, but the largest motion occurred in most patients on the side of the tumor prior to any treatment. Following treatment the trend reversed, with the larger motion occurring on the side opposite the tumor. Hence the technique of DISC provides a non-invasive method of monitoring both the progression of the VS, as well as post-surgical recovery following treatment.

## 6. FIGURES

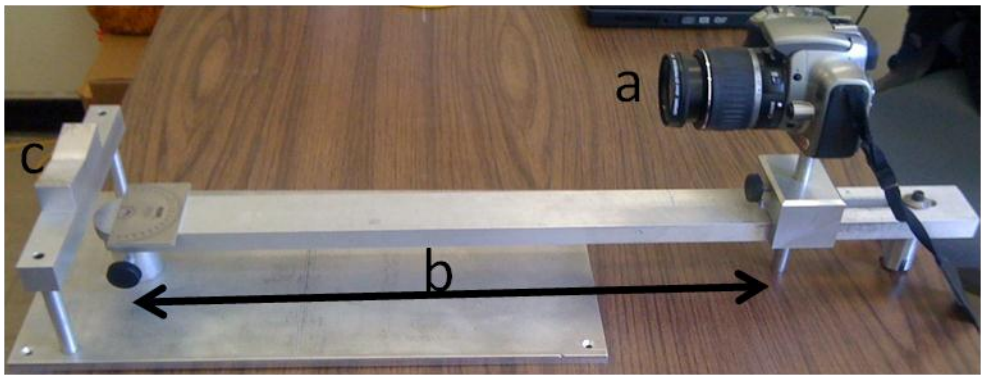


FIGURE 4- 1: SCHEMATIC OF A DISC SET UP. (A) CAMERA (B) TRACK HOLDING THE CAMERA AT A FIXED DISTANCE (C) STAND FOR PLACING THE CHIN

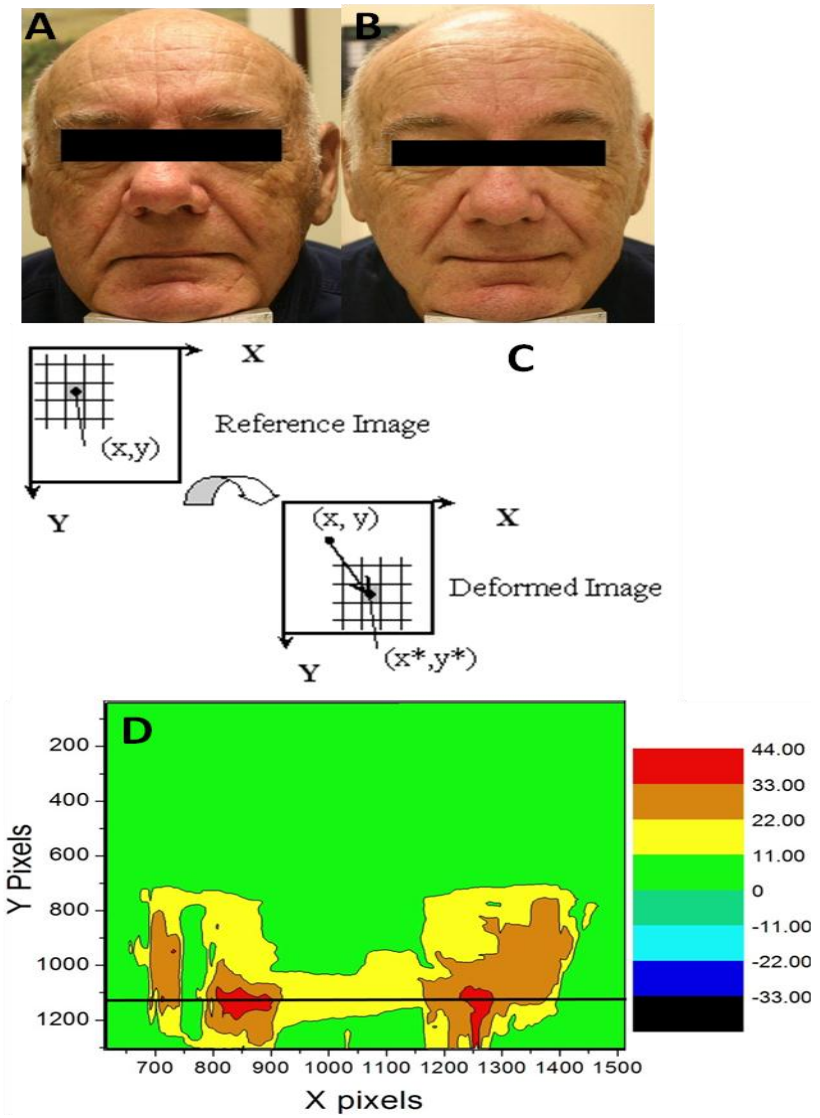


FIGURE 4- 2: (A) PATIENT'S FACE AT REST OR NEUTRAL MOTION (REFERENCE IMAGE) (B) PATIENT'S FACE WITH A SLIGHT SMILE (DEFORMED IMAGE) (C) SCHEMATIC OF WORKING PRINCIPLE OF DISC (D) QUANTIFYING THE MAGNITUDE OF DISPLACEMENT ON RIGHT AND LEFT SIDE OF THE FACE USING A COLOR DISPLACEMENT MAP.

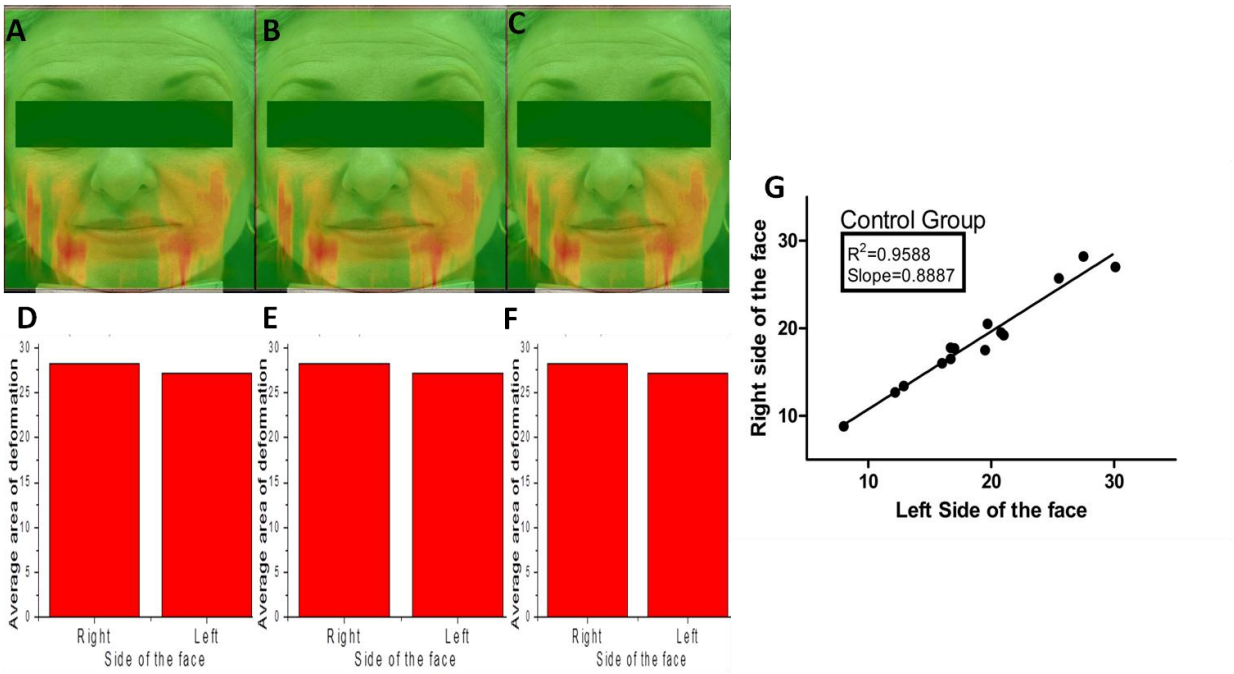


FIGURE 4- 3: DISC GENERATED COLOR DISPLACEMENT MAP OF CONTROL FOR (A) FIRST SET OF IMAGES (B) SECOND SET OF IMAGES (C) THIRD SET OF IMAGES. AVERAGE AREA OF DEFORMATION BETWEEN RIGHT AND LEFT SIDE OF THE FACE FOR (D) FIRST SET OF IMAGES (E) SECOND SET OF IMAGES (F) THIRD SET OF IMAGES (G) LINEAR CORRELATION BETWEEN THE RIGHT AND LEFT SIDE OF THE FACE FOR CONTROL POPULATION INDICATING SYMMETRY.

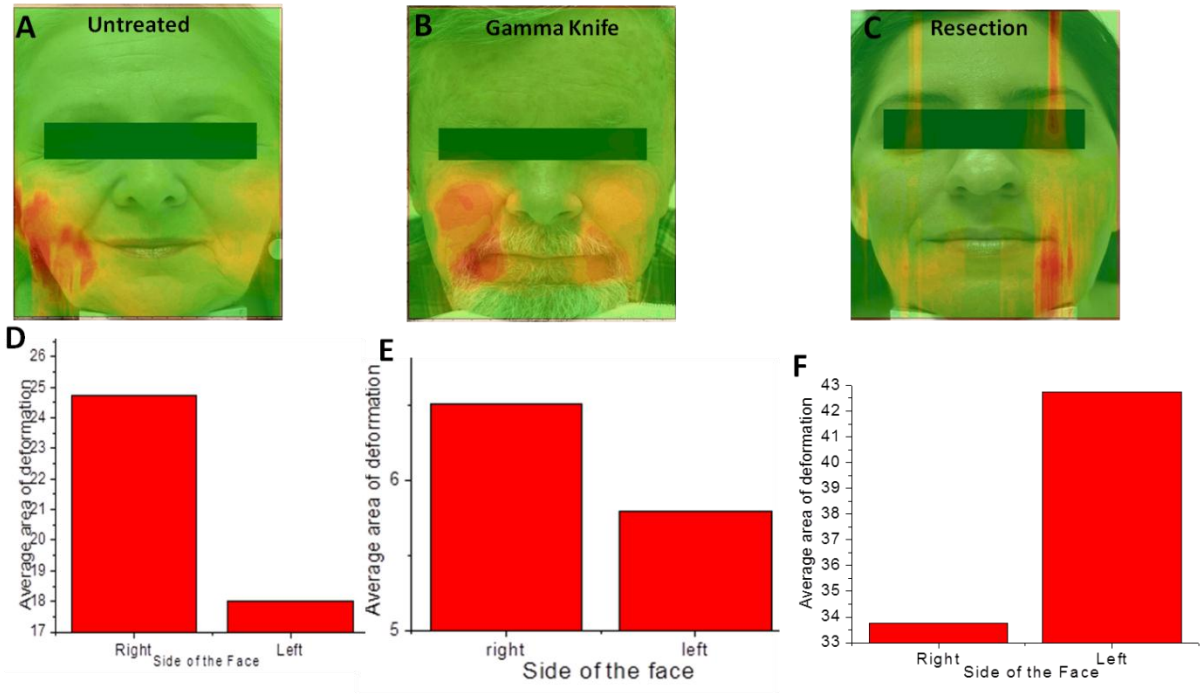


FIGURE 4- 4: OVERLAY OF DISC GENERATED COLOR MAP ON THE DEFORMED IMAGE OF (A) UNTREATED/NO SURGERY PATIENT (B) GAMMA KNIFE TREATED PATIENT (C) RESECTION TREATED PATIENT. AVERAGE AREA OF DEFORMATION BETWEEN RIGHT AND LEFT SIDE OF THE FACE FOR

(D) UNTREATED/ NO SURGERY PATIENT (E) GAMMA KNIFE TREATED PATIENT (F) RESECTION TREATED PATIENT

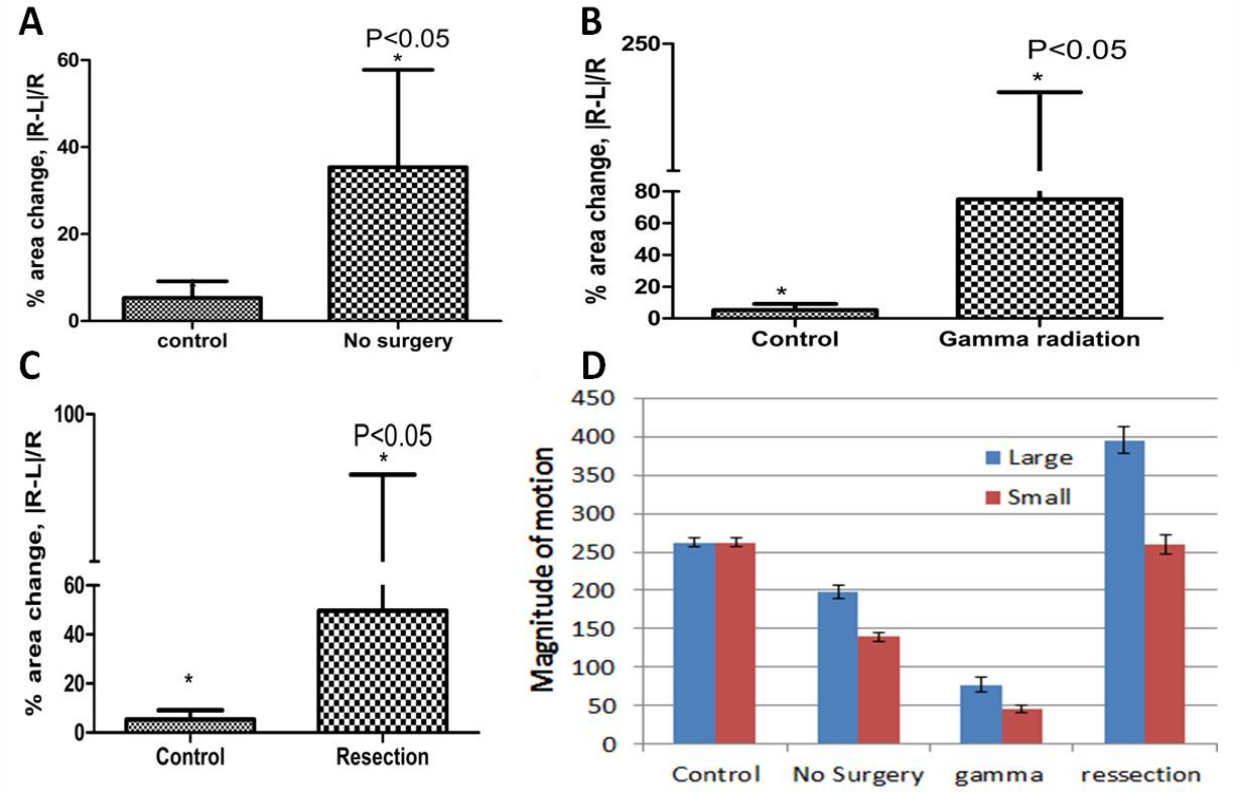


FIGURE 4- 5: PERCENT AREA CHANGE BETWEEN RIGHT AND LEFT SIDE, |R-L|/R COMPARING CONTROL POPULATION AND (A) NO SURGERY/UNTREATED (B) GAMMA RADIATION TREATED (C) RESECTION TREATED. (D) LARGE AND SMALL MAGNITUDE OF MOTION ON THE FACE

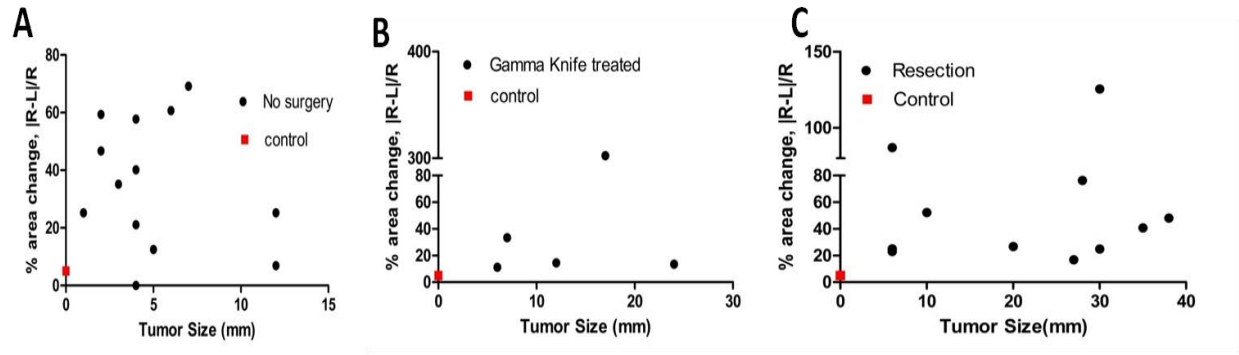


FIGURE 4- 6: NO CORRELATION BETWEEN PERCENT AREA CHANGE BETWEEN RIGHT AND LEFT SIDE, |R-L|/R AND TUMOR SIZE OF (A) NO SURGERY/UNTREATED (B) GAMMA KNIFE TREATED (C) RESECTION TREATED

# BIBLIOGRAPHY


1. Karp, J. and R. Langer, *Development and therapeutic applications of advanced biomaterials.* Curr Opin Biotechnol, 2007. **18**(5): p. 454–459.
2. Langer, R. and D. Tirrell, *Designing materials for biology and medicine* Nature, 2004. **428**(6982): p. 487–492.
3. Chan, B.P. and K.W. Leong, *Scaffolding in tissue engineering: general approaches and tissue-specific considerations.* Eur Spine J, 2008. **17**(Suppl 4): p. S467-s479.
4. Langer, R. and J. Vacanti, *Tissue Engineering.* Science, 1993. **260**: p. 920-926.
5. Freed, L.E., et al., *Biodegradable Polymer Scaffolds for Tissue Engineering.* Bio-Technology 1994. **12**: p. 689-693.
6. Rosso, F., et al., *From cell-ECM interactions to tissue engineering.* J. Cell. Physiol. , 2004. **199**: p. 174-180.
7. Slaughter, B.V., et al., *Hydrogels in Regenerative Medicine.* Advanced Materials, 2009. **21**: p. 3307-3329.
8. Nayak, S. and L.A. Lyon, *Soft Nanotechnology with Soft Nanoparticles.* Angew. Chem. Int. Ed. , 2005. **44**: p. 7686-7708.
9. Peppas, N.A., et al., *Hydrogels in pharmaceutical formulations* Eur. J. Pharm. Biopharm. , 2000. **50**(1): p. 27–46.
10. Moreira Teixeira, L.S., et al., *Enzyme-catalyzed crosslinkable hydrogels: Emerging strategies for tissue engineering.* Biomaterials, 2012. **33**: p. 1281-1290.
11. Wichterle, O. and D. Lim, *Hydrophillic gels for biological use.* Nature, 1960. **185**: p. 117-118.
12. Drury, J.L. and D.J. Mooney, *Hydrogels for tissue engineering: scaffold design variables and and applications.* Biomaterials, 2003. **24**: p. 4337-4351.

13. Vlierberghe, S.V., P. Dubruel, and E. Schacht, *Biopolymer-Based Hydrogels As Scaffolds for Tissue Engineering Applications: A Review.* Biomacromolecules, 2011. **12**: p. 1387-1408.

14. Wu, Y., P. Kalra, and N.M. Thalmann, *Physically-based Wrinkle Simulation & Skin Rendering.* Eurographics Workshop on Computer Animation and Simulation, 1997: p. 69-79.

15. Staloff, A.I., et al., *An in vivo study of the mechanical properties of facial skin and influence of aging using digital image speckle correlation.* Skin Research and Technology, 2007. **14**(2): p. 127-134.

16. Abe, S., S. Yamaguchi, and T. Amagasa, *Multilineage cells from apical pulp of human tooth with immature apex.* Oral Sci. Int., 2007. **4**: p. 45-58.

17. Wang, J., et al., *The odontogenic differentiation of human dental pulp stem cells on nanofiborous poly(L-Lactic acid) scaffolds in vitro and in vivo.* Acta Biomaterialia, 2010. **6**: p. 3856-3863.

18. Dietschi, D., et al., *Biomechanical considerations for the restoration of endodontically treated teeth: a systematic review of the literature—Part I. Composition and micro- and macrostructure alterations.* Quintessence Int, 2007. **38**(9): p. 733-43.

19. Dietschi, D., et al., *Biomechanical considerations for the restoration of endodontically treated teeth: a systematic review of the literature—Part II. Evaluation of fatigue behavior, interfaces, and in vivo studies.* Quintessence Int., 2008. **39**(2): p. 117-129.

20. Nakashima, M. and A. Akamine, *The application of tissue engineering to regeneration of pulp and dentin in endodontics.* J. Endod, 2005. **31**: p. 711-718.

21. Nakashima, M. and A.H. Reddi, *The application of bone morphogenetic proteins to dental tissue engineering.* Nat Biotechnol, 2003. **21**: p. 1025-1032.

22. Sloan, A.J. and A.J. Smith, *Stem cells and the dental pulp: potential roles in dentine regeneration and repair.* Oral Dis., 2007. **13**: p. 151.

23. Gronthos, S., et al., *Postnatal human dental pulp stem cells (DPSC) in vitro and in vivo.* Proc Natl Acad Sci, 2000. **97**(25): p. 13625-30.

24. Zhang, W., et al., *Differentiation ability of rat postnatal dental pulp cells in vitro.* Tissue Eng 2005. **11**(3-4): p. 357-368.

25. Mina, M. and A. Braut, *New insight into progenitor/stem cells in dental pulp using Col1a1-GFP transgenes.* Cells Tissues Organs, 2004. **176**(1-3): p. 120-33.

26. Iohara, K., et al., *Dentin regeneration by dental pulp stem cell therapy with recombinant human bone morphogenetic protein 2.* J Dent Res, 2004. **83**(8): p. 590-595.

27. Brigitte, A.-L., et al., *Dexamethasone stimulates differentiation of odontoblast-like cells in human dental pulp cultures.* Cell Tissue Res, 2005. **321**: p. 391-400.

28. Yu, J., et al., *Differentiation of dental pulp stem cells into regular-shaped dentin-pulp complex induced by tooth germ cell conditioned medium.* Tissue Eng, 2006. **12**: p. 3097–3105.

29. Gronthos, S., et al., *Stem cell properties of human dental pulp stem cells* J Dent Res, 2002. **81**(8): p. 531-535.

30. Gennari, C., *Differential Effect of Glucocorticoids on Calcium Absorption and Bone Mass.* Rheumatology, 1993. **32**(2): p. 11-14.

31. Ma, P., *Biomimetic materials for tissue engineering.* Adv Drug Deliv Rev, 2008. **60**: p. 184.

32. Young, C., et al., *Tissue engineering of complex tooth structures on biodegradable polymer scaffolds.* Dent Res, 2002. **81**(10): p. 695–700.

33. Choi, R. and J. Vacanti, *Preliminary studies of tissue-engineered intestine using isolated epithelial organoid units on tubular synthetic biodegradable scaffolds.* Transplant Proc, 1997. **29**: p. 848-851.

34. Duailibi, M., et al., *Bioengineered teeth from cultured rat tooth bud cells.* J Dent Res, 2004. **83**: p. 523-528.

35. El-Backly, R., et al., *Regeneration of dentine/pulp-like tissue using a dental pulp stem cell/poly(lactic-co-glycolic) acid scaffold construct in New Zealand white rabbits.* Aust Endod J, 2008. **34**: p. 52-67.

36. Zhang, W., et al., *The performance of human dental pulp stem cells on different three-dimensional scaffold materials.* Biomaterials, 2006. **27**: p. 5658-68.

37. Bostman, O. and H. Pihlajamaki, *Adverse tissue reactions to bioabsorbable fixation devices.* Clin Orthop Relat Res, 2000. **371**: p. 216-227.

38. Linde, A., *Dentin matrix proteins: composition and possible functions in calcification.* Anat Rec, 1989. **224**: p. 154.

39. Sumita, Y., et al., *Performance of collagen sponge as a 3-D scaffold for tooth-tissue engineering.* Biomaterials, 2006. **27**: p. 3238.

40. Prescott, R., et al., *In vivo generation of dental pulp-like tissue by using dental pulp stem cells, a collagen scaffold, and dentin matrix protein 1 after subcutaneous transplantation in mice.* J Endod, 2008. **34**: p. 421-426.

41. Yang, X., et al., *The performance of dental pulp stem cells on nanofibrous PCL/gelatin/nHA scaffolds.* Journal of Biomedical Materials Reseach Part A, 2010. **93**(1): p. 247-257.

42. Kuo, T., et al., *Regeneration of dentinpulp complex with cementum and periodontal ligament formation using dental bud cells in gelatin-chondroitin-hyaluronan tri-copolymer scaffold in swine.* J Biomed Mater Res A, 2008. **86**: p. 1063-8.

43. Liang, H.-C., et al., *Genipin-crosslinked gelatin microspheres as a drug carrier for intramuscular administration: In vitro and in vivo studies.* Journal of Biomedical Materials Reseach Part A, 2003. **65A**(2): p. 271-282.

44. Kishimoto, J., et al., *In-Vivo detection of human vascular endothelial growth factor promotor activity in transgenic mouse skin [see comments].* Am J Pathol 2000. **157**: p. 103-110.

45. Zhang, Y., et al., *Surface characterization of cross-linked elastomers by shear modulation force microscopy.* Polymer, 2003. **44**: p. 3327-3332.

46. Zhang, Y., et al., *Surface characterization of cross-linked elastomers by shear modulation force microscopy.* Polymer, 2003. **44**: p. 3327-32.

47. Ghosh, K., et al., *Cell adaptation to a physiologically relevant ECM mimic with different viscoelastic properties.* Biomaterials, 2007. **28**: p. 671-679.

48. Huang, G.T.-J., K. Shagramanova, and S.W. Chan, *Formation of Odontoblast-Like Cells from Cultured Human Dental Pulp Cells on Dentin In Vitro.* Journal of Endodontics, 2006. **32**(11): p. 1066-73.

49. Fromigue, O., P.J. Marie, and A. Lomri, *Differential effects of transforming growth factor beta 2, dexamethasone and 1,25-dihydroxyvitamin D on human bone marrow stromal cells.* Cytokine, 1997. **9**(8): p. 613-623.

50. Mikami, Y., et al., *Bone morphogenetic protein 2 and dexamethasone synergistically increase alkaline phosphatase levels through JAK/STAT signaling in C3H10T1/2 cells.* J Cell Physiol. , 2010. **223**(1): p. 123-33.

51. Smith, A., et al., *Reactionary dentinogenesis* Int J Dev Biol, 1995. **39**: p. 273.

52. Zhang, W., et al., *Hard tissue formation in a porous HA/TCP ceramic scaffold loaded with stromal cells derived from dental pulp and bone marrow* Tissue Eng Part A, 2008. **14**: p. 285.

53. Kim, N., et al., *Distinct differentiation properties of human dental pulp cells on collagen, gelatin, and chitosan scaffolds.* Oral Surg Oral Med Oral Pathol Oral Radiol Endod., 2009. **108**(5): p. 94-100.

54. Dick, H. and D. Carmichael, *Reconstituted antigen-poor collagen preparations as potential pulp-capping agents* J Endod 1980. **6**(7): p. 641-4.

55. Carmichael, D., H. Dick, and C. Dodd, *Histologic effects of antigenically altered collagen as a heterograft for mammalian pulp exposures* Arch Oral Biol 1974. **19**(12): p. 1121-6.

56. Butler, W., et al., *Extracellular matrix proteins and the dynamics of dentin formation.* Connect Tissue Res, 2002. **43**: p. 301-7.

57. Butler, W., *Dentin specific proteins.* Methods Enzymol 1987. **145**: p. 290-303.

58. Yamada, Y., et al., *Cluster analysis and gene expression profiles: a cDNA microarray system-based comparison between human dental pulp stem cells (hDPSCs) and human mesenchymal stem cells (hMSCs) for tissue engineering cell therapy.* Biomaterials, 2006. **27**: p. 3766-81.

59. Kasugai, S., et al., *Characterization of a system of mineralized-tissue formation by rat dental pulp cells in culture.* Arch Oral biol, 1993. **38**: p. 769-777.

60. Lee, K.Y. and D.J. Mooney, *Hydrogels for tissue engineering.* Chemical Reviews, 2001. **101**: p. 1869-1879.

61. Bruce Alberts, D.B., et al., *Molecular Biology of the Cell*, 1994, Garland Science: New York.

62. Fraser, J.R.E., L. T.C., and L. U.B.G., Journal of Intern. Med. , 1997. **242**(1): p. 27-33.

63. Ghosh, K., et al., *Rheological Characterization of in Situ Cross-Linkable Hyaluronan Hydrogels.* BioMacromolecules, 2005. **6(5)**: p. 2857-2865.

64. Elisseeff, J., et al., *Transdermal photopolymerization for minimally invasive implantation.* Proc Natl Acad Sci, 1999. **96**: p. 3104–3107.

65. Hazel, B., et al., *Formaldehyde as a pretreatment for dermal collagen heterografts.* Biochim. Biophys. Acta., 1980. **632**: p. 589-597.

66. Weadock, K., R.M. Olson, and F.H. Silver, *Evaluation of collagen crosslinking techniques.* Biomateri. Med. Dev. Art. Org., 1983. **11**: p. 293-318.

67. Damink, O., et al., *Glutaraldehyde as a crosslinking agent for collagen-based biomaterials.* J. Mater. Sci. Mat. Med., 1995. **6**: p. 460-472.

68. Shalaby, S.W., et al., *Polymers of biological and biomedical significance*, in *ACS Symposium Series*1994, Oxford University Press: Oxford, UK p. 540.

69. Sung, H.W., et al., *Crosslinking characteristics of biological tissue fixed with monofunctional or multifunctional epoxy compounds.* Biomaterials, 1996. **17**: p. 1405-1410.

70. Damink, O., et al., *Crosslinking of dermal sheep collagen using hexamethylene diisocyanate.* J. Mater.Sci. Mat. Med., 1995. **6**: p. 429-434.

71. Schacht, E.H., et al., *Crosslinkage of gelatin by dextran dialdehyde.* Polym. Gels Networks, 1993. **1**: p. 213-224.

72. Choi, Y.S., et al., *Study on gelatin-containing artificial skin: I. Preparation and characteristics of novel gelatin-alginate sponge.* Biomaterials, 1999. **20**: p. 409-417.

73. Choi, Y.S., et al., *Studies on gelatin-containing artificial skin. II. Preparation and characterization of cross-linked gelatin-hyaluronate sponge.* J Biomed. Mater. Res., 1999. **48**: p. 631-639.

74. Williams, C.G., et al., *Variable cytocompatibility of six cell lines with photoinitiators used for polymerizing hydrogels and cell encapsulation.* Biomaterials, 2005. **26**: p. 1211-1218.

75. Gendler, E., S. Gendler, and M.E. Nimni, *Toxic reactions evoked by glutaraldehyde-fixed pericardium and cardiac valve tissue bioprosthesis.* J Biomed Mater Res, 1984. **18**: p. 727-736.

76. Liang, H.C., et al., *Genipin-crosslinked gelatin microspheres as a drug carrier for intramuscular administration: In vitro and in vivo studies.* J Biomed Mater Res A, 2003. **65**: p. 271-282.

77. Shu, X.Z., et al., *Disulfide Crosslinked Hyaluronan Hydrogels.* Biomacromolecules, 2002. **3**(6): p. 1304-11.

78. Luo, Y., K.R. Kirker, and G.D. Prestwich, 69, 169-184 (2000), *"Cros-Linked Hyaluronic Acid Hydrogel Films: New Biomaterials for Drug Delivery.* J.Controlled Rel., 2000. **69**: p. 169-184.

79. Prestwich, G.D., et al., *Chemical modification of hyaluronic acid for drug delivery, biomaterials, and biochemical probes.* J. Controlled Release, 1998. **53**: p. 93-103.

80. Kuo, J.-W., D.A. Swann, and G.D. Prestwich, *Chemical modification of hyaluronic acid by carbodiimides.* Bioconjug. Chem., 1991. **2**: p. 232-241.

81. Fujiwara, J., et al., *Gelation of hyaluronicac id through annealing.* Polym Int, 2000. **49**: p. 1604-1608.

82. Vercruysse, K.P., et al., *Synthesis and in vitro degradation of new polyvalent hydrazide cross-linked hydrogels of hyaluronic acid.* Bioconjug. Chem., 1997. **8**: p. 686-694.

83. Prestwich, G.D., et al., *Controlled chemical modification of hyaluronic acid: synthesis, applications, and biodegradation of hydrazide derivatives.* Journal of Control Release, 1998. **53**: p. 92-103.

84. Seidlits, S.K., et al., *Fibronectin–hyaluronic acid composite hydrogels for three-dimensional endothelial cell culture.* Acta Biomater., 2011. **7**: p. 2401-2409.

85. Shu, X.Z., et al., *In situ crosslinkable hyaluronan hydrogels for tissue engineering.* Biomaterials, 2004 Mar-Apr. **25**(7-8): p. 1339-48.

86. Shu, X.Z., et al., *Attachment and spreading of fibroblasts on an RGD peptide-modified injectable hyaluronan hydrogel.* J Biomed Mater Res, 2004 Feb 1. **68**(2): p. 365-75.

87. Shu, X.Z., et al., *Disulfide-crosslinked hyaluronan-gelatin hydrogel films: a covalent mimic of the extracellular matrix for in vitro cell growth.* Biomaterials, 2003 Sep. **24**(21): p. 3825-3834.

88. Pozzo, D. and L. Walker, *Reversible shear gelation of polymer–clay dispersions.* Colloids Surf, A Physicochem Eng Asp, 2004. **240**(1-3): p. 187-198.

89. Can, V. and O. Okay, *Shake gels based on Laponite–PEO mixtures: effect of polymer molecular weight. .* Des Monomers Polym. Gels Networks, 2005. **8**(5): p. 453-462.

90. Baghdadi, H., H. Sardinha, and S. Bhatia, *Rheology and gelation kinetics in Laponite dispersions containing poly(ethylene oxide).* J Polym Sci, B, Polym Phys, 2005. **43**(2): p. 233-240.

91. Loizou, E., et al., *Large scale structures in nanocomposite hydrogels. .* Macromolecules 2005. **38**(6): p. 2047-2049.

92. Schexnailder, P. and G. Schmidt, *Nanocomposite Polymer Hydrogels.* Colloid Polym Sci, 2009. **287**: p. 1-11.

93. Wang, S.F., et al., *Biopolymer chitosan/montmorillonite nanocomposites: preparation and characterization.* Polym. Degrad. Stabil., 2005. **90**: p. 123-131.

94. Zhuang, H., et al., *In vitro biodegradation and biocompatibility of gelatin/montmorillonite-chitosan intercalated nanocomposite.* J. Mater.Sci. Mater. Med., 2007. **18**: p. 951-957.

95. Bhavesh, D.K., et al., *Biopolymer–clay hydrogel composites as drug carrier: Host–guest intercalation and in vitro release study of lidocaine hydrochloride.* Applied Clay Science 2011. **52**: p. 364-367.

96. Depan, D., A.P. Kumar, and R.P. Singh, *Cell proliferation and controlled drug release studies of monohybrids based on Chitosan-g-lactic acid and montmorillonite.* Acta Biomater., 2009. **5**: p. 93-100.

97. Haraguchi, K., *Synthesis and properties of soft nanocomposite materials with novel organic/inorganic network structures.* Polymer Journal, 2011. **43**: p. 223-241.

98. Wu, C.-J., et al., *Development of Biomedical Polymer-Silicate Nanocomposites: A Materials Science Perspective.* Materials, 2010. **3**: p. 2986-3005.

99. Jin, Q., et al., *Silicate cross-linked bio-nanocomposite hydrogels from peo and chitosan.* Macromol. Biosci. , 2009. **9**: p. 1028-1035.

100. Gaharwar, A.K., et al., *Highly extensible bio-nanocomposite films with direction-dependent properties.* Advan. Funct. Mater., 2010. **20**(429-436).

101. Shazia, R., *Short term exposure to high glucose has multiple adverse effects on wound provisional matrix molecules and a bioengineered matrix.*, in *Biomedical Engineering*2007, Stony Brook University.

102. Deguine, V., et al., *Free radical depolymerization of hyaluronan by Maillard reaction products: role in liquefaction of aging vitreous.* International Journal of Biomacromolecules, 1998 Feb. **22**(1): p. 17-22.

103. Katsumura, C., et al., *Effects of advanced glycation end products on hyaluronan photolysis: a new mechanism of diabetic vitreopathy.* Opthalmic Res. , 2004. **36**: p. 327-331.

104. Arne, N., et al., *High molecular weight hyaluronic acid inhibits advanced glycation endproduct-induced NF-UB activation and cytokine expression.* FEBS Letters, 1999. **453**: p. 283-287.

105. Brown, M.B. and S.A. Jones, *Hyaluronic acid: a unique topical vehicle for the localized delivery of drugs to the skin.* Journal of European Academy of Dermatology and Venereology, 2005. **19**: p. 308-318.

106. Chiou, B.-S., et al., *Rheology of starch–clay nanocomposites.* Carbohydrate Polymers 2005 **59**: p. 467-475.

107. Suprakas, S.R. and O. Masami, *Polymer/layered silicate nanocomposites:a review from prepataion to processing.* Prog. Polym. Sci., 2003. **28**: p. 1539-1641.

108. Kavangh, G.M. and S.B. Ross-Murphy, *Rheological characterization of polymer gels.* Prog. Polym. Sci., 1998. **23**(3): p. 533-562.

109. Moller, L., et al., *Preparation and evaluation of hydrogel-composites from methylacrylated hyaluronic acid, alginate and gelatin for tissue engineering.* Int. J. Artif. Organs, 2011. **34**(2): p. 93-102.

110. Almdal, K., et al., *Towards a phenomenological definition of the term 'gel'.* Polymer Gels and Networks, 1993. **1**(1): p. 5-17.

111. Jiang, J., et al., *The effect of physiologically relevant additives on the rheological properties of concentrated Pluronic copolymer gels.* Polymer, 2008. **49**: p. 3561-3567.

112. Ghosh, K., et al., *Cell Adaption to the physiologically relevant ECM mimic with different viscoelastic properties.* Biomaterials, 2007. **28**: p. 671-679.

113. Frampton, J.E. and S.E. Easthope, *Botuinum Toxin-A (Botox Cosmetic) A Review of its use in treatment of glabellar frown lines.* Am J Clin Dermatology, 2003. **4**(10): p. 709-725.

114. Ferguson, J. and J.C. Barbenel, *Skin surface patterns and the directional mechanical properties of the dermis*, in *Bioengineering Skin*, P.P. Marks R., Editor 1981, Kluwer academic Publishers: London. p. 83-92.

115. Fongo, A., E. Ferraris, and M. Bocca, *Skin tension lines and wrinkles.* Minerva Chir., 1966. **21**(13): p. 627-630.

116. Wu, Y., P. Kalra, and N.M. Thalmann, *Simulation of Static and Dynamic Wrinkles of Skin.* Proc. Computer Animation, IEEE Computer Society, 1996: p. 90-97.

117. Carruthers, J.D. and J.A. Carruthers, *Treatment of glabellar Frown Lines with C. botilinum -A exotoxin.* Journal of Dermalogic Surgery and Oncology, 1992. **18**(1): p. 17-21.

118. Carruthers, A. and J. Carruthers, *Patient-reported outcomes with botulinum neurotoxin type A.* Journal of Cosmetic Laser Therapy, 2007. **9**(1): p. 32-37.

119. Carruthers A., C.J., *Botulinum toxin type A treatment of multiple upper facial sites: patient-reported outcomes.* Dermatol Surgery, 2007. **1 Spec No.**(33): p. S10-7.

120. Carruthers, A., J. Carruthers, and N.J. Lowe, *One-year, randomised, multicenter, two-period study of the safety and efficacy of repeated treatments with botulinum toxin type A in patients with glabellar lines.* Journal of Clinical Research, 2004. **7**: p. 1-20.

121. Stotland, M.A., J.W. Kowalski, and B.B. Ray, *Patient-reported benefit and satisfaction with botulinum toxin type A treatment of moderate to severe glabellar rhytides: Results from a prospective open-label study.* Plastic Reconstructive Surgery 2007. **120**(5): p. 1386-93.

122. Heckmann, M. and G. Schön-Hupka, *Quantification of the Efficacy of Botulinum Toxin-A by Digital Image Analysis.* Journal of American Academy of Dermatology, 2001. **45**(4): p. 508-514.

123. Hanin, L., *Surface topography method to determine the effect of botulinum toxin upon a muscle*, U.S.P.a.T. Office, Editor 2007, Allergan Inc.: USA.

124. Flynn, T.C., *Botulinum Toxin: Examining duration of effect in facial aesthetic applications.* American Journal of Clinical Dermatology, 2010. **11**(3): p. 183-189.

125. Guan, E., et al., *Determining the mechanical properties of rat skin with digital image speckle correlation.* Dermatology, 2004. **208**(2): p. 112-119.

126. Zhou, P. and K. Goodson, *Subpixel displacement and deformation gradient measurement using digital image speckle correlation (DISC).* Society of Photo-Optical Instrumentation Engineers, 2001. **40**(8): p. 1613-1620.

127. Guan, E., et al., *An assesment of DISC.* Proc SEM Annual Conference Theoretical, Experimental Comput Mech, Cincinnati, 1992. **1**: p. 19-22.

128. Peters, W.H. and W.F. Ranson, *Digital imaging techniques in experimental stress analysis.* Optical Enginineering, 1982. **21**(3): p. 427-431.

129. Choi, S. and S.P. Shah, *Measurement of deformations on concrete subjected to compression using image correlation.* Experimental Mechanics, 1997. **37**(3): p. 307-313.

130. Schreier, H.W., J.R. Braasch, and M. Sutton, *Systematic errors in digital image correlation caused by intensity interpolation.* Optical Enginineering, 2000. **39**: p. 2915-2921.

131. Bruck, H.A., et al., *Digital Image Correlation using Newton-Raphson method of partial differential correction.* Experimental Mechanics, 1989. **29**(3): p. 261-267.

132. Sutton, M.A., et al., *Effect of subpixel image restoration on digital correlation error estimates.* Optical Enginineering, 1988. **27**(10): p. 870-877.

133. Chao, Y.J. and P.F. Luo, *An Experimental study of the deformation fields around a propagating crack tip.* Experimental Mechanics, 1988. **38**(2): p. 79-85.

134. Afriat, I.S. and M. Rafailovich, *Measurement of skin stretch using digital image speckle correlation.* Skin Research and Technology, 2008. **14**: p. 298-303.

135. Carruthers, J.D., R.G. Glogau, and A. Blitzer, *Advances in facial rejuvenation: botulinum toxin type a, hyaluronic acid dermal fillers, and combination therapies--consensus recommendations.* Plastic Reconstrucctive Surgery, 2008. **5 Suppl**(121): p. 5S-30S; quiz: 31S-35S

136. Filipo, R., et al., *Botulinum Toxin in the Treatment of Facial Synkinesis and Hyperkinesis.* Laryngoscope, 2012. **122**(February): p. 266-270.

137. de Maio, M. and R.F. Bento, *Botulinum Toxin in Facial Palsy: An Effective Treatment for Contralateral Hyperkinesis.* Plastic Reconstrucctive Surgery, 2007. **120**(4): p. 917-927.

138. Matthies, C. and M. Samii, *Management of 1000 vestibular schwannomas (acoustic neuromas): clinical presentation.* Neurosurgery 1997. **40**: p. 1-9 Discussion 9-10.

139. Samii, M. and C. Matthies, *Management of 1000 vestibular schwannomas (vestibular schwannomas): The Facial Nerve-Preservation and Restitution of Function.* Neurosurgery 197. **40**: p. 684-695.

140. Colletti, V., F. Fiorino, and M. Camer, *La conservazione dell'udito nella chirurgia del neurinoma dell'acustico.* CRS Amplifon, Milano, 1994.

141. Møller, A., *Evoked potentials in intraoperative monitoring*1988, Baltimore: Williams & Wilkins.

142. Møller, A. and P. Jannetta, *Preservation of facial function during removal of acoustic neuromas. Use of monopolar constantvoltage stimulation and EMG.* Journal of Neurosurgery, 1984. **61**: p. 757-760.

143. Kartush, J., J. Niparko, and S. Bledsoe, *Intraoperative facial monitoring: comparison of stimulating electrodes.* Laryngoscope, 1985. **95**: p. 1536-1540.

144. Prass, R. and H. Luders, *Constant current versus constant voltage stimulation.* Journal of Neurosurgery, 1985. **62**: p. 622-623.

145. Prass, R. and H. Luders, *(Acoustic loudspeaker) facial electromyography monitoring: Evoked electromyographic activity during acoustic tumor resection.* Neurosurgery, 1986. **19**: p. 392-400.

146. Colletti, V. and F. Fiorino, *Continuous retrograde monitoring of the facial nerve during cerebellopontine angle surgery: Normative data.* Skull Base Surg, 1996. **6**: p. 47-51.

147. House, J. and D. Brackman, *Facial nerve grading system.* Otolaryngol Head Neck Surg., 1985. **93**: p. 146-147.

148. Vrabec, J., et al., *Facial Nerve Grading System 2.0.* Otolaryngol Head Neck Surg., 2009. **140**(4): p. 445-450.

149. Pamudurthy, S., et al., *Dynamic Approach for Face Recognition using Digital Image Skin Correlation*, 2005, Springer-Verlag Berlin, Heidelberg AVBPA Proceedings of the 5th international conference on Audio- and Video-Based Biometric Person Authentication. p. 1010-1018.

150. Bhatnagar, D., et al., *Digital image speckle correlation (DISC) analysis for quantifying the effect and duration of cosmetic treatment with botulinum toxin(BT) type A*, 2011: 71st Society of Investigative Dermatology Annual Meeting. p. 476.

151. Chiang, F., *A family of 2D and 3D experimental stress analysis techniques using laser speckles.* Solid Mech Archives 1978. **3**(1): p. 1-32.

152. Chiang, F., *Evolution of white light speckle method and its application to micro/nanotechnology and heart mechanics.* Opt Eng 2003. **42**(5): p. 1288-1292.

153. Wynne, M.K., A.O. Diefendorf, and M.H. Fritsch, *Sudden Hearing Loss*, in *The ASHA Leader*December 26, 2001.